UNIVERSIDADE ESTADUAL DE CAMPINAS
FACULDADE DE ENGENHARIA ELÉTRICA E DE COMPUTAÇÃO

DIEGO TERUO MENDES DE SOUZA

HIGH-VOLTAGE HIGH-FREQUENCY CONVERTER FOR RESISTIVE LOAD WITH UNPREDICTABLE VARIATION

CONVERSOR DE ALTA TENSÃO E ALTA FREQUÊNCIA PARA CARGA RESISTIVA COM VARIAÇÃO IMPREVISÍVEL

CAMPINAS
2018

UNICAMP

UNIVERSIDADE ESTADUAL DE CAMPINAS
FACULDADE DE ENGENHARIA ELÉTRICA E DE COMPUTAÇÃO

DIEGO TERUO MENDES DE SOUZA

HIGH-VOLTAGE HIGH-FREQUENCY CONVERTER FOR RESISTIVE LOAD WITH UNPREDICTABLE VARIATION

CONVERSOR DE ALTA TENSÃO E ALTA FREQUÊNCIA PARA CARGA RESISTIVA COM VARIAÇÃO IMPREVISÍVEL

Master dissertation presented to the Electrical Engineering Post-graduation Program of the School of Electrical and Computing Engineering of the University of Campinas to obtain the M.Sc grade in Electrical Engineering, in the field of Electrical Energy.

Dissertação de Mestrado apresentada ao Programa de Pós-Graduação em Engenharia Elétrica da Faculdade de Engenharia Elétrica e de Computação da Universidade Estadual de Campinas para obtenção do título de Mestre em Engenharia Elétrica, na área de Energia Elétrica.

Orientador: Prof. Dr. José Antenor Pomilio

ESTE EXEMPLAR CORRESPONDE À VERSÃO FINAL DA DISSERTAÇÃO
DEFENDIDA PELO ALUNO DIEGO TERUO MENDES DE SOUZA
E ORIENTADO PELO PROF. DR. JOSÉ ANTENOR POMILIO

Assinatura do Orientador

____

CAMPINAS
2018

Agência(s) de fomento e nº(s) de processo(s): Não se aplica.
ORCID: https://orcid.org/0000-0002-2308-3174

Ficha catalográfica
Universidade Estadual de Campinas
Biblioteca da Área de Engenharia e Arquitetura
Luciana Pietrosanto Milla - CRB 8/8129

Souza, Diego Teruo Mendes de, 1992-
So89h High-voltage high-frequency converter for resistive load with unpredictable variation / Diego Teruo Mendes de Souza. – Campinas, SP : [s.n.], 2018.

Orientador: José Antenor Pomilio.
Dissertação (mestrado) – Universidade Estadual de Campinas, Faculdade de Engenharia Elétrica e de Computação.

1. Energia Elétrica - Distribuição - Alta tensão. 2. Eletrônica de potência. 3. Conversores elétricos. 4. Transformadores elétricos. 5. Parasitas. I. Pomilio, José Antenor, 1960-. II. Universidade Estadual de Campinas. Faculdade de Engenharia Elétrica e de Computação. III. Título.

Informações para Biblioteca Digital

Título em outro idioma: Conversor de alta tensão e alta frequência para carga resistiva com variação imprevisível
Palavras-chave em inglês:
Electric power - Distribution - High voltage
Power electronics
Electric converters
Electric transformers
Parasites
Área de concentração: Energia Elétrica
Titulação: Mestre em Engenharia Elétrica
Banca examinadora:
José Antenor Pomilio [Orientador]
Alfeu Joãozinho Sguarezi Filho
Pedro Xavier de Oliveira
Data de defesa: 06-08-2018
Programa de Pós-Graduação: Engenharia Elétrica

COMISSÃO JULGADORA - DISSERTAÇÃO DE MESTRADO

Candidato: Diego Teruo Mendes de Souza RA: 163717

Data da Defesa: 06 de agosto de 2018

Título da Tese (Inglês): "High-voltage high-frequency converter for resistive load with unpredictable variation".

Título da Tese (Português): "Conversor de alta tensão e alta frequência para carga resistiva com variação imprevisível".

Prof. Dr. José Antenor Pomilio (Presidente, FEEC/UNICAMP)
Prof. Dr. Alfeu Joãozinho Sguarezi Filho (UFABC)
Prof. Dr. Pedro Xavier de Oliveira (FEEC/UNICAMP)

A ata de defesa, com as respectivas assinaturas dos membros da Comissão Julgadora, encontra-se no processo de vida acadêmica do aluno.

I dedicate this work to all people who run after their dreams and try to do the right thing, besides all the unfavorable circumstances.

ACKNOWLEDGMENTS

The acknowledgments are written in Portuguese language.

Gostaria de agradecer primeiramente a Deus, pelo dom da vida e por ter me permitido chegar até aqui.

Ao professor Antenor pela orientação e todas as inestimáveis contribuições, pois sem elas não seria possível a realização deste trabalho.

A Zasso Brasil, pelo suporte financeiro na realização da pesquisa.

Ao professor Celi Hipólito Dutra, por ter aberto minha mente para as possibilidades que o estudo pode proporcionar e por ter aguçado em mim, mesmo que em estágio amador na época, a curiosidade científica.

Aos meus pais, Carlos e Maria, pelos bons ensinamentos e valores que passaram em minha educação.

Aos meus irmãos Jonathan, Michele e Diana, por sempre acreditarem em mim e me apoiarem.

A Rita por todo o amor, companheirismo e apoio na realização de meus sonhos, mesmo com toda a dificuldade da minha ausência, e por ser minha maior fonte de inspiração. Te amo!

Aos colegas do LCEE por todas as contribuições diretas e indiretas na realização deste trabalho e em especial ao Bruno, por toda a ajuda no projeto das placas eletrônicas e na parte de programação, deixo aqui meu muito obrigado.

A minha madrinha e grande amiga Flavia, pelos bons conselhos, amizade, e por sempre saber dar os “puxões de orelha” nas horas certas.

A todos que me apoiaram e contribuíram de alguma forma na realização deste trabalho. Esta vitória também é de vocês.

“*Engineering is not only a learned profession, it is also a learning profession, one whose practitioners first become and then remains students throughout their active careers.*”

(William L. Everitt)

“*Quando se nasce pobre, ser estudioso é o maior ato de rebeldia contra o sistema.*”

(Autor desconhecido)

ABSTRACT

High voltage transformers have specific characteristics, since the effect of some parasitic elements is highlighted, due to its high number of turns, in order to reach the desired voltage levels.

High frequency operation reduces the volume of magnetic devices, making the systems more versatile, however it can give rise to other problems such as switching noise, electromagnetic interference and resonances.

In this dissertation a high voltage converter, with high frequency operation was developed for power transferring to resistive loads with unpredictable variation, from the short circuit to the open circuit condition, taking in account the High Voltage High Frequency Transformer's particularities.

Simulations and theoretical calculations were made to characterize the system's behavior. Protection, control and supervision systems were developed to minimize the effects of parasitic elements and resonances, as well as to ensure the safe and correct converter's operation.

A conceptual prototype was built to validate the simulations and calculations performed.

Keywords: *High Voltage Transformer, High Frequency Transformer, High Voltage Converter, Resonant Converters, Parasitic Elements, Transformer Model.*

RESUMO

Transformadores de alta tensão possuem algumas características específicas, uma vez que o efeito de elementos parasitas é amplificado, devido ao elevado número espiras, necessário para se atingir os níveis de tensão desejados.

A operação em alta frequência reduz o volume de dispositivos magnéticos, tornando os sistemas mais compactos, o que pode, no entanto, dar margem a outros problemas, como ruídos de alta frequência, interferência eletromagnética e manifestação de ressonâncias.

Nesta dissertação foi desenvolvido um conversor de alta tensão, com operação em alta frequência para transferência de potência para uma carga resistiva com variação imprevisível, desde uma situação de curto-circuito até a de circuito aberto, levando em consideração as particularidades do transformador de alta tensão operando em alta frequência.

Simulações e cálculos teóricos foram realizados para caracterização do comportamento do sistema. Sistemas de proteção, controle e supervisão foram desenvolvidos para minimizar os efeitos de elementos parasitas e ressonâncias, bem como para garantir a operação segura do conversor.

Um protótipo conceitual foi construído para validação das simulações e cálculos realizados.

***Palavras-chave**: Transformador de Alta Tensão, Transformador de Alta Frequência, Conversor de Alta Tensão, Conversores Ressonantes, Elementos Parasitas, Modelo de Transformador.*

LIST OF FIGURES

LIST OF TABLES

LIST OF SYMBOLS

A_C	Magnetic core cross section area
B_{max}	Maximum allowed electromagnetic flux density
b	Breadth of the core window
d	strand diameter of a litz wire
C_{cl}	High voltage clamper capacitor
C_{ext}	Series capacitor for inverter's DC components' blocking
Cp	Windings capacitance reflected to the primary
E_s	Energy absorbed by the clamper capacitor in a half of the working period
f	Operating frequency
f_s	Series resonance frequency
f_p	Parallel resonance frequency
I_c	Current through the characteristic impedance of the simplified resonant circuit
I_{in}	Input current of the transformer simplified circuit
I_{input}	Measured transformer primary current for the spectral analysis
I_m	Magnetizing current
I_n	Primary nominal current
I_p	Current due to the series resonance excitation
K	Order of the harmonic component
Ld	Primary leakage inductance
Lds	Secondary leakage inductance reflected to the primary
L_{ext}	External inductor
L_{in}	Input Inductance
Lm	Magnetizing inductance
m	Number of eliminated harmonics by chopping a square wave with m angles
N	Number of turns
N_p	Primary minimum number of turns
n	Transformer turns ratio
n_i	Number of strands in a litz wire
P_{max}	Transformer maximum theoretical power
$P_{R_{cl}}$	Power dissipated at the clamper resistor in a half of the working period
Q_s	Electrical charge per cycle of the resonant current

r	Radio of the cross-section area of a solid electric conductor
R_{cl}	Clamper’s resistive load
Rd	Windings resistance reflected to the primary
R_{dc}	Windings resistance value neglecting the skin and proximity effects
R_L	Variable resistive load
Rp	Core-loss equivalent resistance
T	Working Period
t_1	Zero voltage interval per half-cycle in a quasi-square wave
V_{dc}	Voltage inverter DC link
V_{ext}	External series capacitor voltage drop
V_{in}	Transformer primary voltage
V_{input}	Measured transformer primary voltage for the spectral analysis
V_o	Transformer secondary voltage at normal operation
V_{out}	Transformer secondary voltage at open load condition
V_p	Peak value of the primary voltage
V_{sq}	Inducted electromotive force
X_d	Leakage reactance
Z_c	Characteristic impedance of the simplified resonant circuit
Z_{in}	Transformer input impedance
ΔV	Admissible overvoltage at the transformer’s secondary with the HV Clamper
δ	Skin depth
μ_0	Vacuum permeability
ρ	Electrical resistivity
$\emptyset$	Instantaneous magnetic flux
$\emptyset_{max}$	Maximum allowed magnetic flux
ω_{input}	Primary waveforms angular frequency for the spectral analysis

SUMARY

1 INTRODUCTION

Transformer is an electrical device of great importance in Electrical Engineering and has its operation based on the Faraday's law of Electromagnetic Induction. There are several applications for these devices, like measurement instruments (potential and current transformers), electrical insulation (pulse transformers), and power transmission [1] [2].

There are many aspects that must be considered for the transformer's operation, like its thermal behavior, magnetic coupling, parasitic elements, insulation level between primary and secondary windings, etc. These characteristics depend on the application and power to be transferred. Thus, for their correct design, several models and simulations are adopted, depending on the application's particularity [2].

Transformers used in transmission lines have a low operating frequency (generally 50 or 60 Hz), with a high voltage ratio, being heavy and bulky, transferring high power levels.

If the frequency increases to the order of kHz or MHz, the transformer weight and volume reduces considerably, as can be seen in high frequency transformers used in switched-mode power supplies [3], although it leads to the necessity of a power electronics circuitry to produce high-frequency waveforms [4].

There are several challenges for the high frequency transformers design, especially when the application involves high voltage ratio. In this case, it's usual the strong manifestation of parasitic effects, which can lead to undesired operating conditions, such as overcurrent, overvoltage, waveform distortion, resonances and electromagnetic interference [5] [6] [7] [8] [9] [10] [11] [12] [13].

High frequency transformers can be classified in three categories, according to the operating frequency and transferred power [14]. Transformers commonly used in telecommunications and some computer systems are known as *Low Power Ultra High Frequency Transformers*, and typically operate below 1 kW and above 1 MHz. Devices used in avionics and vehicular systems, known as *High Power Mid Frequency Transformers*, operate below 100 kHz and transmit above 10 kW. The third category is the *Mid Power High Frequency Transformers,* which operating transmitting up to 10 kW and operating in the intermediate frequency between the two other categories.

Several authors had highlighted the importance of High Voltage Transformers operating in a high frequency range (HFHPT-*High Frequency High Power Transformers*), although a general modeling have not been achieved yet, due to the different effects caused by the parasitic elements manifestation and operating frequency noises, in each particular application [1] [15].

In [16] a HFHPT design was proposed for high power DC-DC converters, for medium (MVDC) and high voltage (HVDC) direct current applications. The proposed model is based on a bi-dimensional simulation with a regression algorithm, using the finite elements technique. The methodology also provides an analytical approach which enables the leakage inductance calculation, core dimensions and optimum operating frequency determination. The methodology was validated by a 1 MW prototype.

A methodology for High Voltage High Frequency Transformers (HVHFT) construction for switched-mode power supplies is developed in [3]. The construction procedures are based on a thermal modeling and graphical-algebraic tools. For the procedure's validation, two transformers for microwave heating sources were designed and tested. The values found in the prototypes' measurements agreed with those determined by calculation.

Other applications for the HFHPT are resonant converters [14] [17] [18] [19] [20] [21] [22], due to the possibility of magnetic devices parasitic elements exploration in the applications. In the LCC converter operation for example, the transformer parasitics are used as the converter resonant elements. Ferrite cores in E format were used for the transformer's design and the primary and secondary windings were built in a co-centric way, to reduce the leakage inductance value [22].

In [14] it was explored the use of litz wire to minimize the proximity and skin effect, caused by the windings' high frequency currents [23]. A leakage inductance calculation methodology was developed for transformers using this kind of conductor. Examples about the use of these elements can be found in the literature, like sources for pulsed laser [24], ozone generation [25] [26], ballast for discharge lamps [27] [28], RF amplifiers [29].

For the pulsed laser sources in [24], the converter always operates in a transient condition, obtaining a maximum voltage gain by operating at the resonance frequency, with high power factor and low commutation losses as additional benefits. For the ozone generation [25] [26], the ozonizer device behaves like a variable capacitance, the transferred power behaves like a resistance, for the transformer. Therefore, the power can be changed modulating the frequency, so controlling the ozone production.

There are some applications in which the load can vary from the short circuit to the open-load condition, unpredictably [30] [31] [32]. If the load variation is slow, control strategies can be implemented for compensating the perturbation. However, when the variation is too fast, protection against dangerous situations that can damage the system, like overcurrent and overvoltage, must be guaranteed by the converter itself.

A practical example for load with unpredictable variation is the device for plant electrocution, used for controlling weeds [33] [34]. The traditional implementation consists of a 60 Hz transformer whose low voltage side is fed by a generator. The device is driven by a tractor or truck, and the transformer's high voltage side is connected to the applicators and grounders electrodes.

As the tractor moves, the grounders electrodes are kept connected at the soil, and the applicators electrodes touch the aerial part of the plants. The electrical current circulates through the plant heating and killing it. As the plant is electrocuted its "resistance value" decreases, tending to short-circuit, and when the applicator electrodes change from a plant to another, they stay "in the air", causing an open circuit condition. Such changes aren't predictable and can be so fast that it's impossible to wait for the control loop reaction.

The proposed converter makes possible the adaption of these systems to high frequency technologies, turning the device more versatile and slighter, amplifying its possibilities and varieties of applications.

Considering the scenario and the challenges exposed above, the main focus of this work was the design and definition of criteria for the safety operation of a converter that feeds a High Voltage High Frequency Transformer connected to a resistive load with unpredictable variation, taking in account the HVHFT particularities. Taking this general objective, the following specific objectives are given:

- Study, modeling, design and application of a single-phase converter for variable load;
- Study and characterization of behavior particularities of high voltage transformers in a high frequency range;
- Simulate the converter, to get a better understanding and general characterization of the system;
- Protection and supervisory systems development to guarantee the converter's safety operation;
- Studies validation by experimental measurements in conceptual prototypes.

This dissertation is divided as follows: Chapter 1 gives a brief introduction, contextualize the problem, gives the practical motivation and the objectives to be achieved in the work; Chapter 2 focus on the high voltage transformer with high frequency operation, its modeling, the parasitics, the definition of its technical specifications and characterize its behavior; Chapter 3 presents the converter topology, characterize its dynamics and defines criteria for its safety operation through simulations and analytical calculations; Chapter 4 validate the studies developed in Chapter 3 by experimental measurements in prototypes of 1 and 3 kW, and Chapter 5 presents the achieved conclusions and propositions of this work's continuity from the achieved points.

This work generated the publication of the paper "*Overvoltage protection procedures for high voltage high frequency transformers*" in the 14th Brazilian Power Electronics Conference (COBEP), at Juiz de Fora, MG, Brazil, in 2017.

2 HIGH VOLTAGE HIGH FREQUENCY TRANSFORMER

Various high frequency transformer models can be used depending on the analysis to be performed. When the interest is the transient behavior and the propagation time is relevant, distributed parameters models can be used [10] [11]. If the frequency is not too much high (below 1 MHz) and the propagation delay can be neglected, lumped models can be used [7] [8] [9].

This dissertation uses a lumped model, as in Figure 2.1. The transformer parameters, reflected to the primary (low voltage) side, are listed below. The winding capacitance represents the total effect of the intrinsic adjacent winding turns and is mainly due to the secondary winding capacitance reflected to the primary side *Cp*. Other lumped models can use additional capacitances and inductances [7] [8] [9] [35].

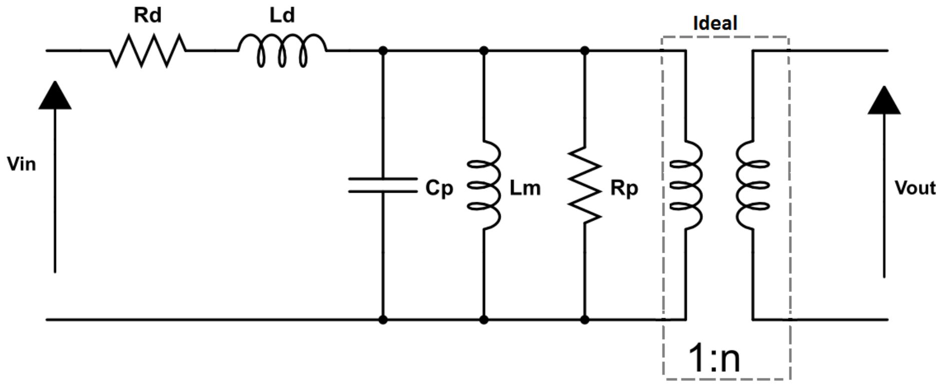

Figure 2.1- High Voltage Lumped Model Transformer.

- ***Rd*** = Total Windings Resistance;
- ***Ld*** = Leakage Inductance;
- ***Cp*** = Winding Capacitance;
- ***Lm*** = Magnetizing Inductance;
- ***Rp*** = Core Loss Resistance
- ***n*** = turns ratio.

2.1 PARASITIC ELEMENTS

2.1.1 Leakage Inductance

Figure 2.2 shows a magnetic core with the primary (N1) and secondary (N2) windings. When one of the windings is excited, a magnetic flux is generated and "flows" through the core, achieving the other winding. If the two windings have a perfect magnetic coupling, all the flux generated by one will link the other. The magnetic flux linked by the two windings is called mutual flux (ϕ_m) and is essentially confined in the magnetic core.

The perfect magnetic coupling is never possible, and part of the flux generated by a winding does not link the other. This flux is generally lost in the air and is called leakage flux [36]. Figure 2.2 shows the leakage flux for primary and secondary windings as being ϕ_1 and ϕ_2 respectively. An inductance is used for modeling this behavior in simulations and design procedures [37] [38] [39]. The leakage inductance appears connected in series with the primary side, as showed in Figure 2.1.

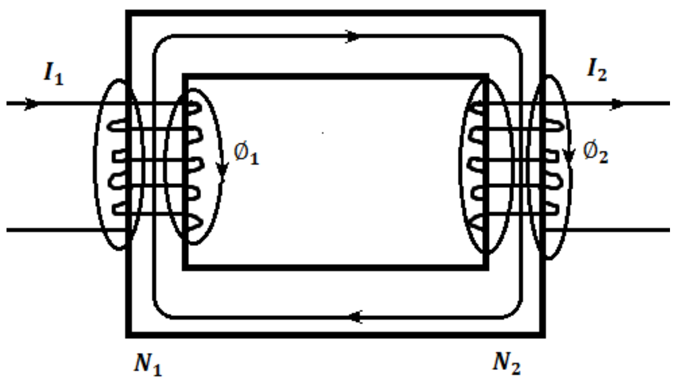

Figure 2.2 -Two windings magnetic circuit with imperfect magnetic coupling.

The primary and secondary disposition [40] has stray influence on the leakage inductance value. If a high insulation level is needed between the two windings, they must be allocated in separated branches, like in Figure 2.2, what increases the leakage flux and, consequently, the leakage inductance.

The primary and secondary windings can be allocated in a convenient way to improve the magnetic coupling between them, like in Figure 2.3. The windings disposition is normally made in U or E core format. The dashed lines show the core branch in which the windings are allocated. All these winding dispositions have lower leakage inductance compared to Figure 2.2, for the same number of turns. Although, they have more thermal and isolation issues.

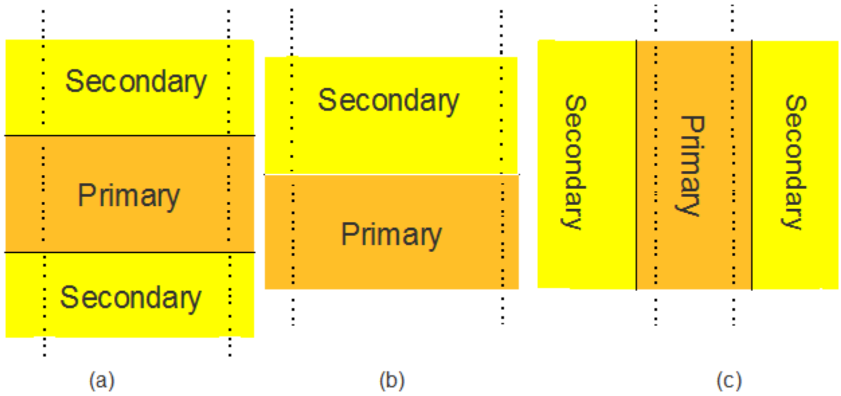

Figure 2.3-Cross-section representation of primary and secondary windings disposition with lower leakage inductance: (a) primary between a secondary divided in two layers; (b) primary and secondary in the same branch; (c) primary winding surrounded by the secondary.

To illustrate the winding disposition influence on the leakage inductance, its value was measured (by the procedure described in Section 2.2) for a 1 kVA @311 V @ 20 kHz ferrite core transformer with the winding disposition of section a of Figure 2.3 and compared with a similar transformer with the winding disposition of Figure 2.2, the total number of turns for the primary and secondary windings were the same in both transformers. The leakage inductance measured in the first case was 63.5 μH and in the second one was 656 μH. The great discrepancy between both values reflects how the first windings disposition is better magnetically coupled compared to the second. Figure 2.4 shows the two transformers.

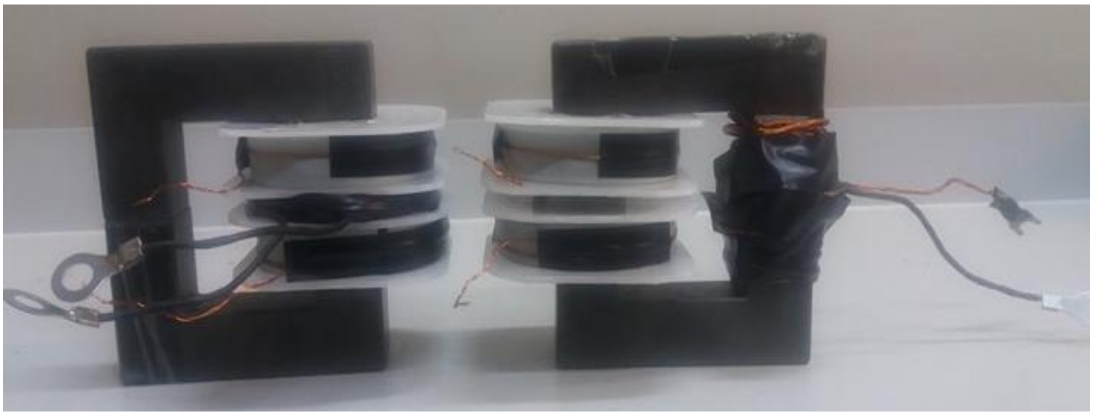

Figure 2.4 - 1 kVA @311 V @ 20 kHz ferrite core transformers with different windings disposition: Primary between secondary layers at the same core branch (left), and primary and secondary in different core branches (right).

2.1.2 Windings Capacitance

Wherever there are two electrical conductors separated by a dielectric, there is the manifestation of a capacitive effect. High Voltage Transformers secondary windings are generally built in several layers, separated by an insulation material from each other, so they can support the high voltage. Figure 2.5 shows an example of the cross-section of a secondary construction when it's the high voltage side.

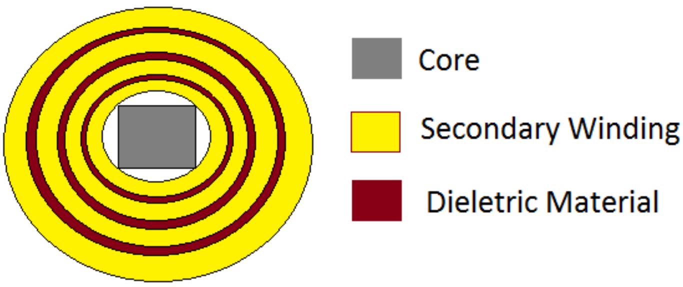

Figure 2.5-Cross-section of a High Voltage Transformer Secondary construction.

There are several stray capacitances in the non-ideal transformer's operation, but the most considered for its modeling are the capacitance between the two windings and the determined by each winding [6] [7]. The capacitance calculated by (5), (6), (11) and (12) takes all the transformer capacitive effects in consideration, and is due mainly to the secondary winding capacitance, because of its high number of turns.

The capacitances seen from the primary side are responsible for the resonance frequencies, and the parasitic capacitances between the windings may mainly contribute to electromagnetic interference [2] [41].

Table 1 shows different values of winding capacitances measured for three ferrite cores transformers. The 20 kHz transformers have the winding disposition of Figure 2.3, section a, and the 15 kHz transformer of section c of Figure 2.3. The winding capacitance increases when the secondary voltage is higher, because in this situation, a higher number of turns is necessary, what increases the capacitive effects.

Table 1- Winding Capacitance measurement for different types of High Frequency High Voltage Transformers.

Nominal Power (kVA)	**Frequency (kHz)**	**Primary Nominal Voltage (V)**	**Turns Ratio**	**Capacitance Reflected to the Primary (nF)**
1	20	311	12.19	2.36
3	20	311	20.14	6.26
10	15	600	18.48	31

2.2 PARAMETERS ESTIMATION PROCEDURES

The winding resistance *Rd* has, in general, a relatively small value and can be determined by direct measurement, with a DC source (Ohmmeter). Nevertheless, in high frequency range, the skin and the proximity effects must be taken in consideration for the effective determination of the resistance [42] [43]. Both effects vary with the frequency, making difficult to include the correct value in the circuit model.

The skin depth can be determined for any conductor by (1), where ρ is the conductor electrical resistivity and f is the operating frequency. The AC resistance factor can be calculated by (2), for a solid conductor with circular cross-section area of radio *r* [44] [45].

$$\delta = \sqrt{\frac{\rho}{\pi \mu_0 f}} \tag{1}$$

$$\frac{R_{ac}}{R_{dc}} = \frac{r}{2\delta} \tag{2}$$

All transformers used in this work have their primary windings made of litz wire to minimize these effects. In [23] is presented a simplified approach to determine the number and diameter of strands in a litz wire based on the skin depth, the frequency of operation, the number of turns, the breadth of the core window and a constant. The approach was applied here in a reverse way to determine the effective winding resistance at the nominal operating frequency.

The AC resistance factor for a litz wire can be calculated by (3), where d is the strand diameter, N the number of turns, n_i the number of strands and b is the breadth of the core window. The AC resistance can be estimated at any frequency, once the transformer parameters are known and the DC winding resistance is measured.

$$\frac{R_{ac}}{R_{dc}} = 1 + \frac{(\pi n_i N)^2 d^6}{192\delta^4 b^2} \tag{3}$$

Figure 2.6 shows the AC resistance factor variation with frequency for a common solid conductor and a litz wire with the same cross-section area. The ac resistance increases faster in the case of the solid conductor. Considering the operating frequency of 20 kHz, the AC resistance would be almost 64% more than the DC value for the solid conductor, while it would only 19.1% with the use of litz wire, about 3 times less. The graphs of Figure 2.6 show the effectiveness of litz wire to minimize the skin effect.

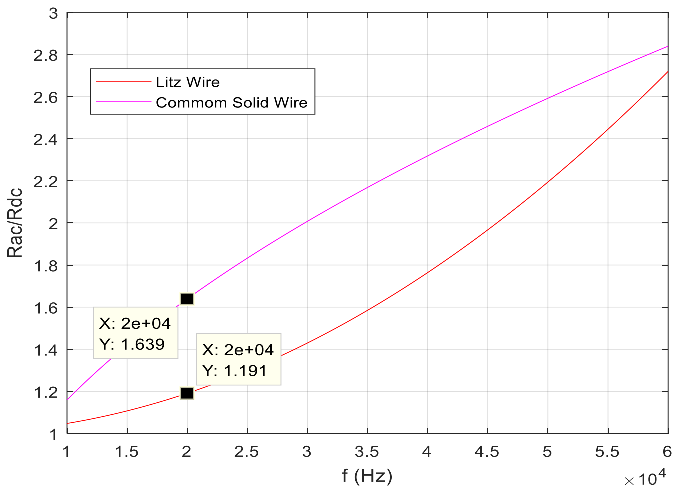

Figure 2.6-AC resistance factor variation with frequency for a common and litz wire.

The core loss resistance *Rp* can be determined by using an adaptation of the Steinmetz's equation [46] and, in general, has a high value. The data from the core manufacturer allows the losses estimation and so, the shunt equivalent resistance.

Since the magnetic design guarantees the core will not saturate, the parameters of the transformer's model can be estimated through a spectral analysis, by applying a sinusoidal signal at the primary winding, with the secondary in open load condition. For example, at low frequency, the measurement of the applied voltage, current and frequency, allows to determinate the input inductance by (4).

$$L_{in} = \frac{V_{input}}{I_{input}} \frac{1}{\omega_{input}} \tag{4}$$

In the low frequency range, the winding capacitance effect can be neglected, because of its high reactance value, so the resulting input impedance is the sum of the magnetizing and leakage reactances. Since the magnetizing inductance is much higher than the leakage's, the *Lm* approximated value can be determined.

Using the same approach, but in the high frequency range, the capacitive reactance is too small, canceling the effect of the magnetizing reactance (once they are both in parallel), so the equivalent input impedance is only due to the leakage reactance and the *Ld* value can be determined. After this calculation, the magnetizing inductance value can be determined more precisely, correcting the value calculated in the low frequency analysis.

The low frequency resonance *fp* (parallel resonance) occurs between *Lm* and *Cp*. At this point the input impedance achieves its maximum value, which regards *Rp*. Nevertheless, like this essay uses a low voltage source, it's difficult to get the correct value of *Rp*.

Above this frequency, the input impedance presents a capacitive behavior, so the primary current leads the voltage. The high frequency resonance, at *fs* (series resonance), occurs between *Ld* and *Cp* and gives the minimum input impedance. This minimum value represents the resistance at this frequency. However this value, due to the skin effect, doesn't represent the resistance at lower frequencies. The *Cp* value can be calculated using both parallel and series resonances by (5) and (6) respectively, and the resulting values must be close, if the model correctly represents the device.

$$C_p = \frac{1}{(2\pi f_p)^2 L_m} \tag{5}$$

$$C_p = \frac{1}{(2\pi f_s)^2 L_d} \tag{6}$$

The input impedance of the transformer showed in Figure 2.1 is given by (7) and the voltage gain can be determined at any operating point by (8).

$$Z_{in} = \frac{s^3 L_m L_d C_p + s^2 L_m \left(\frac{L_d}{R_p} + C_p R_d\right) + s\left[L_m\left(1 + \frac{R_d}{R_p}\right) + L_d\right] + R_d}{s^2 L_m C_p + s\frac{L_m}{R_p} + 1} \tag{7}$$

$$\frac{V_{out}}{V_{in}} = \frac{snL_m R_p}{s^3 L_m L_d C_p R_p + s^2 L_m\left(L_d + R_d R_p C_p\right) + s[R_d L_m + R_p(L_d + L_m)] + R_p R_d} \tag{8}$$

The transformer open circuit analysis, as described before, doesn't take in consideration the secondary leakage inductance. A lumped model with this inductance and without the respective resistive losses is presented in [35]. To measure the secondary leakage inductance, the transformer's input impedance is measured in the high frequency range, with the secondary in a short-circuit condition. As the magnetizing reactance is too high, and the capacitive reactance was "removed" by the short-circuit, the total leakage reactance is determined. As the primary leakage inductance can be determined by the open-circuit analysis, the secondary leakage inductance can be determined by this approach. By adding the resistive losses to the model presented in [35], the lumped model shown in Figure 2.7 is derived. The input impedance and voltage gain for this model are given by (9) and (10) respectively, and the windings capacitance can be calculated by (11) and (12) using the parallel and series resonance frequencies respectively. Which model is more adequate will be discussed later.

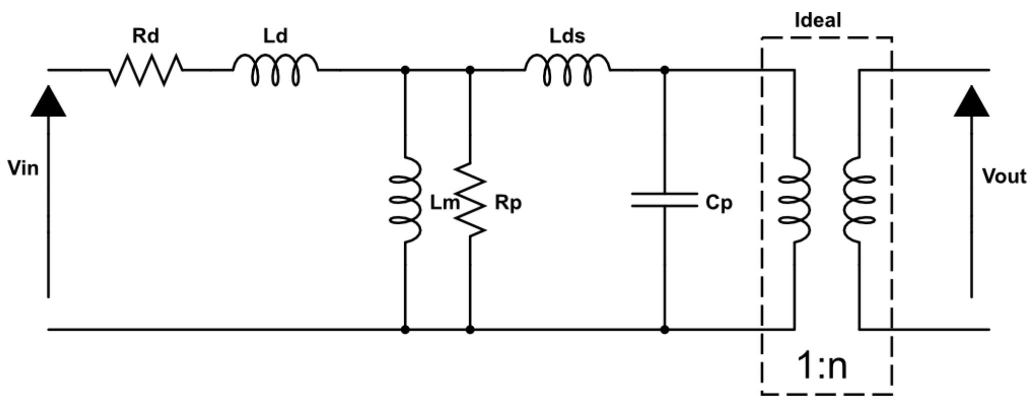

Figure 2.7-High-Voltage Transformer lumped model considering the secondary leakage inductance and resistive losses.

$$Z_{in} = \frac{\begin{array}{c} s^4 L_m L_d L_{ds} C_p + s^3\left[R_p L_{ds} C_p (L_m + L_d) + L_m C_p\left(R_d L_{ds} + R_p L_d\right)\right] + \\ s^2\left[R_d R_p C_p (L_{ds} + L_m) + L_m L_d\right] + s\left[L_m\left(R_p + R_d\right) + L_d R_p\right] + R_d R_p \end{array}}{s^3 L_m L_d C_p + s^2 R_p C_p (L_{ds} + L_m) + sL_m + R_p} \tag{9}$$

$$\frac{V_{out}}{V_{in}} = \frac{snL_mR_p}{s^4L_mL_dL_{ds}C_p + s^3\left[R_pL_{ds}C_p(L_m + L_d) + L_mC_p\left(R_dL_{ds} + R_pL_d\right)\right] + s^2[R_dR_pC_p(L_{ds} + L_m) + L_mL_d] + s\left[L_m\left(R_p + R_d\right) + L_dR_p\right] + R_dR_p} \tag{10}$$

$$C_p = \frac{1}{(2\pi f_p)^2(L_{ds} + L_m)} \tag{11}$$

$$C_p = \frac{L_d + L_m}{(2\pi f_s)^2[L_mL_{ds} + L_d(L_{ds} + L_m)]} \tag{12}$$

2.3 DETERMINATION OF THE TRANSFORMER' SPECIFICATIONS

The transformer's adequate design must take in consideration the several features demanded by the application. First, the device must not saturate at normal operating conditions, what is fundamentally determined by the number of turns of the primary winding. Figure 2.8 shows the magnetic flux waveform, considering a N_p turns winding fed by a T period square wave voltage.

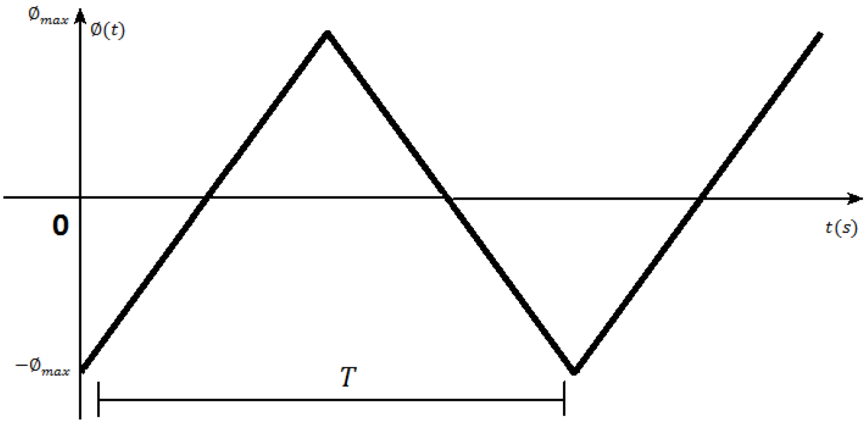

Figure 2.8- Magnetic Flux waveform considering a square wave voltage.

Considering the linear behavior, the magnetic flux may be represented by a simple row equation, as showed in (13):

$$\emptyset(t) = -\emptyset_{max}\left(\frac{4t}{T} - 1\right) \tag{13}$$

The Faraday's Law of Electromagnetic Induction is given by (14), where V_{sq} is the inducted electromotive force:

$$V_{sq} = N_p \frac{d\emptyset(t)}{dt} \tag{14}$$

The magnetic flux is given by (15), where A_c is the core cross section area and B_{max} is the maximum allowed magnetic flux density, whose value is given by the core manufacturer.

$$\emptyset_{max} = B_{max} A_c \tag{15}$$

Combining the expressions (13) and (15) with the Faraday's Law in (14), the minimum number of turns is given by (16).

$$N_p = \frac{V_{sq}\left({T}/{4}\right)}{B_{max} A_c} \tag{16}$$

If the primary number of turns is below the value determined by (16), the magnetic flux density has a value higher than B_{max} and will not be possible operate at the specified voltage and frequency $\left({1}/{T}\right)$. Once the primary number of turns is determined, the secondary can be calculated by using the turns-ratio. Another important feature is the expected power to be transferred, because the windings' conductors must have the correct cross-section, to support the necessary current without overheating.

2.4 SPECTRAL ANALYSIS OF THE HIGH VOLTAGE HIGH FREQUENCY TRANSFORMER

A sinusoidal voltage with low amplitude was applied on the primary side of a 1 kVA @311 V @ 20 kHz ferrite core transformer, with the secondary opened. The expected turns-ratio is 12. The current was measured by a probe with enough frequency band.

Figure 2.9 shows the primary and secondary voltage for the sinusoidal excitation. The measured voltage ratio is 12.19. Figure 2.9 also shows primary voltage and current at 1 kHz.

Neglecting the resistances, the sum of the magnetizing and leakage inductances is given by (4), using the values of Figure 2.9:

$$L_m + L_d = 5.71\ mH$$

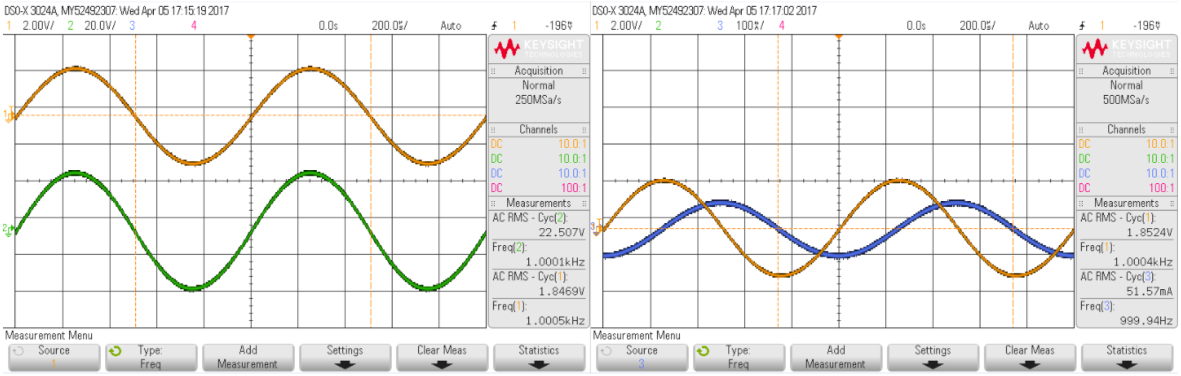

(a) (b)

Figure 2.9 – Primary (yellow) and secondary (green) voltages (a) and primary voltage (yellow) and current (blue) (b) for the transformer excited by a low amplitude sinusoidal signal at 1 kHz.

Figure 2.10 shows the waveforms at 50 kHz at the first resonance (parallel resonance). The primary current achieves its minimum value, since the transformer's input impedance has its maximum value. As the current probe resolution is not high enough, the calculated *Rp* has not a precise value. After the parallel resonance, the input impedance presents a capacitive behavior. At 411 kHz, occurs the series resonance, as can be seen in part (b) of Figure 2.10.

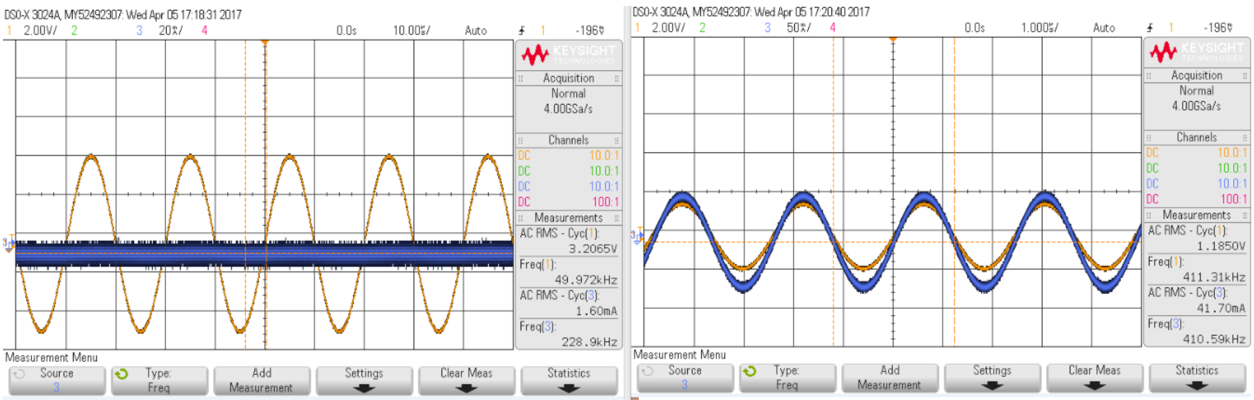

(a) (b)

Figure 2.10 - Primary voltage (yellow) and current (blue) at the parallel (a) and series (b) resonances.

After the series resonance, the input impedance again presents an inductive behavior, as showed in Figure 2.11. For a higher frequency, the estimated leakage inductance can be calculated by adapting (4) for the values of Figure 2.11 and the found value is:

$$L_d = 63.5\ \mu H$$

So, a more precise value for the magnetizing inductance is:

$$L_m = 5.71\ mH - 63.5\mu H = 5.64 mH$$

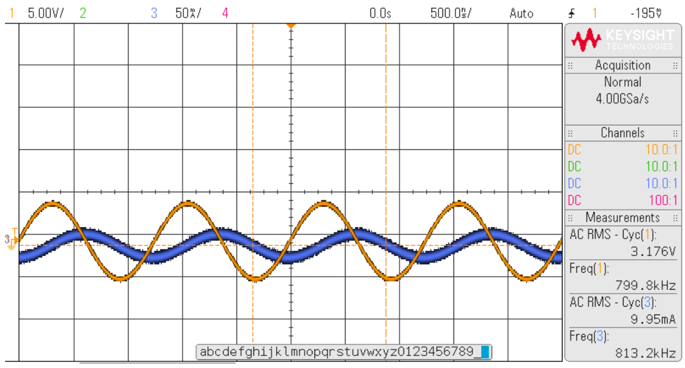

Figure 2.11- Primary voltage (yellow) and current (blue) to estimate the leakage inductance.

Figure 2.12 shows the primary voltage and current in a high frequency value, with the secondary at short-circuit. The "total" leakage inductance is:

$$L_d + L_{ds} = 77.4\ \mu H$$

So, the secondary leakage inductance, reflected to the primary side, can be estimated as:

$$L_{ds} = 77.4\ uH - 63.5uH = 13.9\ \mu H$$

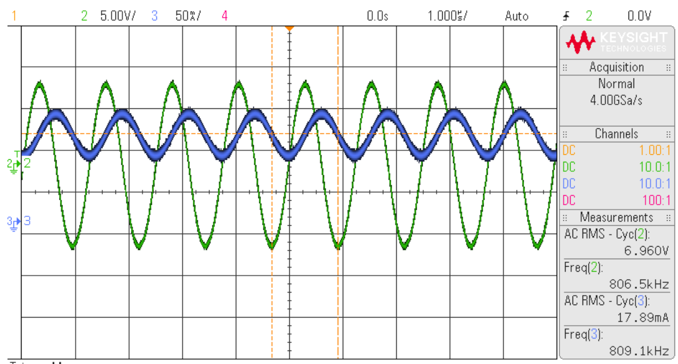

Figure 2.12- Primary voltage (green) and current (blue) to estimate the secondary leakage inductance.

Besides its low value seen from the primary side, the secondary leakage inductance has a value of almost 2.1 mH, when reflected to the secondary.

The windings capacitance value determined by (5) is 1.8 nF, and the value determined by (6) is 2.3 nF. The discrepancy presented in the values (21.7%) is due to the secondary leakage inductance neglecting in this model. The capacitance values determined by (11) and (12) are 1.79 nF and 1.96 nF, respectively, showing that the addition of the secondary leakage inductance increases the precision in the winding capacitance estimation procedure. In both cases, the considered values were the determined by the series resonance, once its excitation produces secondary overvoltage and primary overcurrent. The shunt-loss resistance estimated for the transformer is approximately 880 **Ω** and the winding resistance at 20 kHz is 0.329 **Ω**.

The resonances are not observed in the spectral analysis when it is performed with the secondary short-circuited. As the winding capacitance and the "primary equivalent parallel circuit" are cancelled, the remaining circuit only has the windings resistance and the leakage inductance, which always shows an inductive behavior.

The input impedance is shown in Figure 2.13 and the voltage gain in Figure 2.14 for the transformer model of Figure 2.1 for two situations, the open and nominal load. The voltage gain is amplified in the region next the series resonance, because of the low input impedance value, what can lead to overvoltage problems if this resonance is excited. The load has an important role for minimizing such behavior. As it appears in parallel with the magnetizing branch, it damps the resonance. However, if the transformer operates without load, as the resonance increases the voltage peak, the isolation capability may be compromised if an overvoltage protection procedure is not adopted.

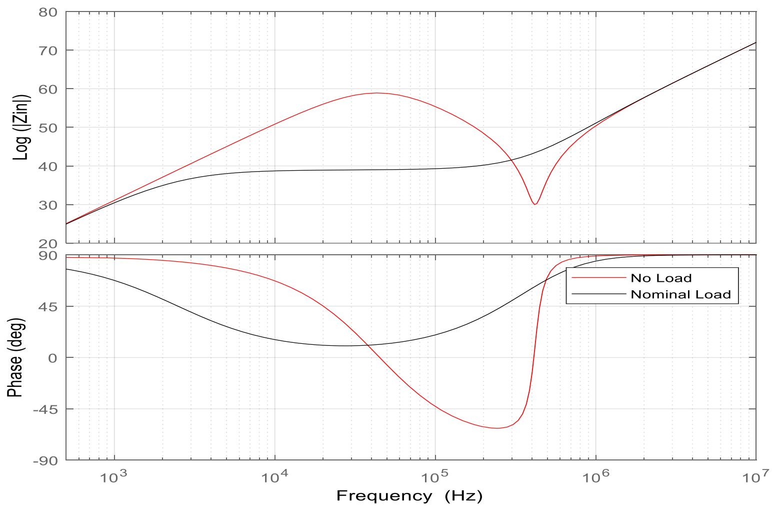

Figure 2.13-Input impedance of the transformer model of Figure 2.1 at nominal (black) and open-load (red) conditions.

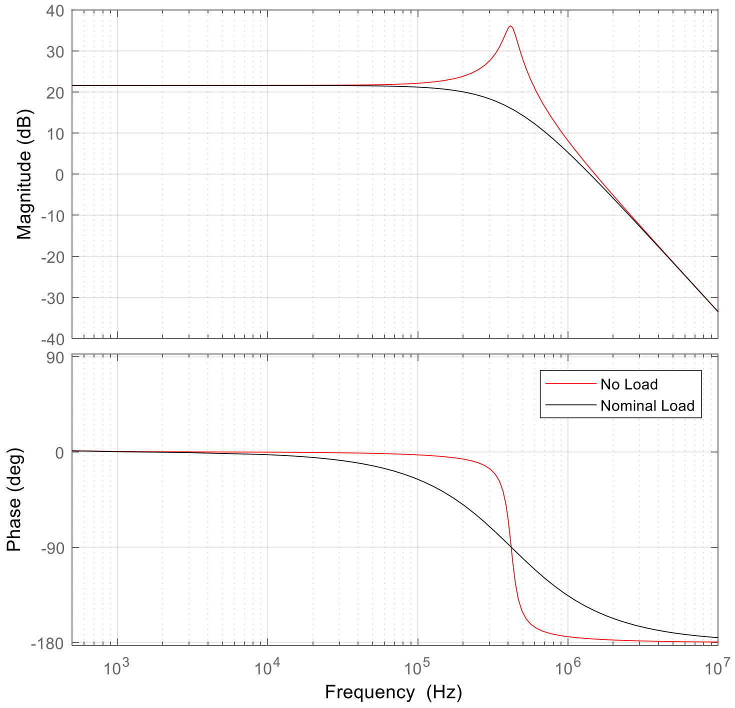

Figure 2.14 - Voltage gain for the transformer model of Figure 2.1 at nominal (black) and open-load (red) condition.

Figure 2.15 shows the open circuit input impedance for the third and fourth order transformer models of Figure 2.1 and Figure 2.7 respectively. The curves format is almost the same, but the parallel resonance frequency is not correctly identified, due to the little discrepancy between the capacitances calculated by (5) and (6). The series resonance was correctly identified in both cases.

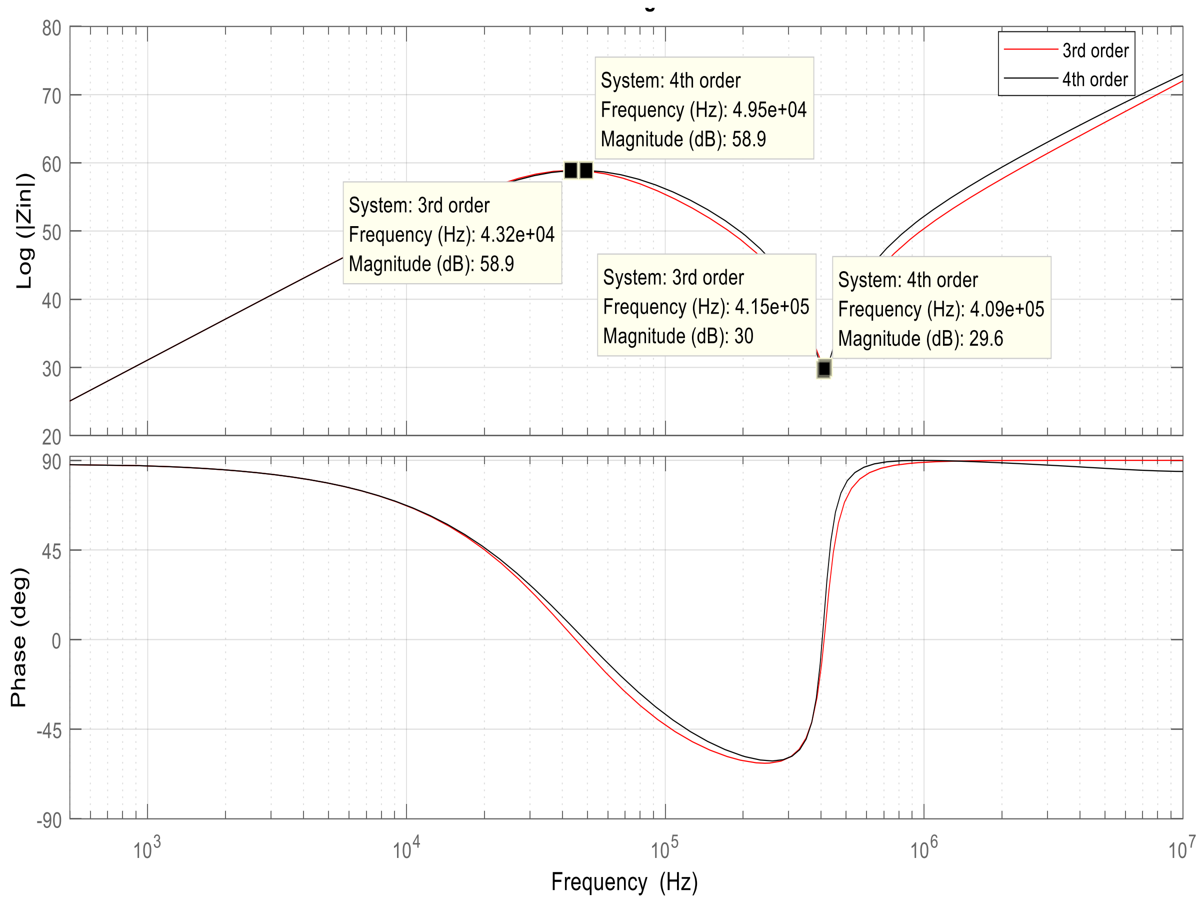

Figure 2.15-Open circuit input impedance for the third and fourth order transformer models.

The voltage gain for both models is showed in Figure 2.16, where it can be seen that the behavior is almost the same in both open and nominal conditions. As the series resonance is correctly identified in both models and the secondary leakage is small in comparison to the other parameters, the third order transformer lumped model is good enough for the system representation.

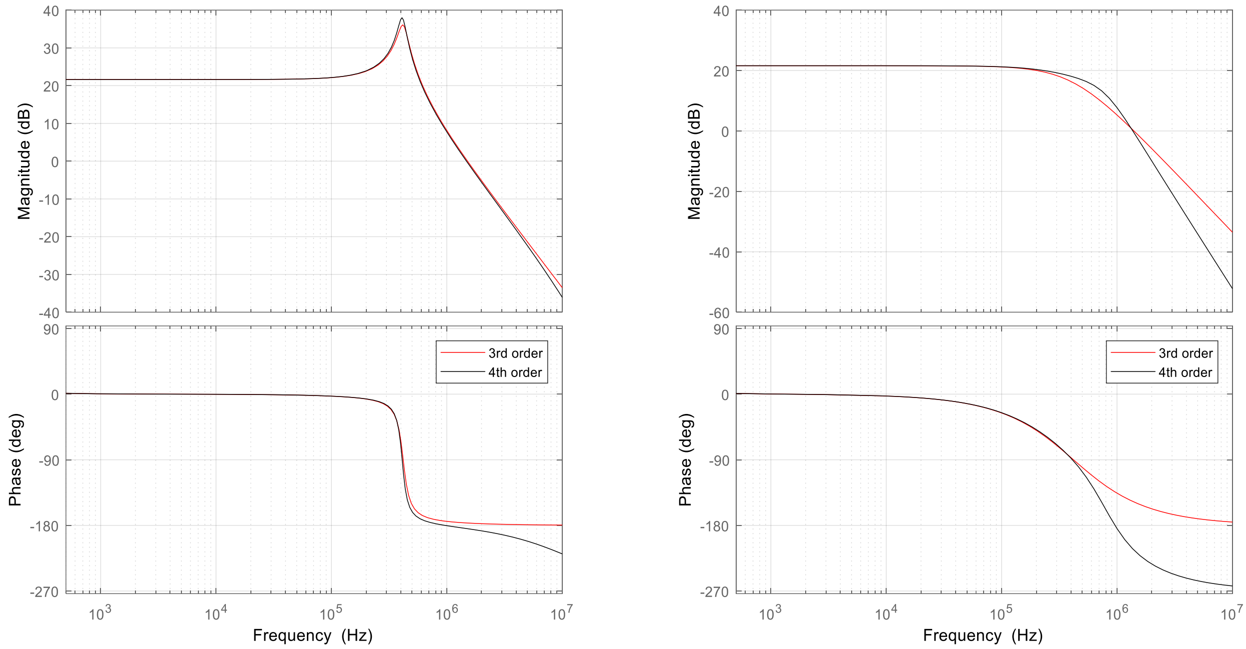

Figure 2.16-Voltage gain at open (left) and nominal (right) conditions, for third and fourth order transformer models.

The ferrite core of this transformer has a cross-section of 6.4 cm^2 and the adopted maximum flux density is 0.15 T, so the minimum number of turns determined by (16) is 41 turns. The number informed by the manufacturer was 42, because one of the transformer requirements was the minimum volume and parasitic effects manifestation.

The Faraday's Law equation can be rearranged to show that the magnetic flux is directly proportional to the voltage peak value, and inversely proportional to the operating frequency, as shown in (17), a modified form of (16).

$$\emptyset_{max} = \frac{V_{sq}}{4fN_p} \tag{17}$$

The flux can be kept constant if the voltage and frequency have the same variation rate. That's the main idea behind the approach used here to verify if the transformer will or not saturate at nominal operating conditions.

If the transformer is supposed to work with an input voltage of 311 V at 20 kHz without core saturation, the same would occurs with 31.1 V at 2 kHz. This situation is shown in Figure 2.17, where it can be seen by the primary current waveform that the saturation is about to begin, confirming the transformer can operate at nominal conditions without saturation.

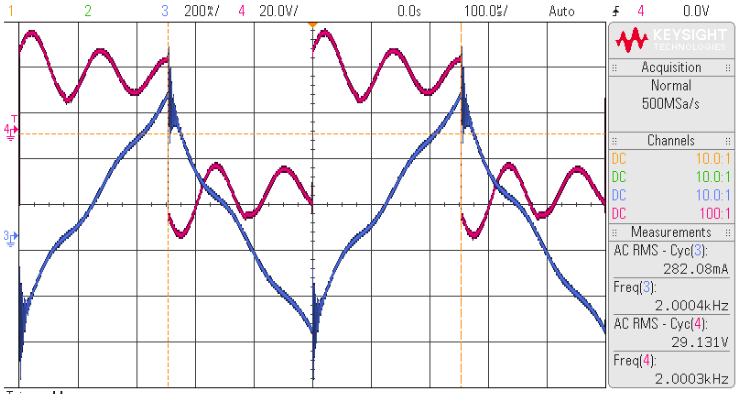

Figure 2.17 - Primary voltage (purple) and current (blue) at 10% of the nominal voltage and frequency.

Figure 2.18 shows the same condition of Figure 2.17 for less than 10% of the operating frequency, showing the saturation's beginning. The voltage distortion presented in the primary voltage is due to the voltage drop on the source internal resistance.

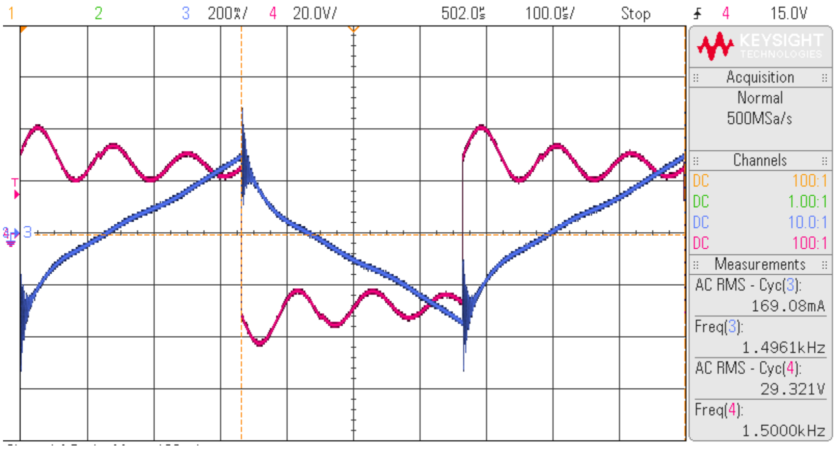

Figure 2.18 - Primary waveforms for 10% of the nominal voltage and less than 10% of the operating frequency, showing the beginning of the saturation.

Figure 2.19 shows the transformer waveforms for the open load operation. Due to the series resonance excitation, the voltage gain increases for the frequencies next to it, achieving more than two times the expected value, what can damage the secondary isolation. The magnetizing current is also affected by the resonance manifestation, causing the current stress shown in Figure 2.19.

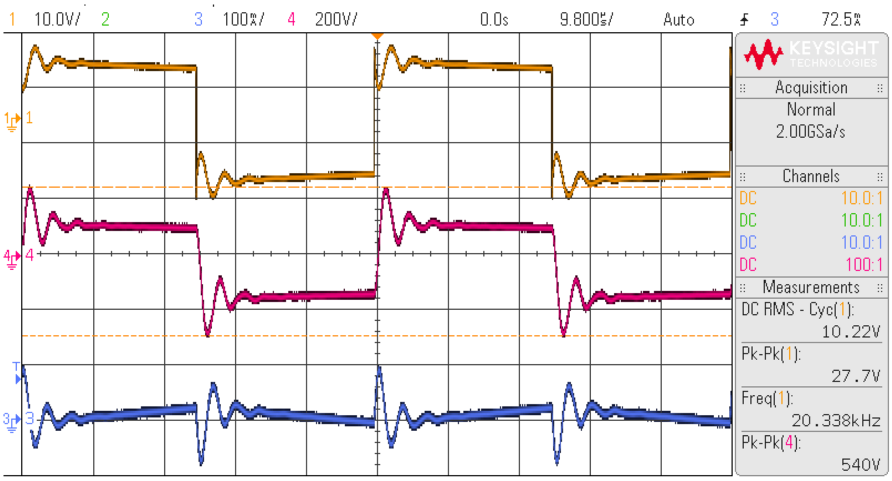

Figure 2.19 - From top to bottom: Primary Voltage, Secondary Voltage and Primary current, for an open load situation.

The oscilloscope “High Voltage Probe” at the secondary side has a capacitance of 15 pF, which represents an effective value of 2.23 nF, reflected to the primary side. This capacitance value cannot be neglected in comparison to the winding capacitance and affects the series resonance in the open load condition.

Figure 2.20 shows a zoom of the waveforms in Figure 2.19. The period of the oscillation showed in the primary current is next to 1+4/5 divisions, given a resonance frequency near 290 kHz. Figure 2.21 shows the same situation, without the high voltage probe. The period this time is next to 1+2/5 divisions, what leads to a resonance frequency of 372 kHz, that’s a value closer to the obtained in the spectral analysis.

The voltage probe changes the resonance frequency to nearly 300 kHz and the value measured by the spectral analysis is 411 kHz. The differences between these values and the measured in Figure 2.20 and Figure 2.21 are probably due to the damping factor, introduced by the transformer resistive losses.

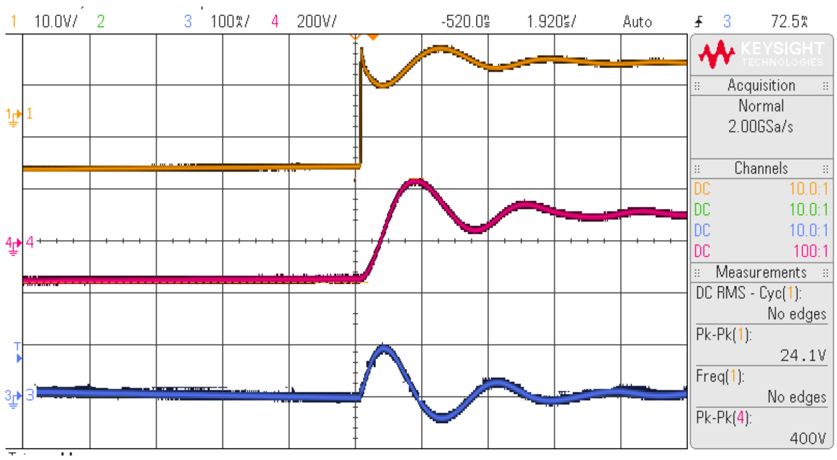

Figure 2.20-Zoom of Figure 2.19.

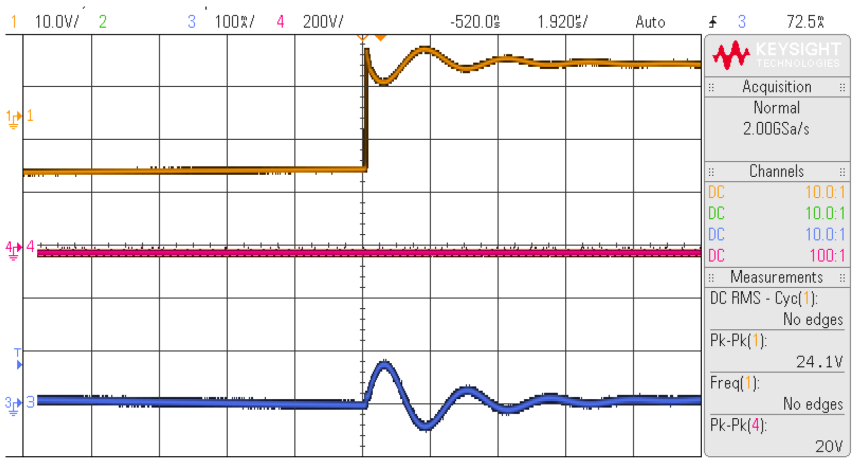

Figure 2.21 - Detail of Figure 2.19 without the voltage probe at the secondary winding.

Although the analysis made here has been performed for a specific transformer, the behavior is the same for any HFHVT. The parameters for all transformers used in this work were determined by the procedure.

3 THE CONVERTER

3.1 PRELIMINARY ANALYSIS OF THE CONVERTER'S POWER

A simplified approach can be adopted to determine the maximum power the converter can transfer, taking in account only the fundamental frequency of the input voltage and the respective reactance values.

If the transformer circuit in Figure 2.1 has a resistive load at the secondary side, it can be reflected to the primary. The magnetizing branch reactance is too high at the working frequency and can be neglected. So, ignoring the transformer losses, the equivalent circuit can be regarded as a simple RL circuit, as Figure 3.1[1] shows.

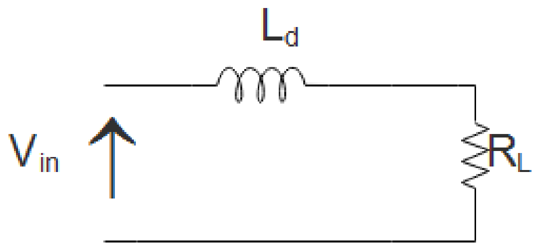

Figure 3.1 - Simplified RL circuit to determine the maximum power that can be transferred by the transformer.

The input current of the circuit shown in Figure 3.1 can be calculated by (18) and the power transferred to R_L, by (19). Differentiating the power equation in (19) and making it equal zero, the maximum power occurs when the resistive load is equal the leakage reactance, and its value can be calculated by (20). The voltage used in the calculation is given by (21), that determines the rms value of the fundamental harmonic component of a square wave.

$$I_{in} = \frac{V_{in}}{\sqrt{(R_L)^2 + (X_d)^2}} \tag{18}$$

$$P = \frac{(V_{in})^2 R_L}{(R_L)^2 + (X_d)^2} \tag{19}$$

---

[1] Ferrite core @ 1 kVA @ 20 kHz @ 311V transformer's reactances:
$X_{L_d} = 8\ \Omega$
$X_{L_m} = 708\ \Omega$
$X_{C_p} = 3.4\ k\Omega$

$$P_{max} = \frac{(V_{in})^2}{2X_d} \tag{20}$$

$$V_{in} = \frac{4V_p}{\pi\sqrt{2}} \tag{21}$$

The voltage value determined by (21) for the transformer characterized in section 2.4 is 280 V and its leakage reactance at 20 kHz is 7.98 Ω, reflected to the primary side. The maximum power that can be transferred to the load is 4.9 kW. Figure 3.2 shows the power transferred for several resistive load values, where it can be confirmed the maximum value calculated. It's important to note that the power values in Figure 3.2 can only be transferred by the system if the physical elements, like transformer, power switches, etc., can support. The Figure 3.2 also shows the power expected to be transferred to a resistive load of 12.5 kΩ connected at the transformer's secondary side, that corresponds to 84.12 Ω reflected to the primary.

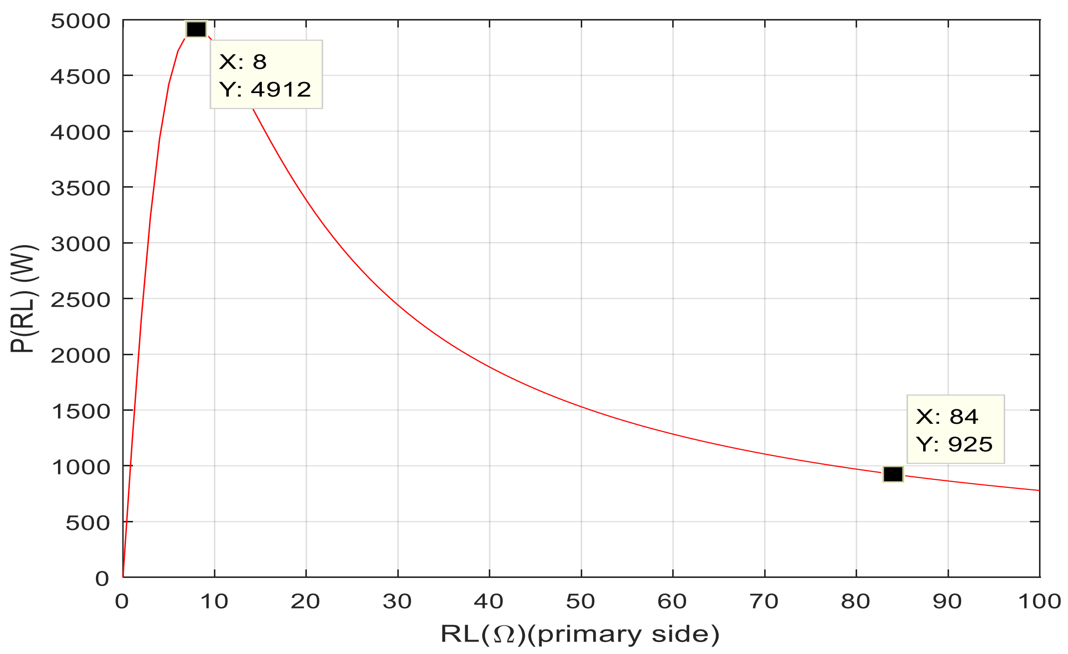

Figure 3.2 - Power Transfer Curve for the 1 kVA @ 20 kHz Transformer.

Figure 3.3 shows the power factor variation for the 1 kVA transformer, depending on the resistive load. For the maximum power transfer, the power factor is only 0.7, so high primary currents are necessary at this point. The power factor tends to the unity, at resistive loads next to the transformer nominal value.

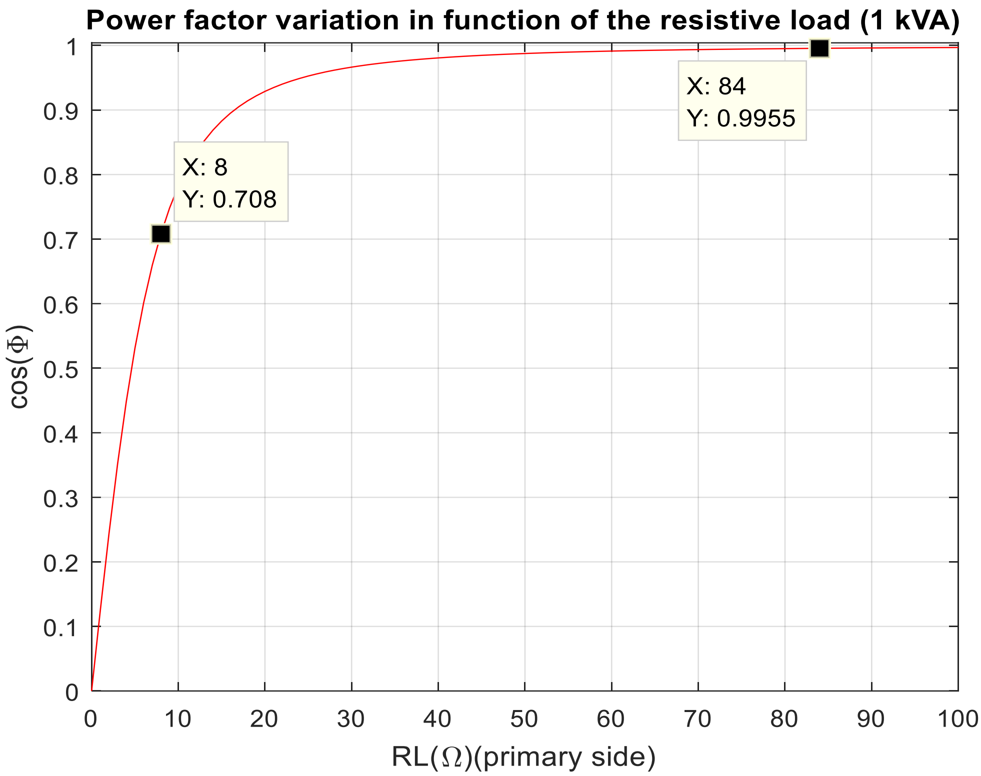

Figure 3.3 - Power factor variation for the curve of Figure 3.2.

The Power Transfer and power factor curve for the 3 kVA transformer are shown in Figures 3.4 and 3.5 respectively, where it can be seen the maximum possible power achievable, respecting the same circuit conditions. Figure 3.4 also shows the expected power to be transferred for a resistive load of 25 and 12.5 kΩ, that reflects 61.6 and 30.8 Ω to the primary side respectively. Figure 3.6 shows the expected power to be transferred to these same loads, but also shows the expected power for a 10 kΩ load (30.1 Ω reflected to the primary), considering the 10 kVA transformer. Figure 3.7 shows the corresponding power factor curve.

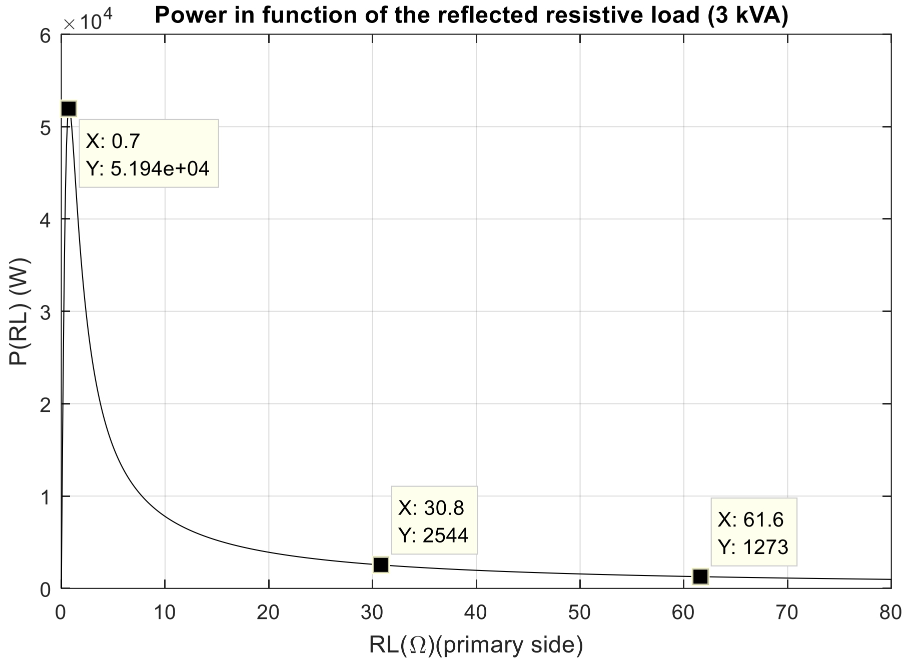

Figure 3.4 - Power Transfer Curve for the 3 kVA @ 20 kHz Transformer.

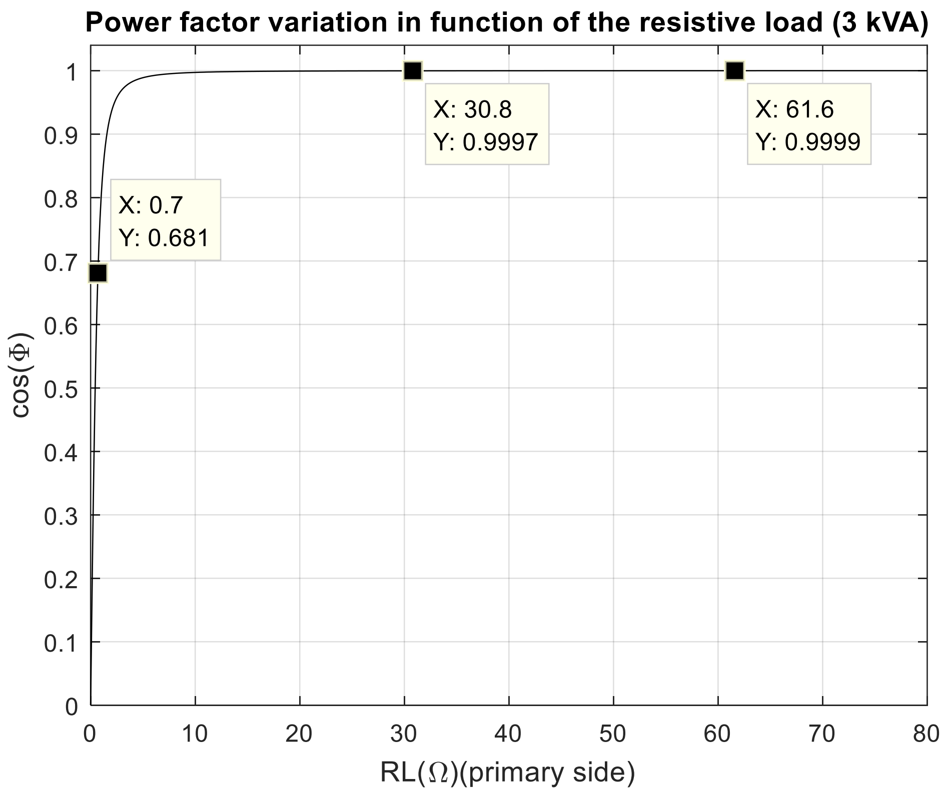

Figure 3.5 - Power factor variation for the curve of Figure 3.4.

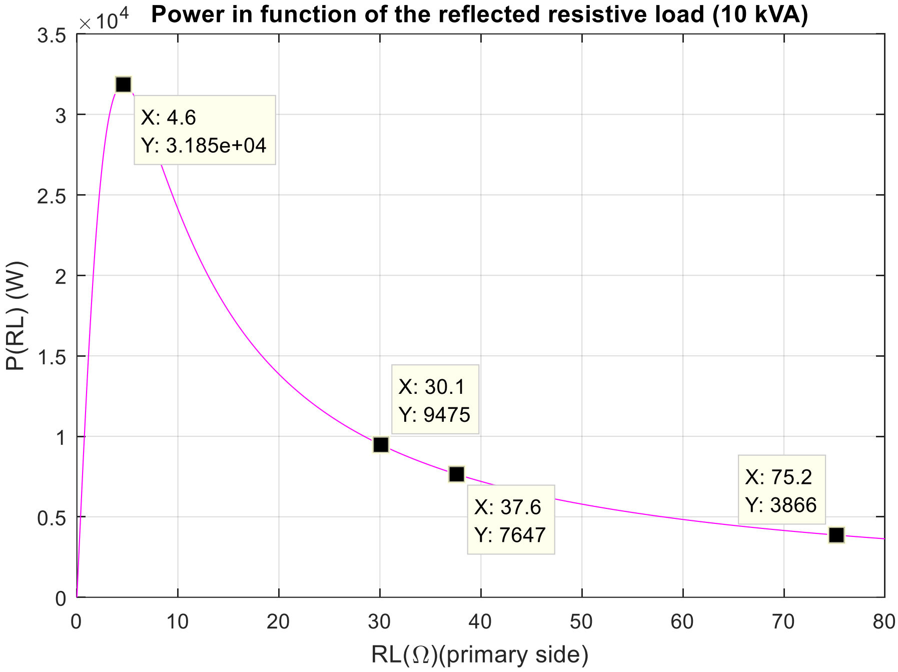

Figure 3.6 - Power Transfer Curve for the 10 kVA @ 15 kHz Transformer.

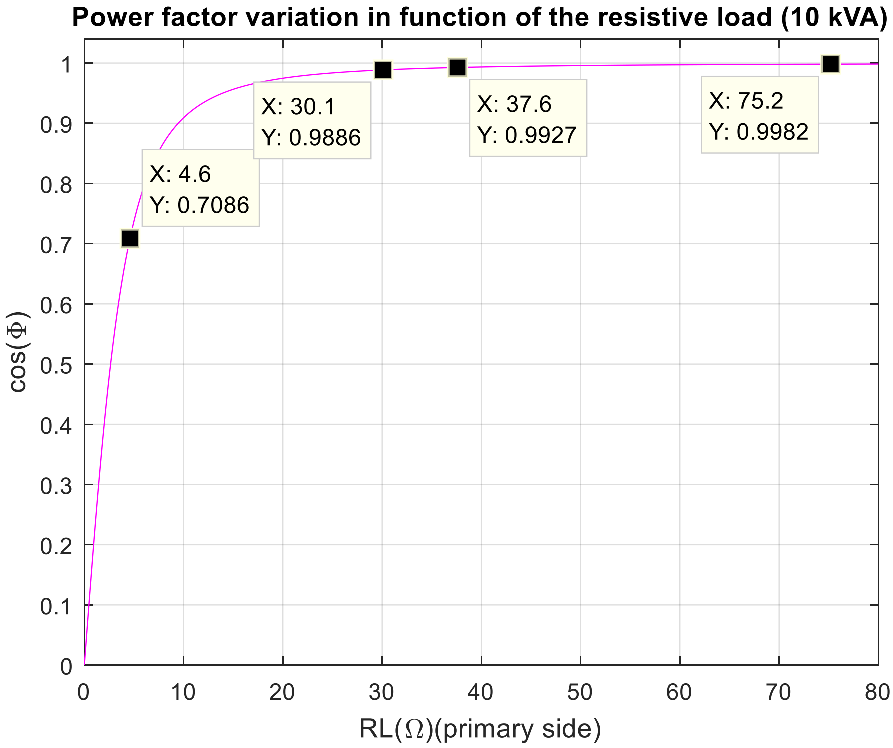

Figure 3.7 - Power factor variation for the curve of Figure 3.6.

3.2 OVERVIEW AND OPERATION

Figure 3.8 shows a full bridge voltage inverter feeding a high voltage, high frequency transformer with a variable resistive load connected at the secondary side. The inverter produces, in principle, a square wave output voltage, whose amplitude is the DC voltage.

In general applications the objective is to control the power transfer to the load, so control and command strategies are implemented for that [14] [16] [18] [24] [47] and are very effective if the load is know or have a slow variation. However, in this work the load varies in a large range, creating some new challenges for the inverter design [33].

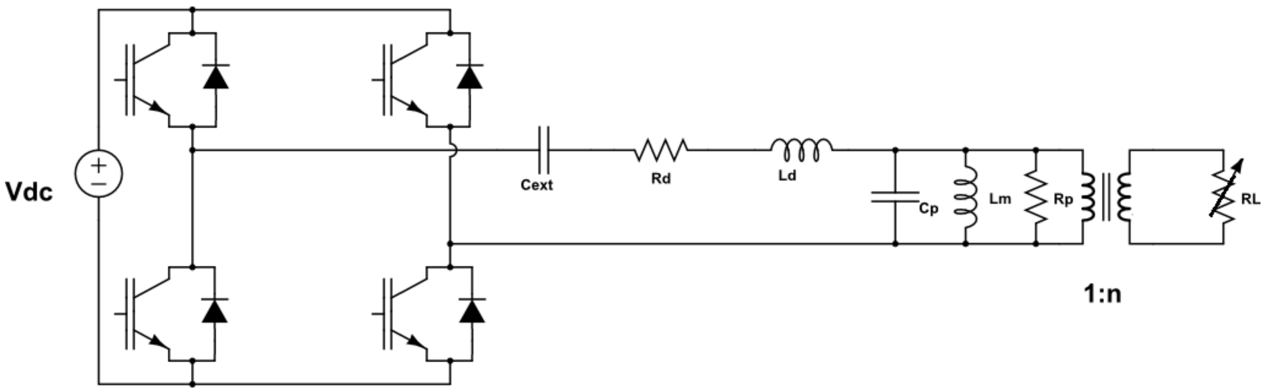

Figure 3.8-Full bridge voltage inverter feeding a HVHFT with a variable resistive load.

The series capacitor C_{ext} has the function of blocking DC components from the inverter, avoiding the transformer saturation [48] [49]. It must have a low impedance value at the operating frequency and a low voltage drop at nominal conditions [48]. If I_n is the primary nominal current and V_{ext} is the capacitor voltage drop, the capacitance of the series capacitor is calculated by (22). The input impedance and the voltage gain with the series capacitor are given by (23) and (24) respectively.

$$C_{ext} = \frac{I_n}{2\pi f V_{ext}} \tag{22}$$

$$Z_{in} = \frac{\begin{array}{c} s^4 L_m L_d C_{ext} C_p R_p + s^3 L_m C_{ext}\left(L_d + C_p R_d R_p\right) + \\ s^2\left(L_m R_p C_{ext} + L_m R_d C_{ext} + L_d R_p C_{ext} + C_p L_m R_p\right) + \\ s(L_m + R_d R_p C_{ext}) + R_p \end{array}}{s^3 L_m C_{ext} C_p R_p + s^2 L_m C_{ext} + s R_p C_{ext}} \tag{23}$$

$$\frac{V_{out}}{V_{in}} = \frac{s^2 n L_m R_p C_{ext}}{\begin{array}{c} s^4 L_m L_d C_{ext} C_p R_p + s^3 L_m C_{ext}\left(L_d + C_p R_d R_p\right) + \\ s^2\left(L_m R_p C_{ext} + L_m R_d C_{ext} + L_d R_p C_{ext} + C_p L_m R_p\right) + \\ s(L_m + R_d R_p C_{ext}) + R_p \end{array}} \tag{24}$$

Considering a primary current of 3.22 A (1000 W/311 V), and a voltage drop of 15 V (4.8 % of the nominal voltage), the series capacitor value is determined as 1.7 µF. Figure 3.9 shows the input impedance with the addition of the series capacitor with a value of 2 µF, and Figure 3.10 the respective voltage gain. The capacitor adds a series resonance at 1.5 kHz, affecting predominantly the low frequency region. As the region next to the operating frequency did not have its behavior changed, the capacitor can be adequately used.

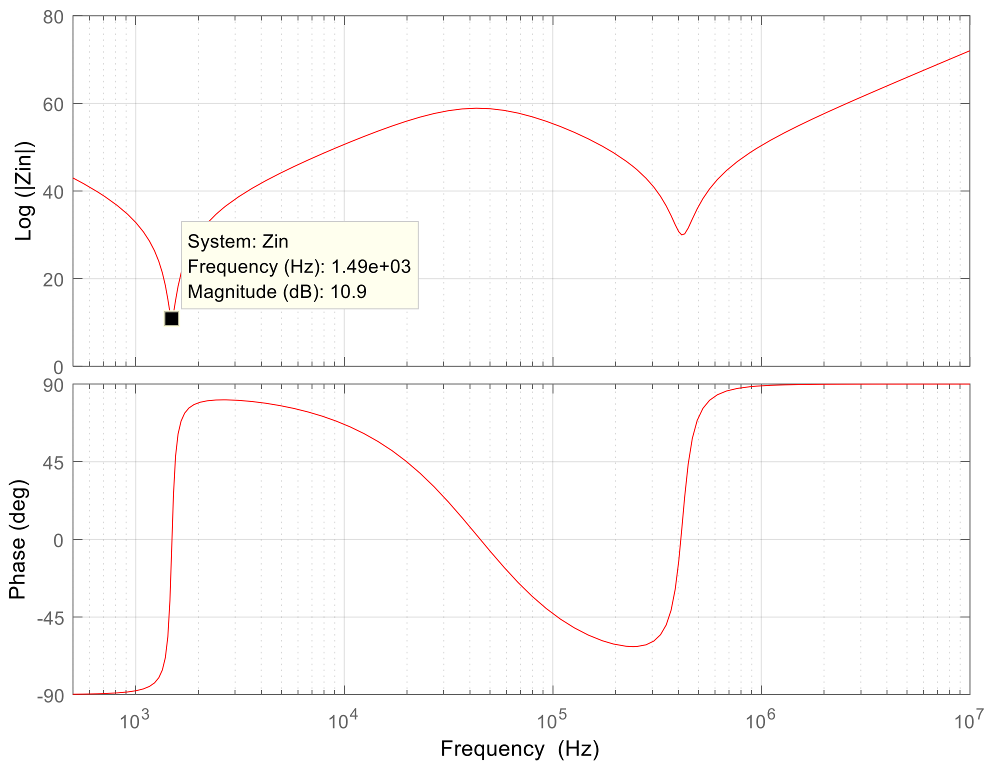

Figure 3.9 - Input impedance of the transformer considering the series capacitor.

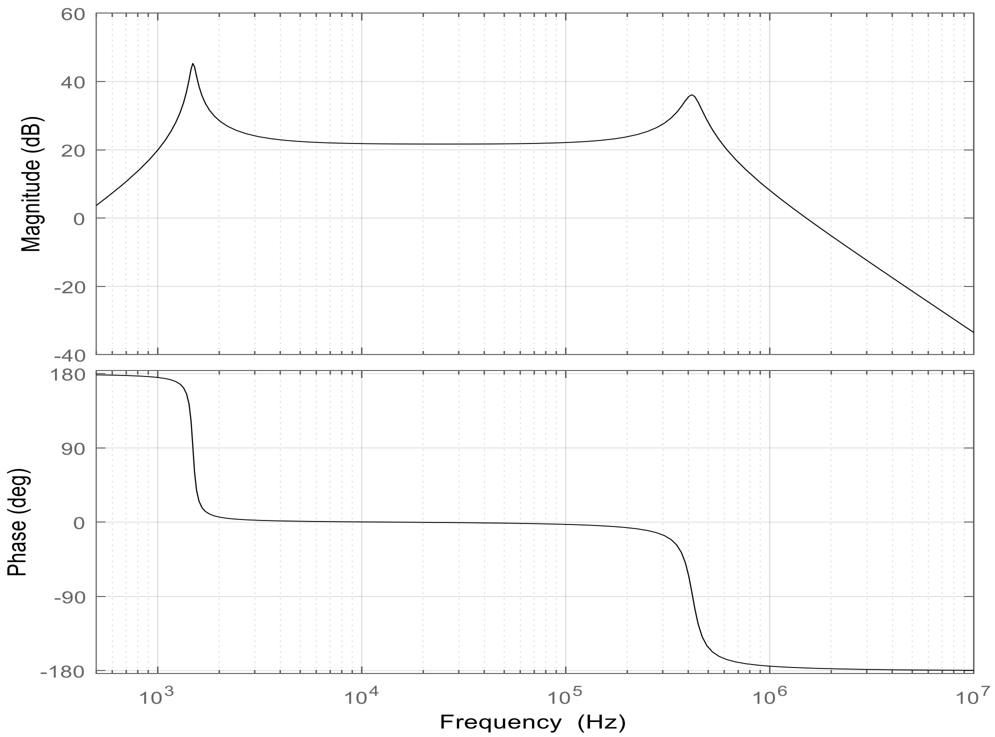

Figure 3.10 - Voltage gain with the series capacitor.

A simulation circuit in the software PSIM® is shown in Figure 3.11. The transformer parameters were obtained in section 2.4. When the converter operates at nominal condition, 1 kW should be transferred to the load. For the open or short circuit situations, the transformer can be damaged by overvoltage or overcurrent due to this extreme load conditions.

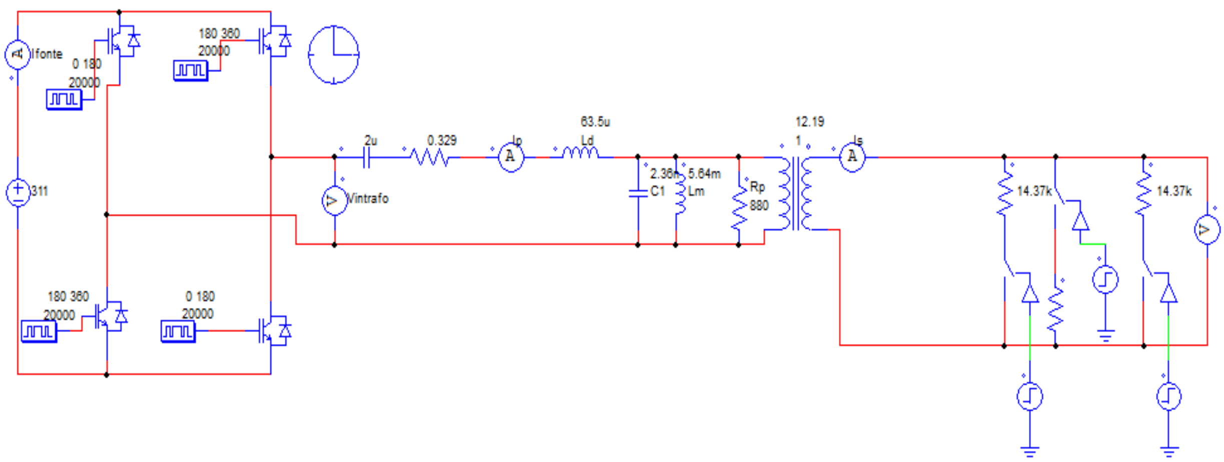

Figure 3.11 - Simulation for the converter proposed, with variable load.

Figure 3.12 shows the transformer output waveforms for the converter feeding a resistive load whose value was determined for a power dissipation of 1 kW at secondary nominal voltage. The apparent power is 1 kVA, and the power factor is nearly 1, showing that's possible for the converter transfer the expected power.

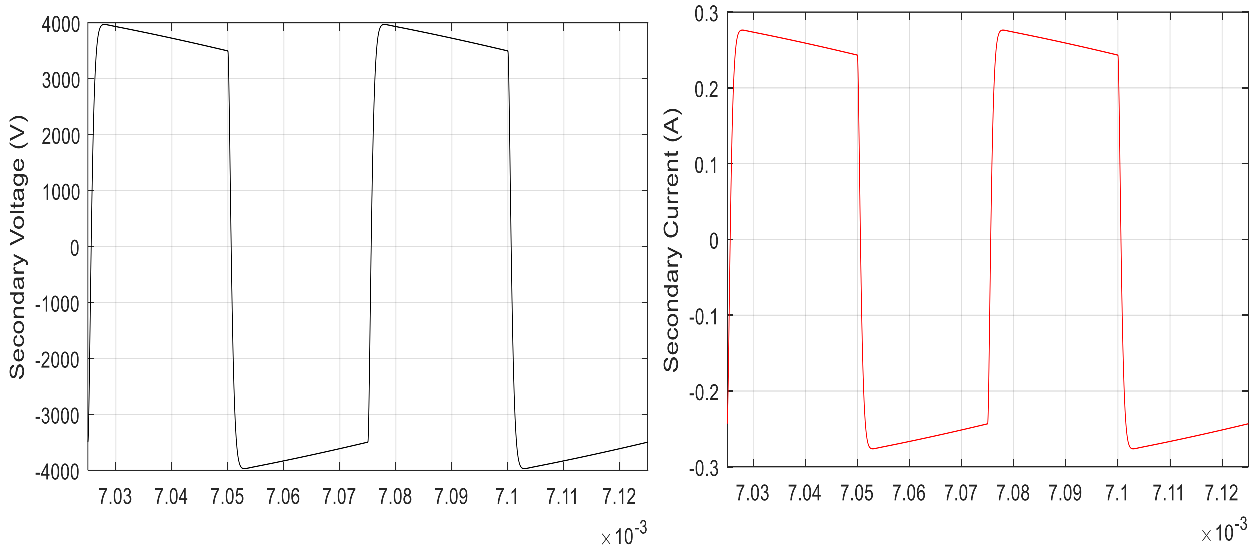

Figure 3.12 - Secondary voltage and current for the converter operating at nominal conditions.

For open circuit load situation, the series resonance is excited by the input voltage harmonic components, amplifying the voltage gain and giving the oscillatory aspect to the output waveform, as Figure 3.13 shows. The voltage peak is almost two times the expected value, what can compromise the isolation. The primary current, that should be only the magnetizing current with a triangular aspect, is affected by the resonance as well, showing the oscillatory behavior that can be seen in Figure 3.13.

Like the resonance is due to leakage inductance and the equivalent winding capacitance, it happens "inside" the transformer. It is not possible to access the tank elements, so their effects can be mitigated only by external procedures, to guarantee the safety operation.

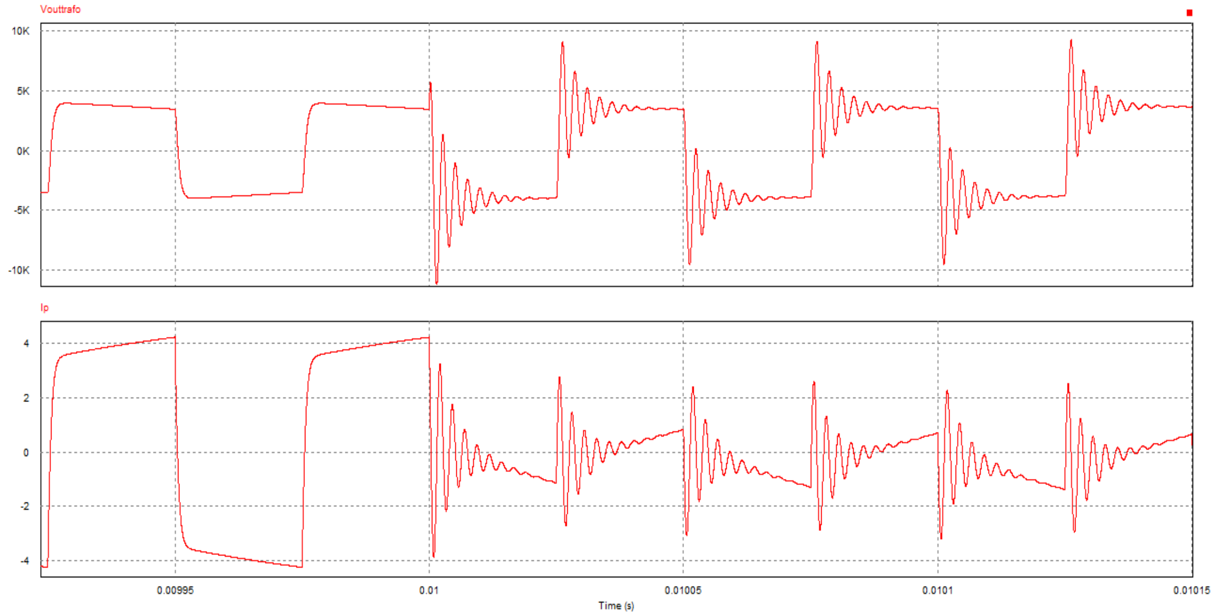

Figure 3.13 - Secondary voltage and primary current for nominal condition, for an open circuit load situation.

The secondary voltage and primary current for the transformer operating at nominal conditions when occurs a short-circuit in the secondary winding is shown in Figure 3.14. The primary current quickly increases, what can damage the inverter and the transformer.

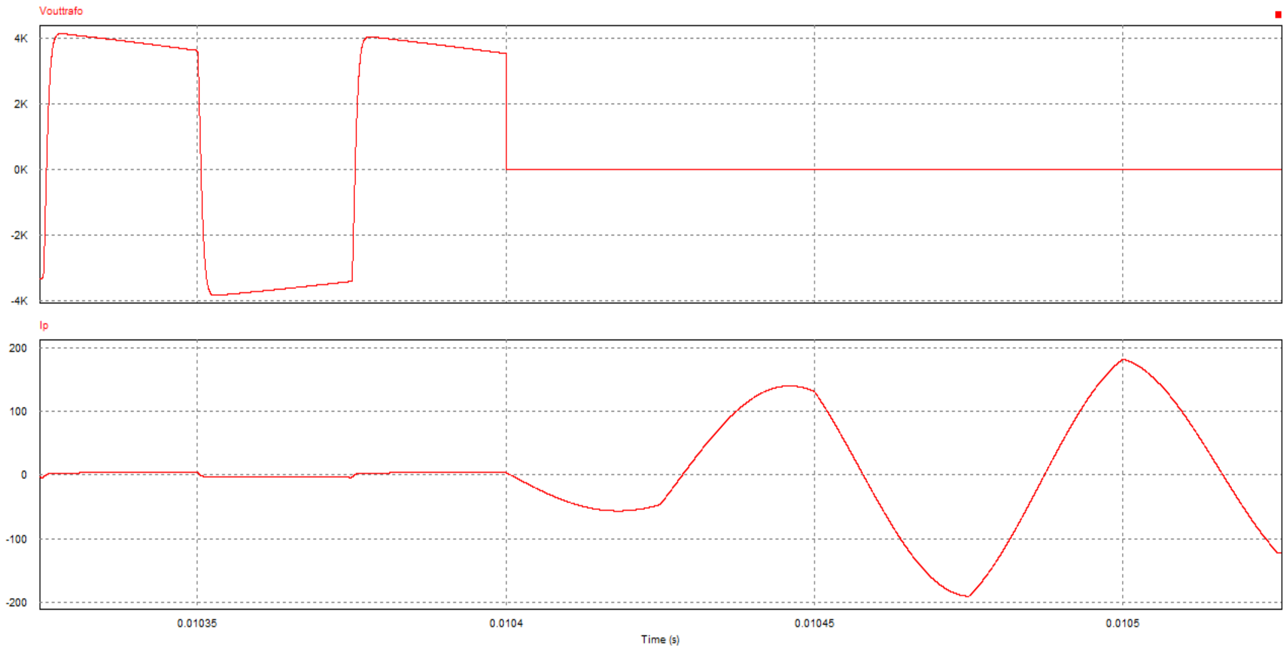

Figure 3.14 - Secondary voltage and primary current, for a short-circuit situation.

The overvoltage and overcurrent situations impose the necessity of protection strategies to guarantee the system safety operation. The limitation in the open load condition can be made by reducing the primary voltage, changing the input impedance, or a combination of both. The primary voltage reduction could be made on real time by implementing a phase-shift modulation, that produces a three-level voltage when a secondary overvoltage is detected. Nevertheless, this reduction would depend on the control lope response time.

As a matter of fact, any control strategy used to limit the open load voltage peaks would have a response time, and the voltage limitation would not be obtained until the effective action of the control loop. As the load presents a fast and unpredictable variation, the system needs the fastest overvoltage limitation, to guarantee the windings integrity. So, a direct action made by fixed components associated to the converter may have a better effect for this application, once they respond instantaneously to the disturbances.

3.3 PROTECTION STRATEGIES FOR THE CONVERTER'S SAFETY OPERATION

3.3.1 Overvoltage Protection Strategies

To protect the transformer against the high voltage peaks caused by the series resonance manifestation, overvoltage limiting strategies must be implemented. Since the equivalent capacitance reflected to the primary side is unreachable, it's impossible to limit its voltage directly on the magnetizing branch. As such voltage reflects to the secondary side, the overvoltage protection strategies can act directly on that winding.

3.3.1.1 High-Voltage Clamper

A Voltage Clamper [50] can be used at the secondary side to limit the voltage during the open load operation, the clamper configuration is shown in Figure 3.15. The clamper uses high voltage high frequency diodes, as well as a high voltage capacitor (C_{cl}) and enough resistive load (R_{cl}).

During the normal operation, the clamper capacitor charges with the secondary nominal voltage. When the series resonance is excited, the clamper absorbs the energy associated with the L_d-C_p tank circuit and dissipates it on the resistor. There's a slightly increase in the voltage peak, but the output AC voltage remains limited by the capacitor voltage peak.

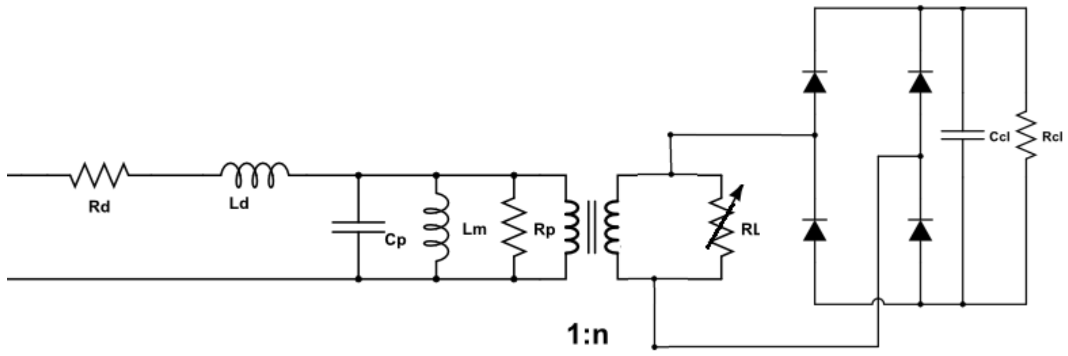

Figure 3.15-Voltage Clamper at the secondary side to protect the transformer against overvoltage.

The magnetizing current "contaminated" by the series resonance manifestation is shown in Figure 3.16. The leakage inductance current peak value with the resonance manifestation is *Ip*. This value is achieved in a quarter of the wave-cycle at the resonant frequency.

To determine *Ip*, the magnetizing current peak *Im* must be taken in consideration and its value subtracted from the total current in the resonant circuit. The value of *Im* can be estimated by (25).

$$I_m = \frac{TV_{dc}}{4L_m} \tag{25}$$

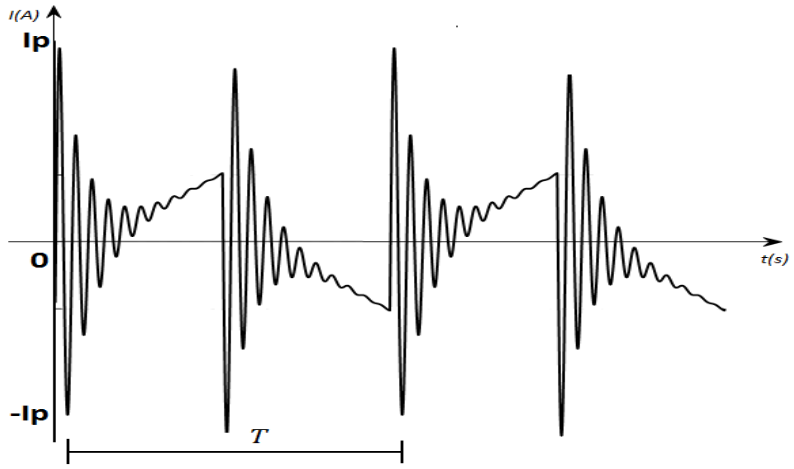

Figure 3.16-Magnetizing current with the series resonance manifestation.

The resonant circuit may be regarded as a simple LC, as Figure 3.17 shows, neglecting the resistive losses, so its characteristic impedance is given by (26), the total contaminated current is given by (27) and the Ip value by (28).

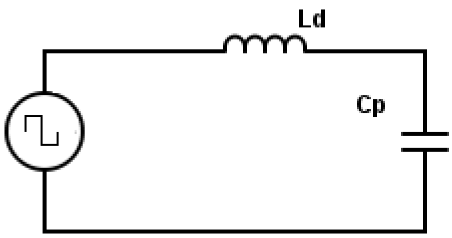

Figure 3.17 - Simplified resonant circuit neglecting the resistive effects.

$$Z_c = \sqrt{\frac{L_d}{C_p}} \tag{26}$$

$$I_c = \frac{2V_{dc}}{Z_c} \tag{27}$$

$$I_p = I_c - I_m \tag{28}$$

The energy accumulated in L_d during a half-cycle can be used to determine the clamper components' values. The total electrical charge delivered by the "resonant current" during this time interval, if f_s is the series resonance frequency, can be calculated by (29) and is determined by the expression in (30). Considering the transformer secondary can handle an overvoltage of ΔV, the clamper capacitor is determined by (31).

$$Q_s = 2\int_0^{\frac{1}{2f_s}} I_p \sin(2\pi f_s t)\, dt \tag{29}$$

$$Q_s = \frac{2I_p}{\pi f_s} \tag{30}$$

$$C_{cl} = \frac{2I_p}{\pi f_s \Delta V} \tag{31}$$

The energy absorbed by C_{cl} in a half period is given by (32) and must be dissipated on the clamper resistor. Considering the voltage on the resistor constant and equals the secondary output voltage V_o in normal operation, the power the resistor must dissipate during the resonance is given by (33), and its value can be calculated by (34).

$$E_s = \frac{I_p \Delta V}{\pi f_s} \tag{32}$$

$$P_{R_{cl}} = \frac{E_s}{T/_2} \tag{33}$$

$$R_{cl} = \frac{(V_o)^2 \pi f_s}{2 I_p \Delta V f} \tag{34}$$

For the 1 kVA transformer analyzed, the output voltage expected at normal operation is nearly 3.8 kV. The magnetizing current given by (25) is 0.69 A. The characteristic impedance given by (26) is 164 Ω and the total resonant current through is 3.79 A, so the Ip value determined by (29) is 3.10 A.

The clamper capacitor determined by (31), considering an overvoltage of 200 V (a secondary voltage peak of 4 kV) is 24 nF and the minimum clamper resistor, at these conditions, calculated by (34) is 748.29 kΩ. The power dissipated on the clamper's resistor, determined by (33) is 19.21 W.

A simulation of the voltage clamper strategy is shown in Figure 3.18. The transformer input current and output voltage at nominal and open load conditions with the clamper are shown in Figure 3.19. The waveforms validate the clamper design procedure and confirm the expecting results. The clamper resistance must be high enough to limit the losses, but not so high in order to limit the overvoltage.

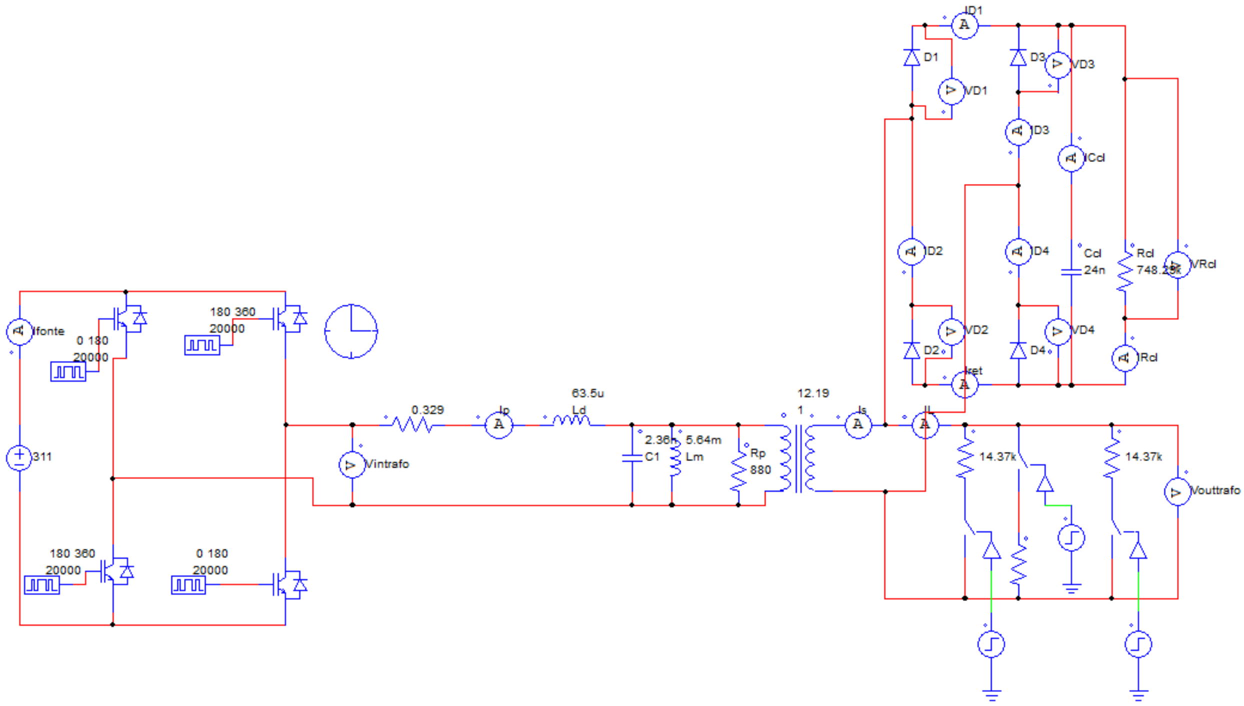

Figure 3.18-Voltage Clamper at the secondary side to protect the load against overvoltage.

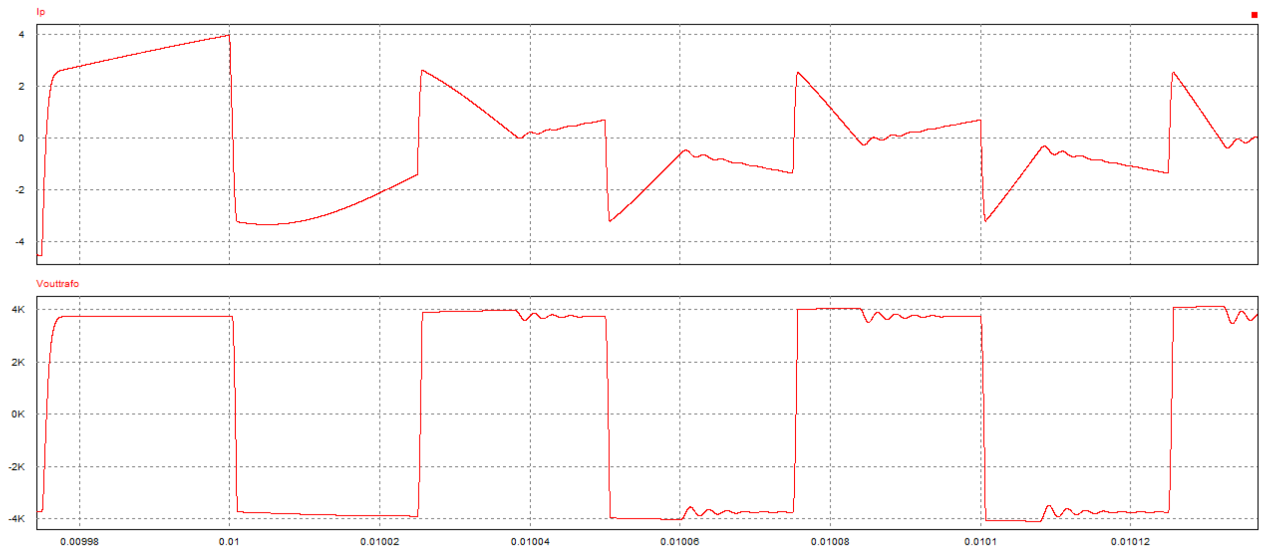

Figure 3.19-Primary current and secondary voltage with the clamper.

Figure 3.20 shows several currents for the simulation of Figure 3.18. The “large initial peak” in the primary current is due to the diodes conducting interval, that causes the peak at the secondary current, and this behavior is reflected to the primary side. This effect is not so expressive at normal operation, once the diodes current are small in comparison to the primary, and their addition don’t have much expression when reflected to the primary current. The main drawbacks of this solution are the cost of the high voltage high frequency components, as well as the additional losses.

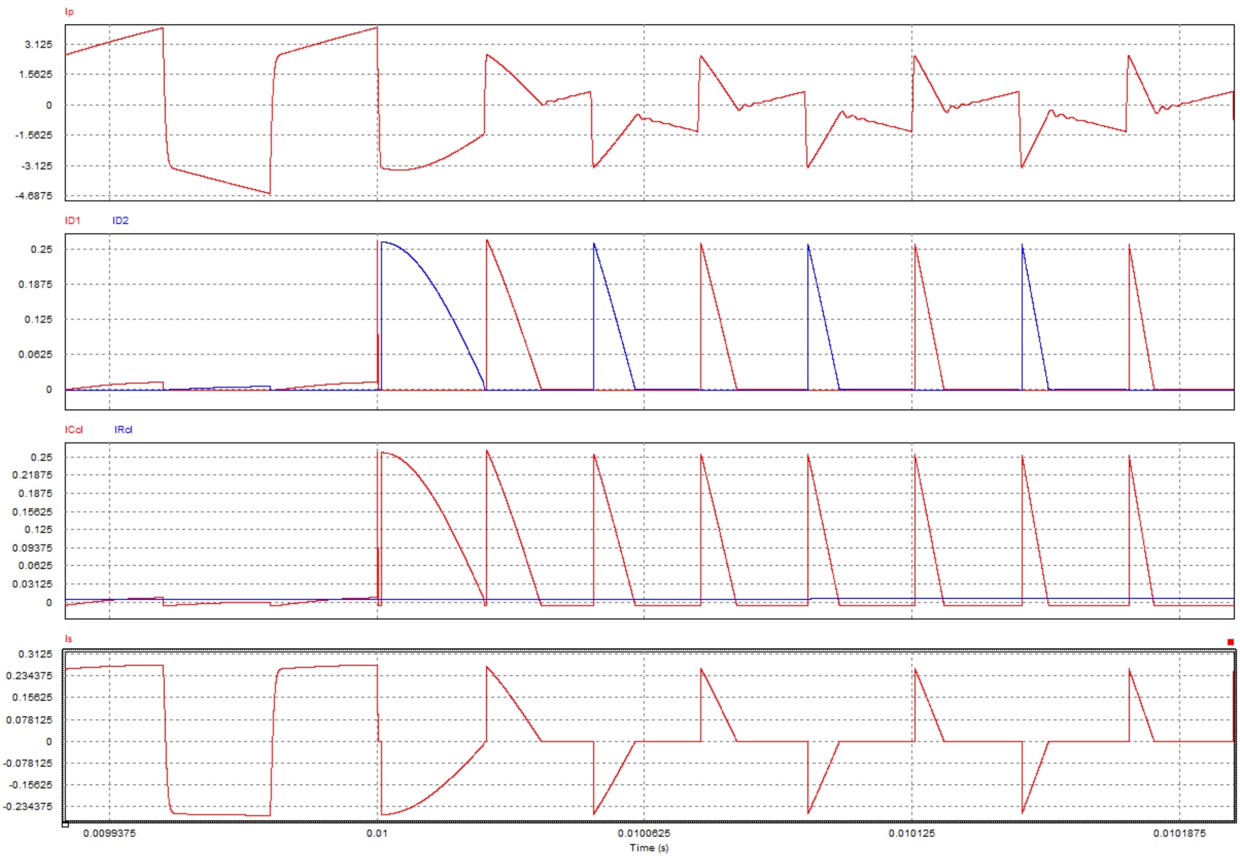

Figure 3.20-High voltage clamper currents. From top to bottom: Primary, diodes, clamper's resistor and capacitor, and secondary currents.

3.3.1.2 External Inductance

If the magnetic coupling between primary and secondary windings was perfect (zero leakage inductance), the voltage would be imposed directly on the magnetizing branch by the inverter and no overvoltage would occur, even in the open circuit situation. Although this ideal case is impossible, an approximation can be made, if the leakage inductance has a small value.

When this is the case, an external inductor, with an inductance value significantly higher than the leakage's, can be connected in series with the primary side to obtain the overvoltage limitation. The external inductance can't be excessively high; otherwise it would limit the primary current and, consequently, the power transfer. The point between the external inductor and the transformer is connected to the intermediary point of a diode branch and then connected to the inverter's DC link [51]. Figure 3.21 shows the connections for this strategy.

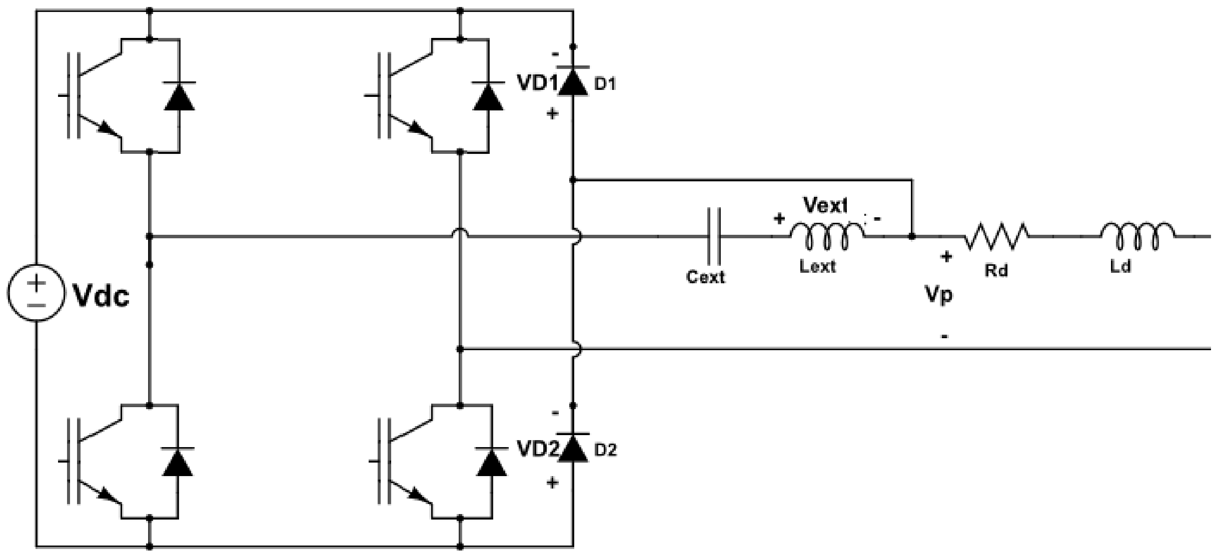

Figure 3.21-External inductor strategy for overvoltage protection.

The diodes branch operates as a clamper and limits the voltage amplitude on the primary to the dc link. As the leakage inductance is small compared to the external inductor, the voltage at the magnetizing branch and at the output is limited, reducing the transformer high voltage peaks.

The efficacy of this strategy is directly related to the ratio between the external and leakage inductances. Figure 3.22 shows a simulation for this strategy and Figure 3.23 the output voltage limitation with the external inductor.

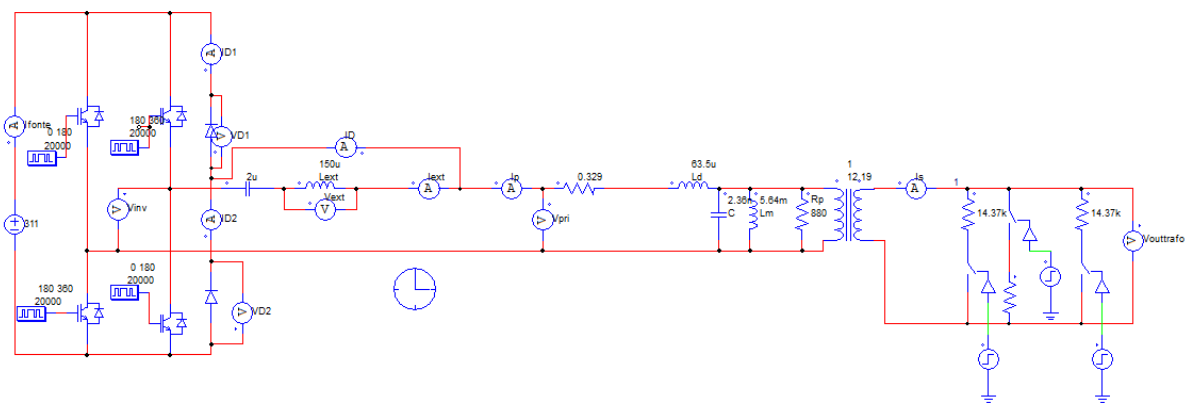

Figure 3.22-Simulation for the external inductor strategy.

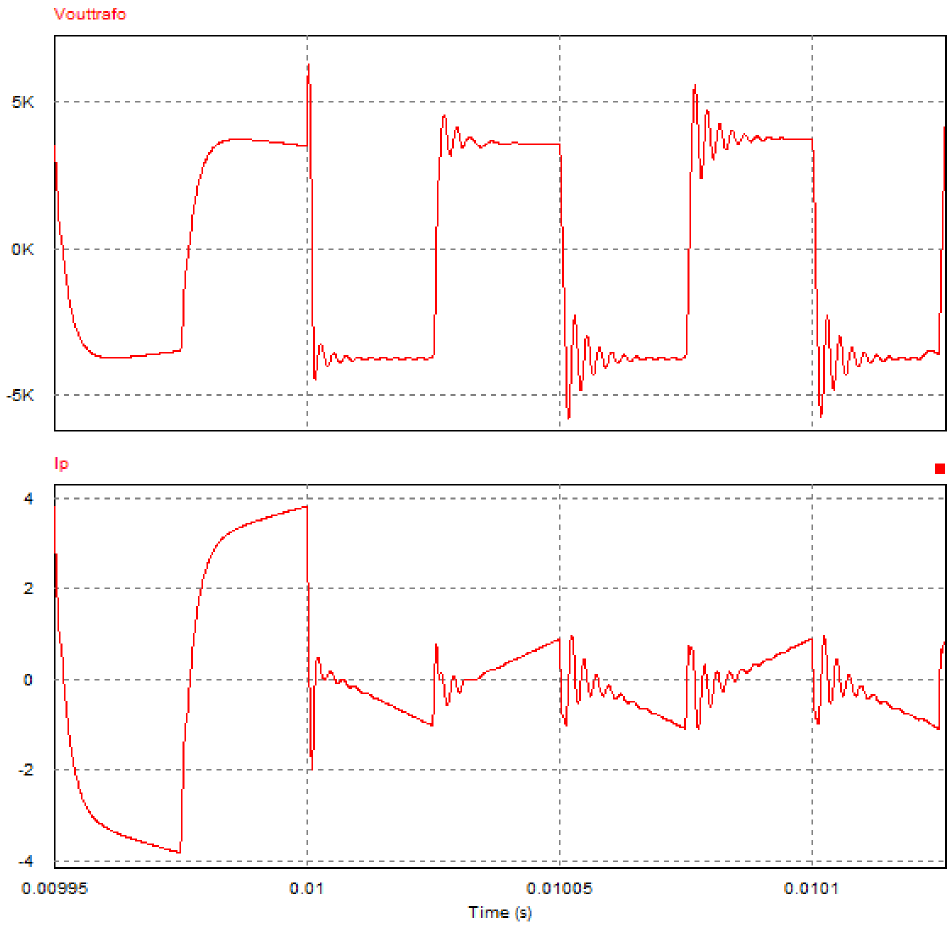

Figure 3.23-Secondary voltage and primary current with the external inductor.

To better understand the converter's behavior with the external inductor, an analysis based on the waveforms will be made at nominal and open load conditions. Figure 3.24 shows the waveforms for the external inductor and the primary winding at nominal conditions, as well as the inverter voltage output.

During the positive half-cycle, the inverter's output is V_{dc}. The external inductor is initially uncharged, so it behaves like an open circuit and its voltage drop is a little more than V_{dc}. The primary voltage is the difference between the inverter and external inductor voltages, so the primary voltage at this moment is 0. The voltage on the diode D1 is -V_{dc} and on the diode D2 is 0, as can be seen in Figure 3.25. The additional initial voltage on the external inductor is due to the capacitor C_{ext} effect. If the capacitor is removed, the initial voltage drop on the inductor is V_{dc}, and its behavior is the same as described above.

The inductor voltage tends to zero and the primary voltage increases gradually to V_{dc}. The voltages on D1 and D2 tend to 0 and -V_{dc} respectively. When the half-cycle changes, the behavior is similar, but the voltage values are opposite, as can be seen in Figure 3.24 and Figure 3.25. The primary, inductor and diode currents for this situation can also be seen in Figure 3.25. There’s a slight difference between the inductor and primary currents, because of the current circulation trough the diodes during their conduction.

The diodes polarization (and consequently their conduction intervals) depends on the voltage at the point between the external inductor and the primary, during the positive half-cycle the diode D2 is conducting, and during the negative, the diode D1, as can be seen in the waveforms of Figure 3.25. When the primary voltage achieves its peak, the voltage on the diode D1 is 0 during the positive (consequently in D2, during the negative) half-cycle, but there’s no current flowing through the diodes in this situation.

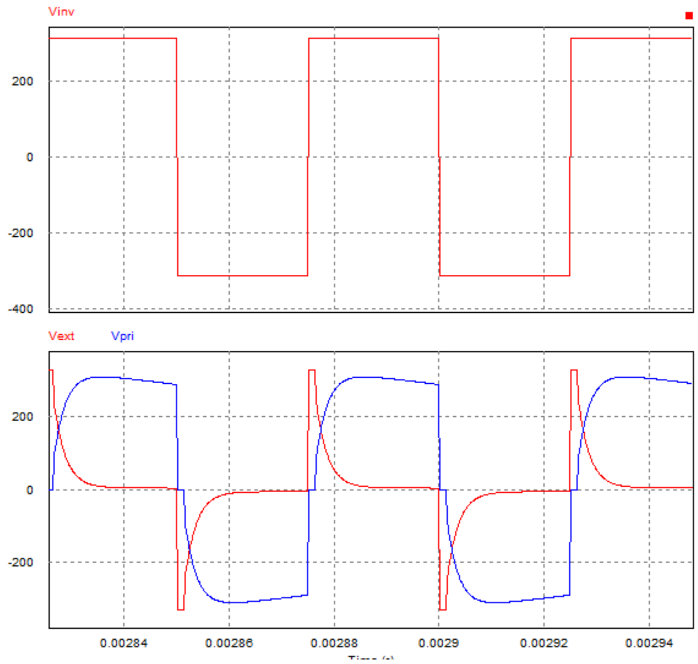

Figure 3.24 - From top to bottom: Inverter output voltage; Primary and external inductor voltages, at nominal conditions.

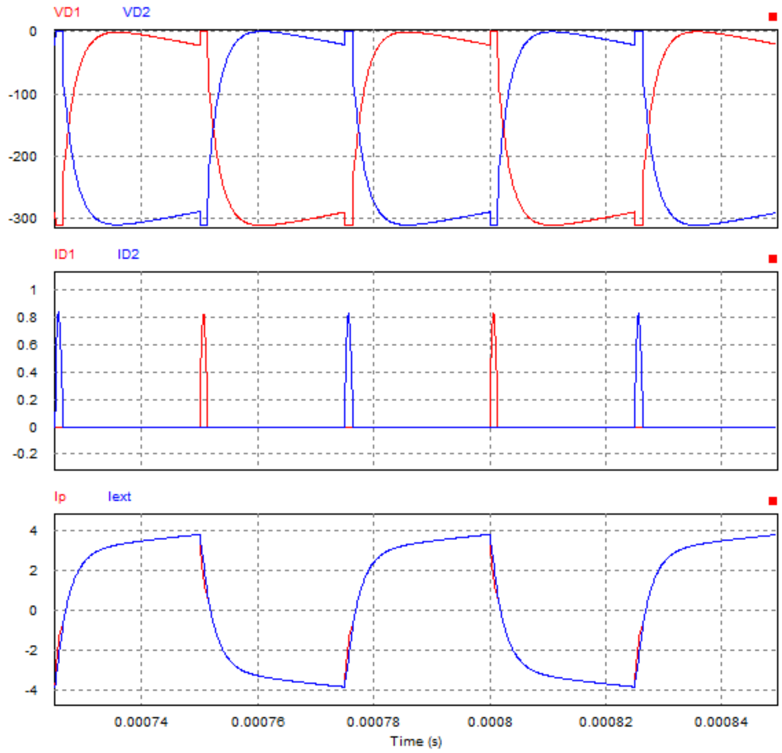

Figure 3.25 - From top to bottom: Diodes voltages, diodes currents, primary and external inductor currents for the external inductor strategy at nominal conditions.

The converter's behavior described above can be represented by two equivalent circuits, one for each half-cycle, as Figure 3.26 shows. In that representation, the primary voltage is represented as a voltage source.

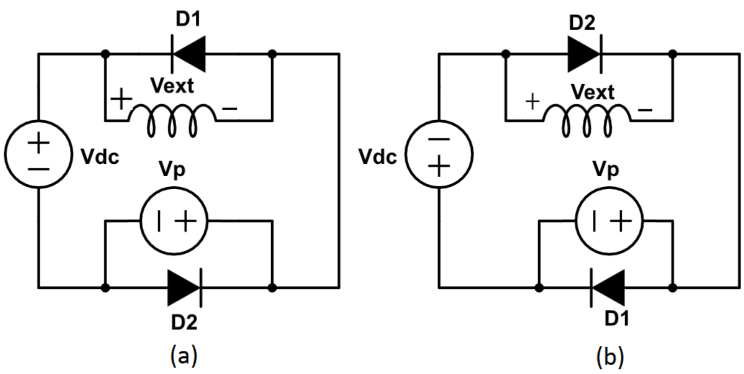

Figure 3.26 - Equivalent circuits for the external inductor strategy: Positive (a) and negative half-cycles (b).

The inductor current increases more quickly when the secondary is in the open load condition, as can be seen in Figure 3.27. The external inductor charges faster, as Figure 3.28 shows. The primary voltage takes less time to achieve its peak value and remains limited to

V_{dc}. The diodes currents and voltages are affected by the resonance manifestation, as shown in Figure 3.27 and Figure 3.28 respectively.

As the primary voltage reaches its peak quickly, the diode D1 conducts before the nominal operation shown in Figure 3.25, and most of the additional current flows through it, reducing the primary current peaks during the open load situation.

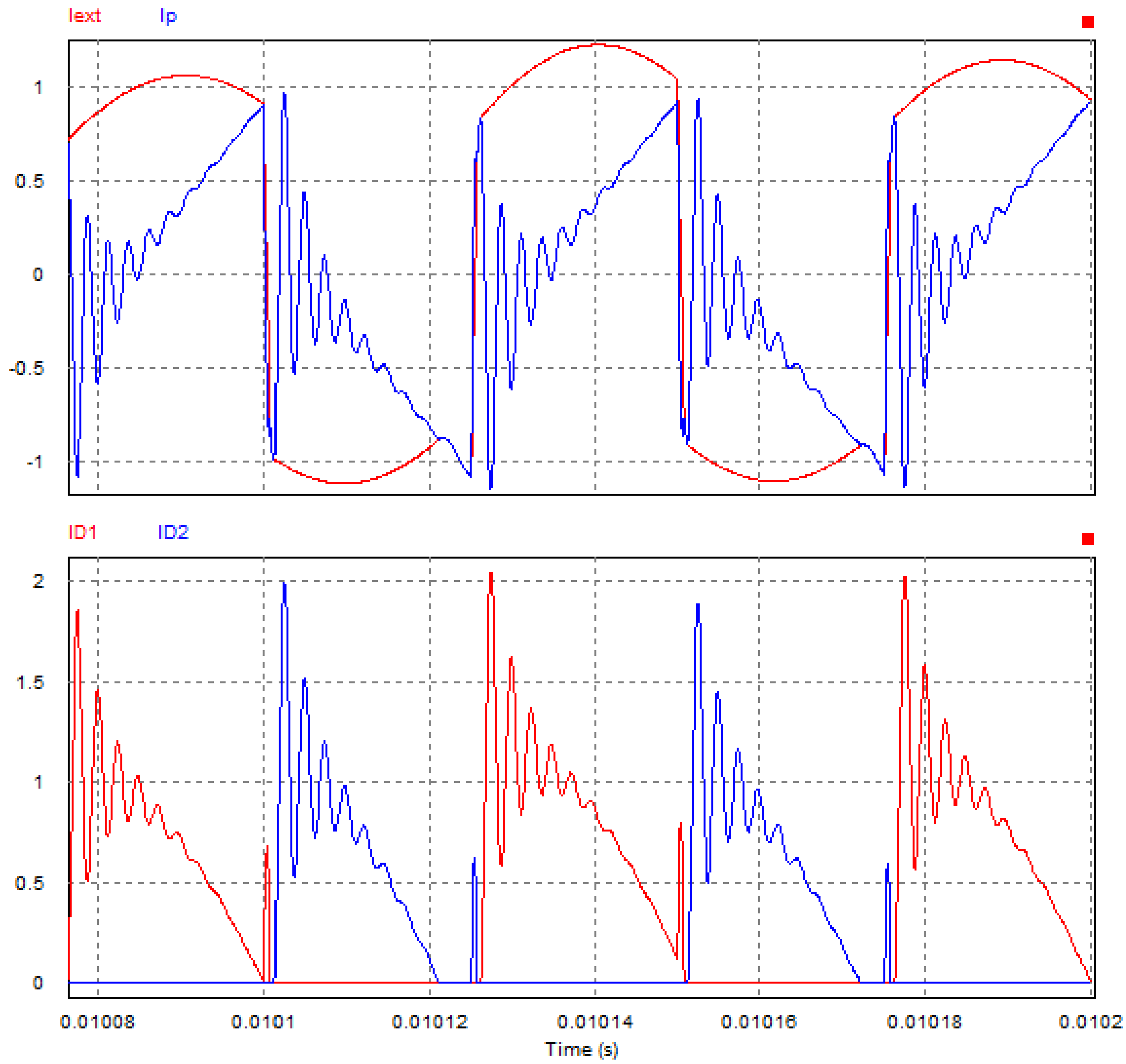

Figure 3.27 - Waveforms for the external inductor strategy at open load condition. From top to bottom: Primary and inductor currents; Diodes currents.

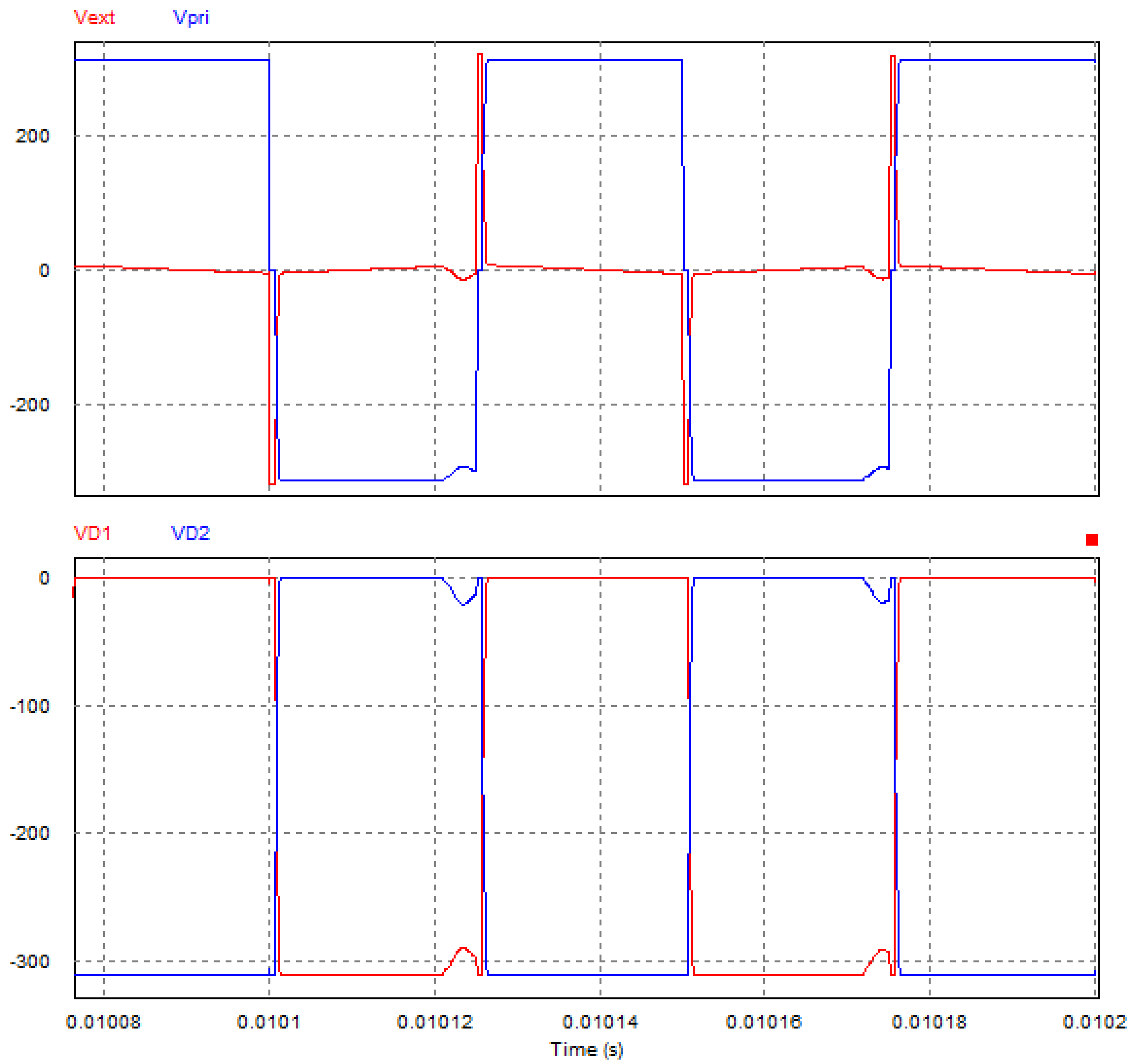

Figure 3.28 - Voltages at open load condition. From top to bottom: Primary and external inductor; Diodes.

The main drawback of the external inductor strategy is the reduction of the power factor due to the higher series inductance. So, for a given output power, the input current will be higher than without the external inductor. If the leakage inductance is high, this solution can't be applied. Tables 2, 3 and 4 show the output power with the nominal load connected at the secondary and the secondary voltage peak in the open load condition for the 1 kVA, 3 kVA and 10 kVA transformers respectively. It can be seen that higher the external inductor, higher the voltage peak reduction at the open load condition, but lower the power delivered to the load. The resistive load considered in each case is the enough expected to dissipate the nominal power in the nominal conditions, considering the system ideal characteristics.

Table 2- Power and overvoltage variation according to the external inductor value, for the 1 kVA transformer (L_d = 63.5 μH).

External inductor (μH)	**Output Voltage rms value (kV)**	**Output power (W)**	**Secondary open load voltage peak (kV)**
0	3.68	944	9.2
100	3.46	834	6.3
150	3.34	778	5.8
200	3.21	720	5.2
300	2.96	610	4.5
600	2.22	350	3.8

Table 3- Power and overvoltage variation according to the external inductor value, for the 3 kVA transformer (L_d = 5.99 μH).

External inductor (μH)	**Output Voltage rms value (kV)**	**Output power (kW)**	**Secondary open load voltage peak (kV)**
0	6.17	2.94	12.9
20	5.34	2.2	8.4
50	5.73	2.5	6.8
100	5.04	1.9	6.3
150	4.26	1.4	5.8

Table 4- Power and overvoltage variation according to the external inductor value, for the 10 kVA transformer (L_d = 48.3 μH).

External inductor (μH)	**Output Voltage rms value (kV)**	**Output power (kW)**	**Secondary open load voltage peak (kV)**
0	10.26	10.5	29.3
100	9.52	9.1	18.8
150	8.86	7.8	17.8
200	8.11	6.6	15.9
300	6.56	4.3	13.1
450	4.79	2.3	12.8

Figure 3.29 shows how the input power transferring and the corresponding power factor values are damped for the same loads as the external inductor increases, Figure 3.30 and Figure 3.31 show the similar behavior of the 3 kVA and 10 kVA transformers respectively.

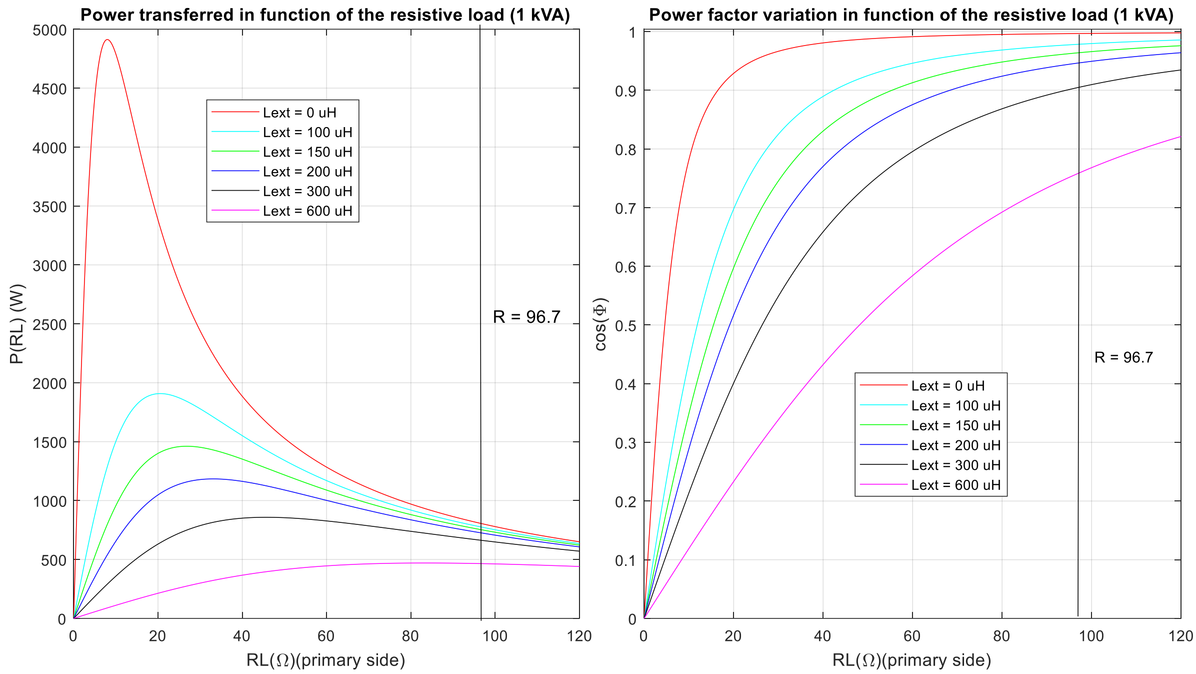

Figure 3.29 - Input power curves and corresponding power factors evolution for the values of Table 2.

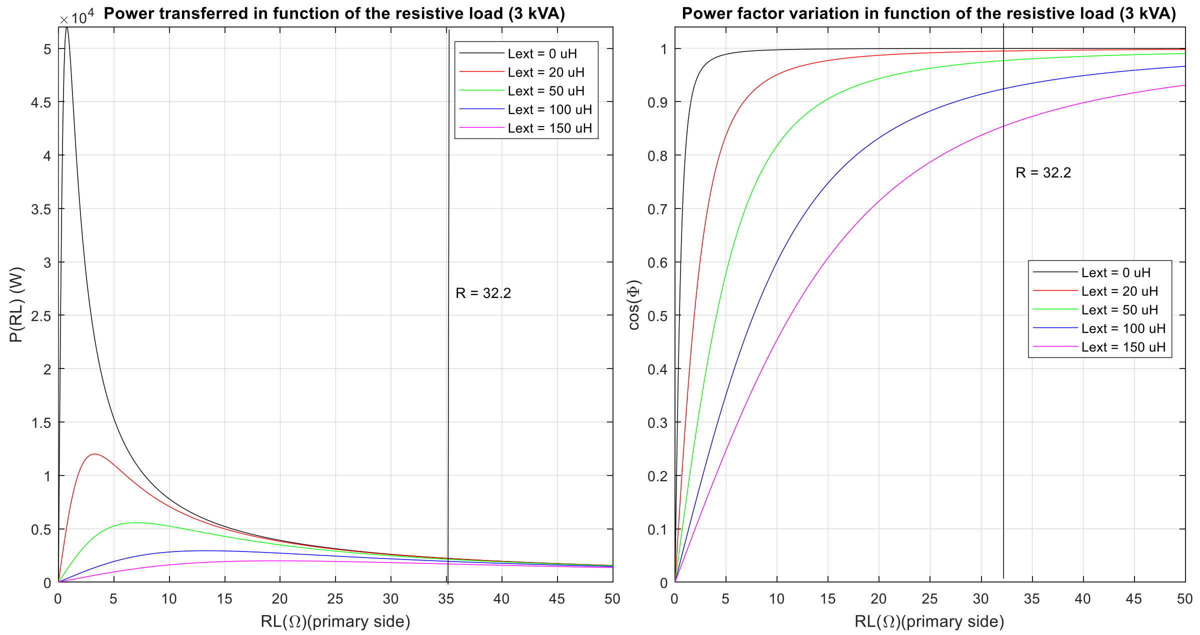

Figure 3.30 - Input power transferring and power factors curves with various external inductor values, for the 3 kVA transformer.

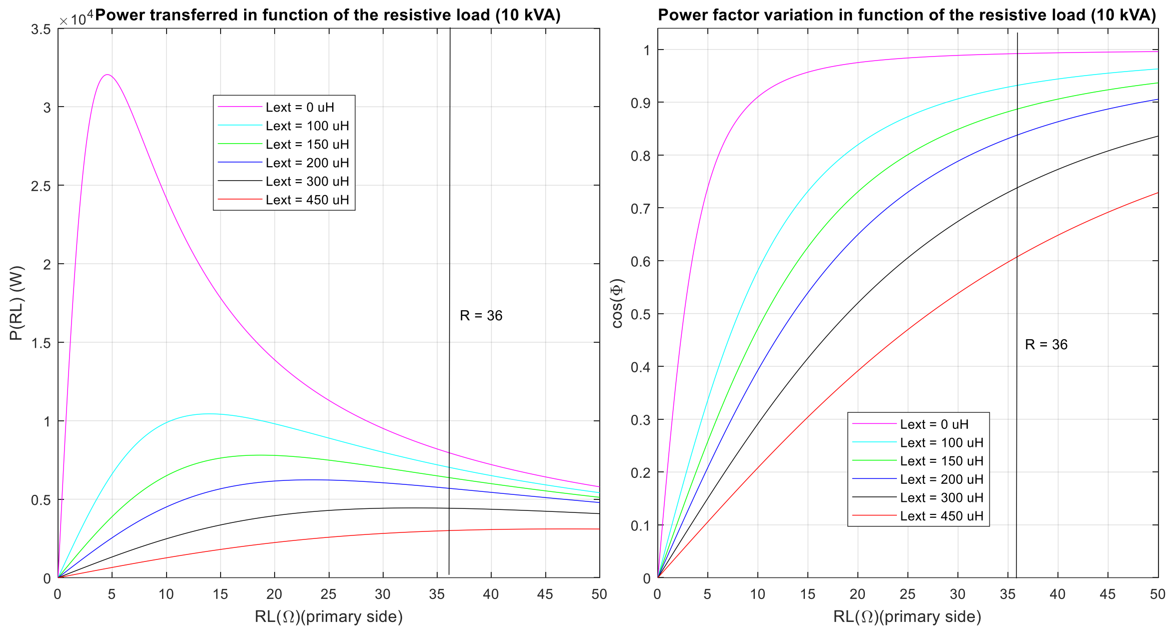

Figure 3.31 - Input power curves and corresponding power factors evolution for the values of Table 4.

The power factor reduction caused by the external inductor use may be overcame by redesign the transformer anticipating its necessity, adapting the winding conductors for the new current levels. Of course this adapting will change the transformer parasitics and, consequently, the transformer dynamics. Thus, a commitment relationship must be found between the external inductor and the transformer dynamics change.

3.3.1.3 Inverter Voltage Conditioning

The series resonance won't be excited if the voltage applied to the transformer doesn't have the respective spectral component. Without compromising the switching frequency, it's possible to produce a three-level waveform, including a zero-voltage step. The length of the zero interval allows eliminating one specific harmonic. For example, if the zero-voltage interval is 1/21 of the period, the 21st harmonic is cancelled.

Figure 3.32 shows the primary waveforms and secondary voltage for the 1 kVA transformer, using this strategy. The 21st harmonic was removed from the input signal because the series resonance frequency is 411 kHz and the operating frequency is 20 kHz (20x21 = 420 kHz). The simulated waveforms validate the overvoltage limitation by this procedure.

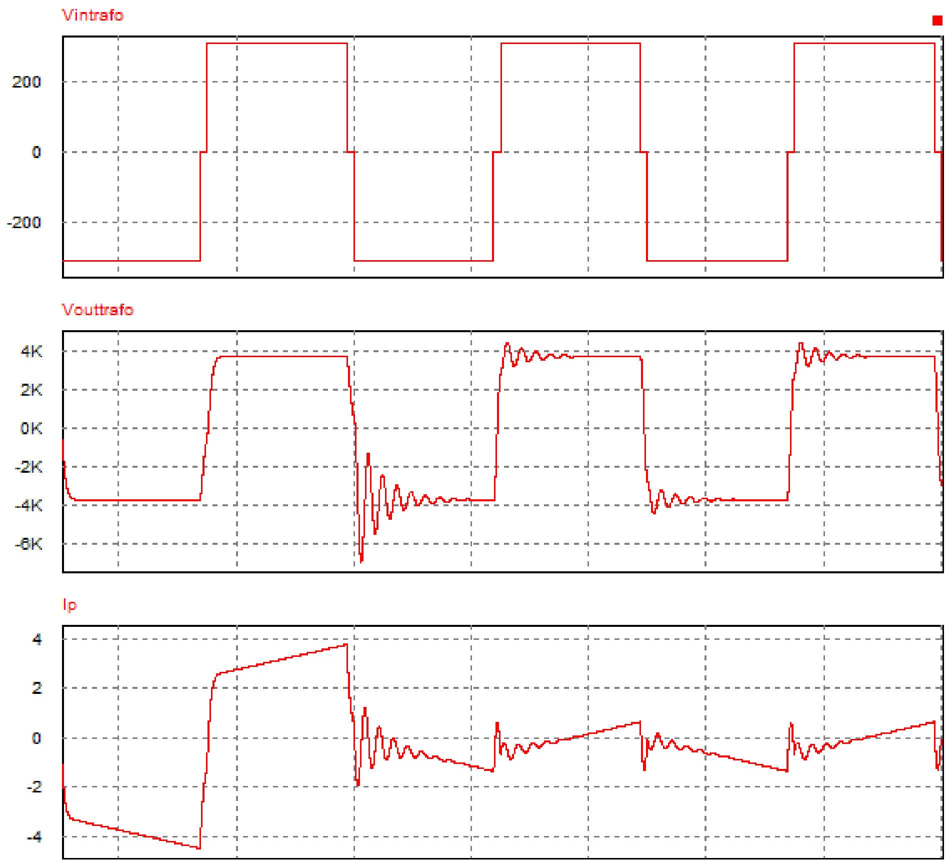

Figure 3.32-From top to bottom: Primary voltage, secondary voltage and primary current, for the harmonic elimination strategy.

It can be seen that the overvoltage was reduced. The frequency associated with the remaining oscillation is due to the components next to the resonance frequency, like the 19th, that remains in the applied rectangular voltage.

Figure 3.33 shows the Fourier Transformer of the primary voltage of Figure 3.32, where it can be verified the effectiveness of the method to eliminate the 21st harmonic from the voltage spectrum.

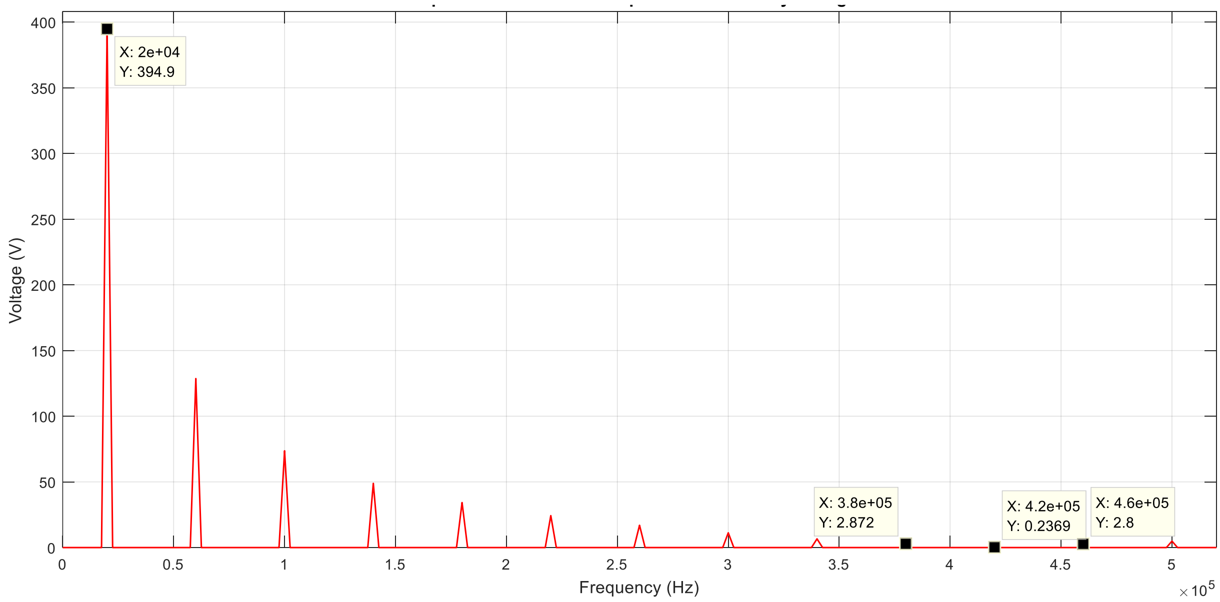

Figure 3.33-Fourier Transformer of the primary voltage of Figure 3.32.

To prove how a zero-step timing equivalent to a period fraction can eliminate a specific harmonic, the Fourier analysis is performed for a square wave with such condition, as showed in Figure 3.34. The total zero time is equal the period divided by the harmonic order to be eliminated, so the zero-time t_1 is given by (35) where K is the order of the harmonic to be eliminated.

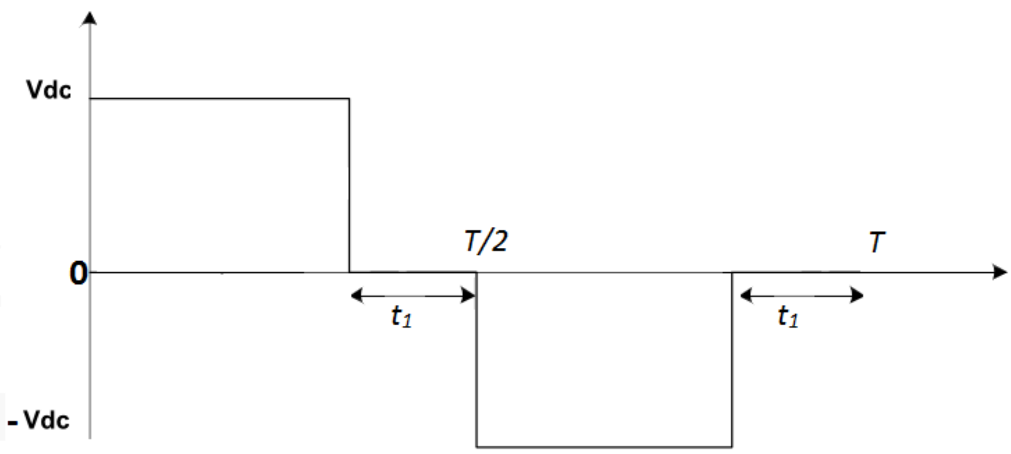

Figure 3.34-Square wave with a zero-step timing.

$$t_1 = \frac{T}{2K} \tag{35}$$

The Fourier series is given by (36), where a_0 is the average value, and a_k and b_k are the Fourier Coefficients, determined by (37) and (38) respectively [52] [53]. If the function has half wave symmetry, its average value is 0. Besides if the function has odd symmetry, the values for a_k are all 0. The signal showed in Figure 3.34 has both properties.

$$f(t) = \frac{a_0}{2} + \sum_{k=1}^{\infty} a_k \cos\frac{2\pi kt}{T} + \sum_{k=1}^{\infty} b_k \sin\frac{2\pi kt}{T} \tag{36}$$

$$a_k = \frac{2}{T}\int_0^T f(t)\cos\left(\frac{2\pi kt}{T}\right)dt \tag{37}$$

$$b_k = \frac{2}{T}\int_0^T f(t)\sin\left(\frac{2\pi kt}{T}\right)dt \tag{38}$$

Figure 3.35 shows the same square wave of Figure 3.34, but in a different representation. The equation for a period of this waveform is given by (39). The symmetry makes that the average value and the Fourier coefficients determined by (37) be zero. The coefficients determined by solving (38) are given by (40).

$$f(t) = \begin{cases} -V_{dc}, & \frac{t_1 - T}{2} < t < \frac{-t_1}{2} \\ V_{dc}, & \frac{t_1}{2} < t < \frac{T - t_1}{2} \end{cases} \tag{39}$$

$$b_k = \frac{4V_{dc}}{\pi k}\cos\frac{\pi k t_1}{T} \tag{40}$$

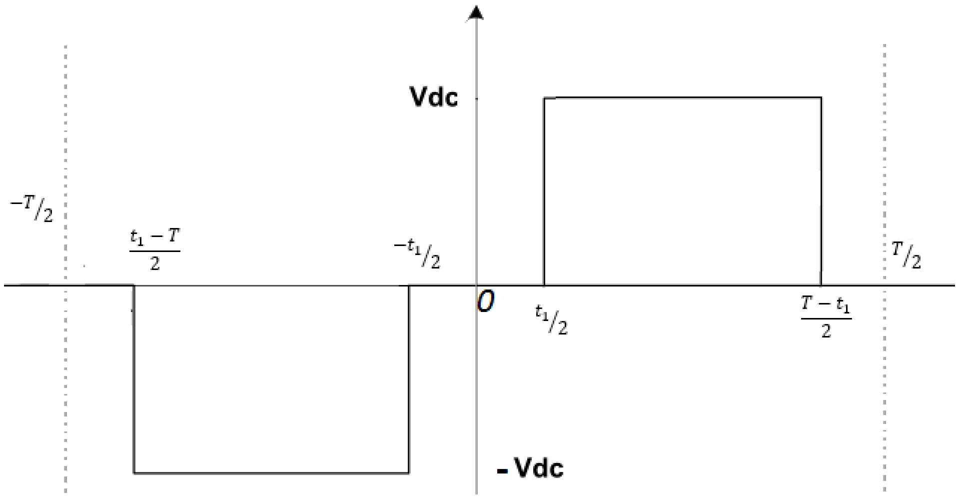

Figure 3.35-Signal of Figure 3.34 in different representation.

By putting (35) in (40), the expression in (41) is obtained. Not only b_K, but all the harmonic orders multiples of K, that is, all yK coefficients' orders, where y is an integer odd number, were eliminated.

$$b_k = \frac{4V_{dc}}{\pi k}\cos\frac{\pi k}{2K} \tag{41}$$

Besides the non-complete elimination of the overvoltage, other drawback of this solution is the reduction of the applied RMS voltage, which impacts the maximum power that can be transferred to the load. For the 1 kVA transformer, if this strategy is applied, the secondary RMS voltage value is reduced to 3.6 kV and output power to 899 W. When this strategy is used, it's necessary to redesign the transformer for the specific input voltage waveform.

The elimination of additional harmonics is possible, at the cost of increase the transistors switching frequency and the reduction of the fundamental component [54] [55] [56] [57] [58]. By chopping a square wave m times, using m+1 chopping angles in a quarter period, m chosen harmonics can be eliminated [57] [58]. Figure 3.36 shows the situation for two harmonics removing.

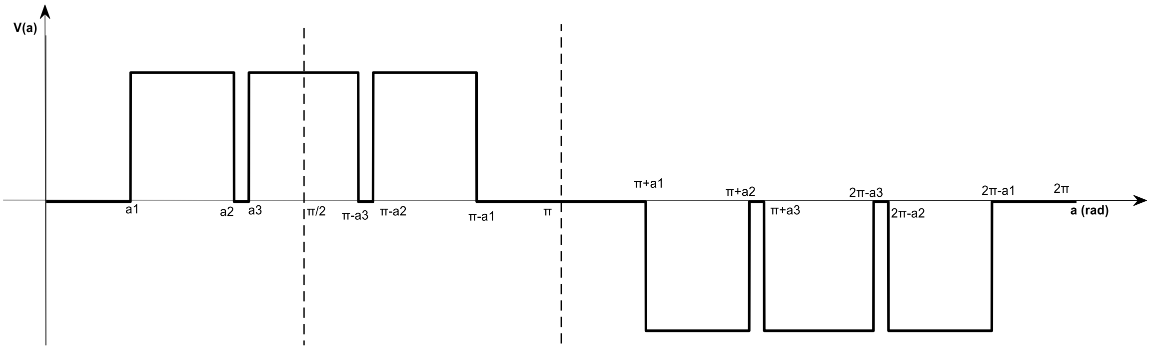

Figure 3.36-Primary waveform with three chop angles, to eliminate two harmonic components.

The Fourier series for the chopped waveform is given by (42) and the Fourier coefficients are given by (43). For the elimination of m harmonics, a nonlinear system of m equations with m variables is obtained, where the variables are the chopping angles.

$$V_{out}(\omega t) = \sum_{k=1}^{\infty} b_k \sin k\omega t \qquad (42)$$

$$b_k = \frac{4V_{dc}}{k\pi} \sum_{u=1}^{m} (-1)^{m+1} \cos k a_u \qquad (43)$$

There’s no analytical solution for such system, so a numeric iterative approach known as the Newton-Raphson method is generally used. In this method initial values for the chopping angles are guessed, and the values are updated in each iteration until a precision criteria for each angle be achieved. The direct disadvantage of this method is the divergence risk. In [57] a suggestion for the initial chopping angles guess is proposed but it’s not quite suitable for the elimination of a great number of harmonics.

Considering the elimination of two harmonics (Figure 3.36 case), like the 19th and 21st, the system in (44) is obtained, where *M* is the ratio between the fundamental component amplitude and the DC link. For a full square wave, *M* presents its maximum value of $^4/_\pi$, when harmonics are eliminated by notching the wave, *M* will decrease, because of the fundamental component reduction.

$$\begin{cases} \cos a_1 - \cos a_2 + \cos a_3 = M\,^{\pi}/_{4} \\ \cos 19a_1 - \cos 19a_2 + \cos 19a_3 = 0 \\ \cos 21a_1 - \cos 21a_2 + \cos 21a_3 = 0 \end{cases} \qquad (44)$$

Considering M = 1.26 ($3.96 / \pi$), the angles determined by solving (44) are:

$$\begin{cases} a_1 = 5.9^o \\ a_2 = 10.9^o \\ a_3 = 12.6^o \end{cases}$$

The waveforms for these harmonics' elimination in the 1 kVA transformer are showed in Figure 3.37. It can be seen the oscillation reduction at the secondary voltage, for the open load condition, due to the less harmonic content. Figure 3.38 shows the spectrum of the primary voltage, where it can be verified the desired harmonics elimination.

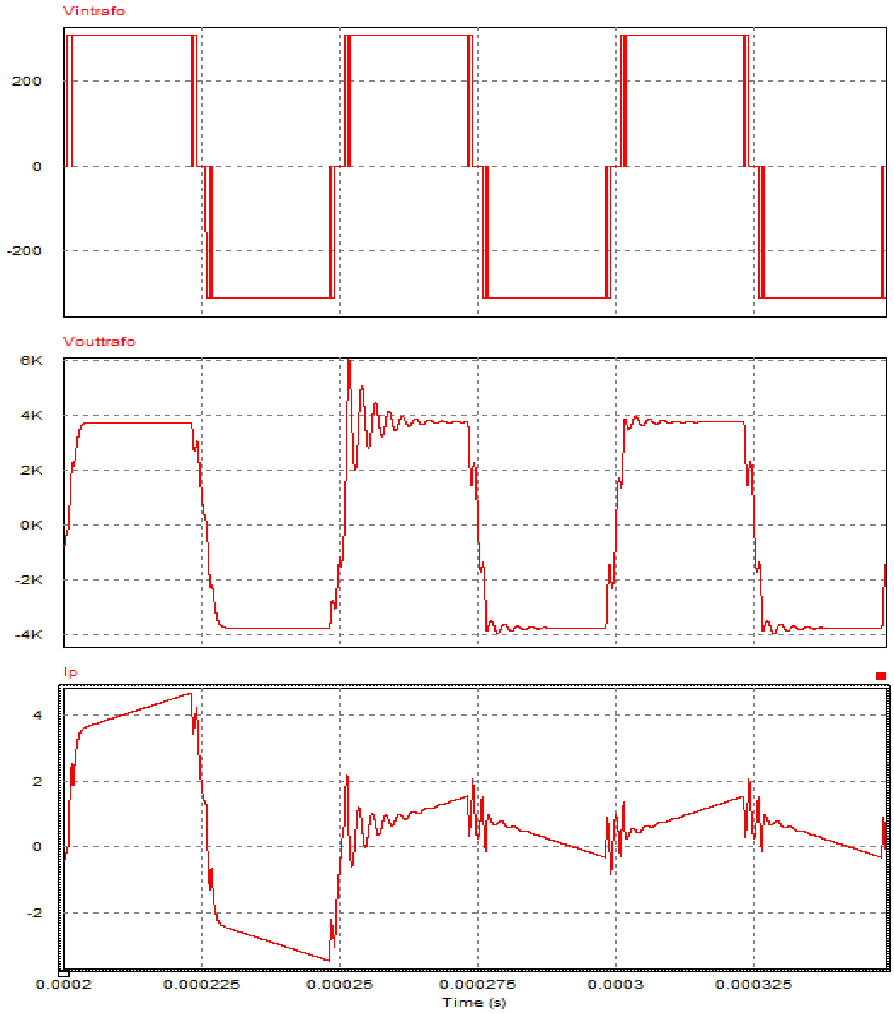

Figure 3.37 - Waveforms for the 1 kVA transformer with the 19th and 21st harmonics elimination. From top to bottom: Primary voltage, secondary voltage and primary current.

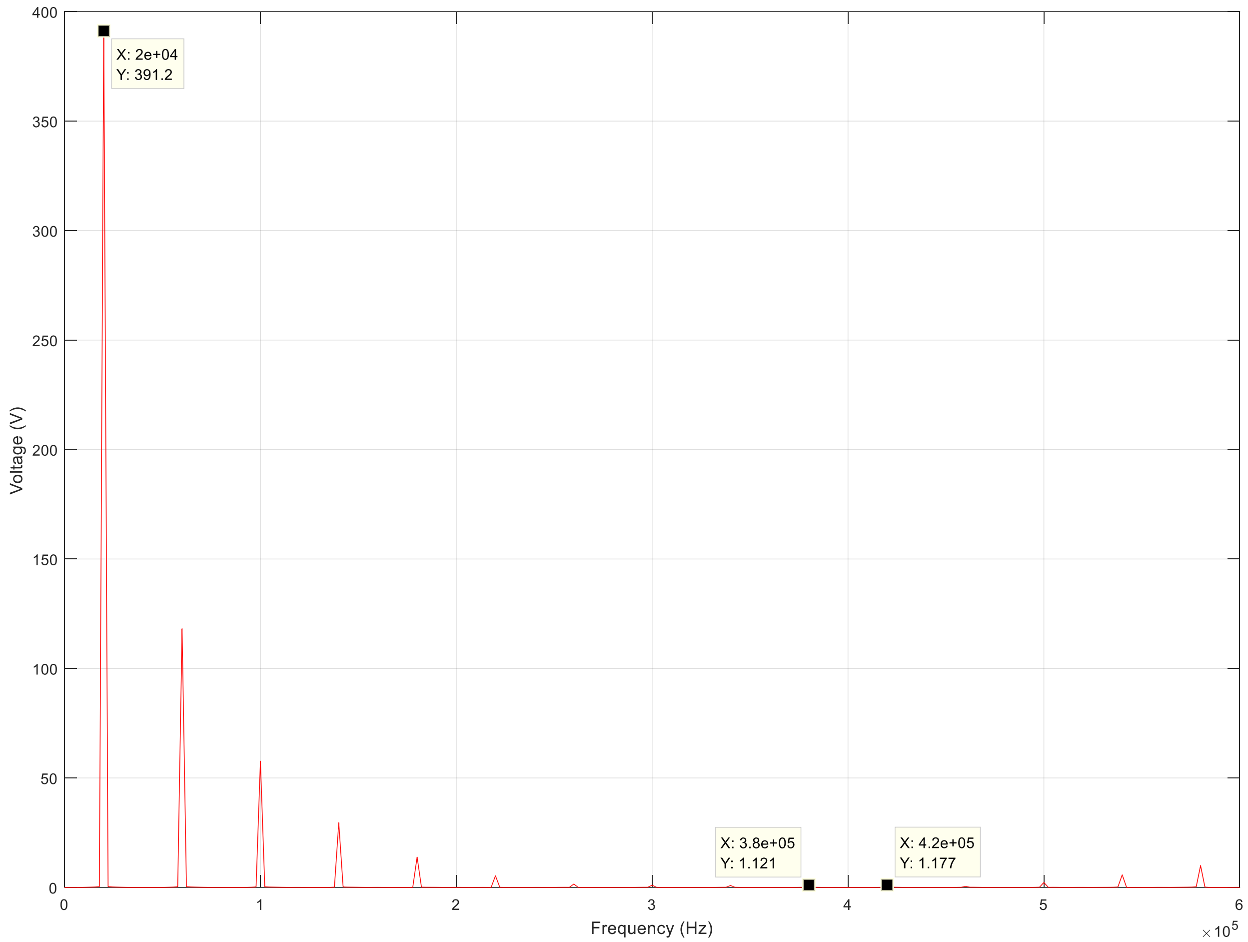

Figure 3.38-Spectral distribution for the primary voltage of Figure 3.37.

Figure 3.39 and Figure 3.41 show the waveforms eliminating respectively three and four harmonic components near the series resonance frequency, with the respective spectra in Figure 3.40 and Figure 3.42. The modulating index M was 1.236 $(3.88 / \pi)$ and 1.18 $(3.7 / \pi)$ respectively. The less harmonic content can be verified, as well as the voltage peaks reduction in the open load condition.

Table 5 shows a comparative analysis of the transformer output power for the different number of eliminated harmonics. The fundamental component amplitude is reduced with the elimination of additional harmonics, reducing the output voltage RMS value and, consequently, the output power. The secondary open load voltage peak is reduced in all cases. By comparing the tendency between the harmonics' elimination output power variation and the open load voltage peak reduction, it can be seen that the better compromising relationship is for the elimination of the two harmonics nearest the resonance.

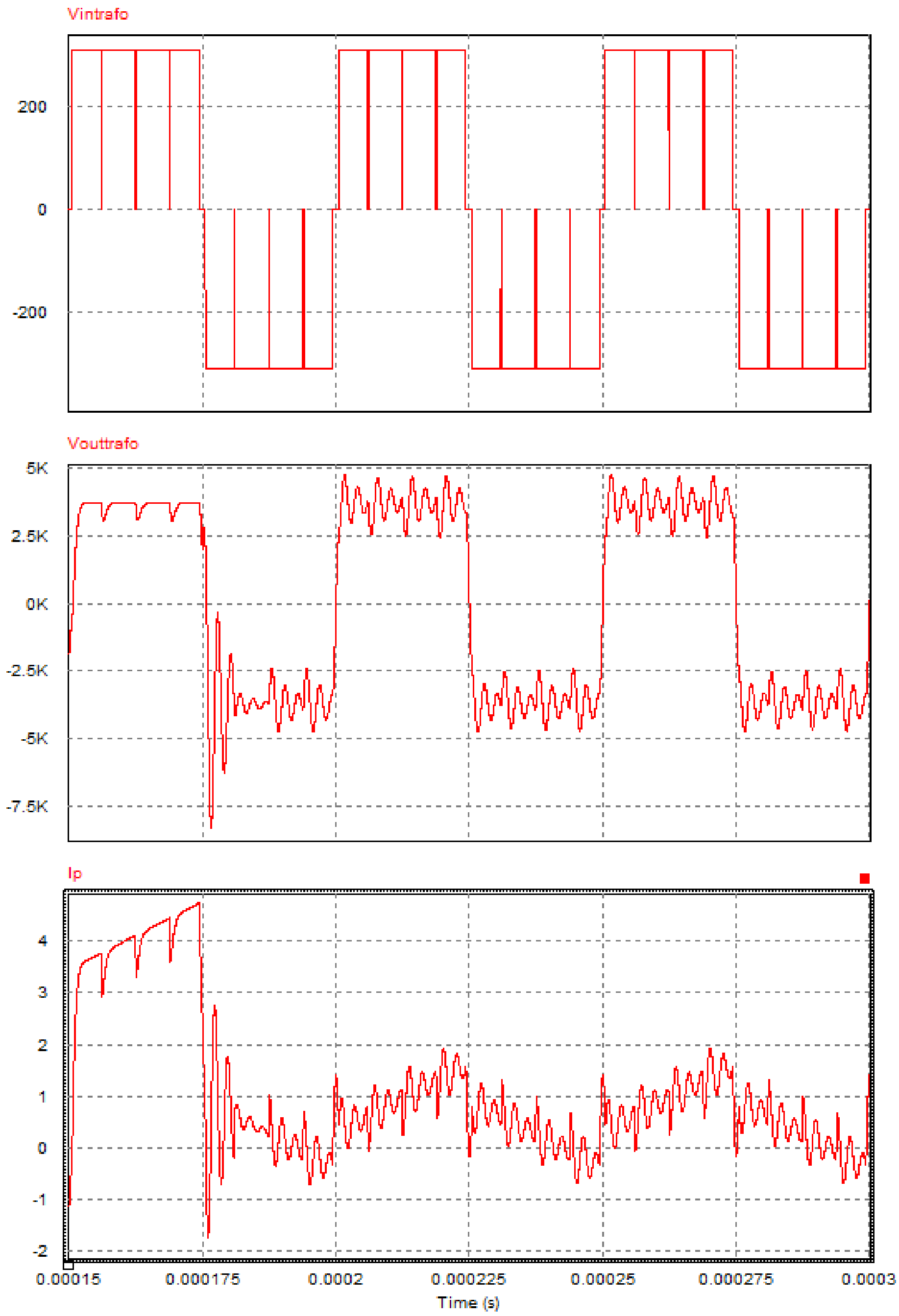

Figure 3.39 - Waveforms for the 1 kVA transformer with the 17th, 19th and 21st harmonics elimination. From top to bottom: Primary voltage, secondary voltage and primary current.

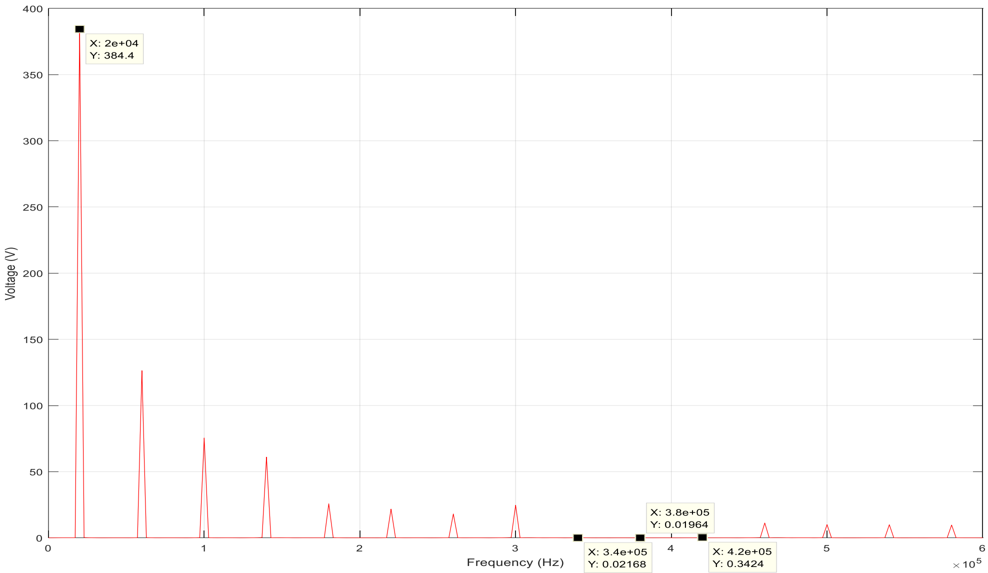

Figure 3.40 - Spectral distribution for the primary voltage of Figure 3.39.

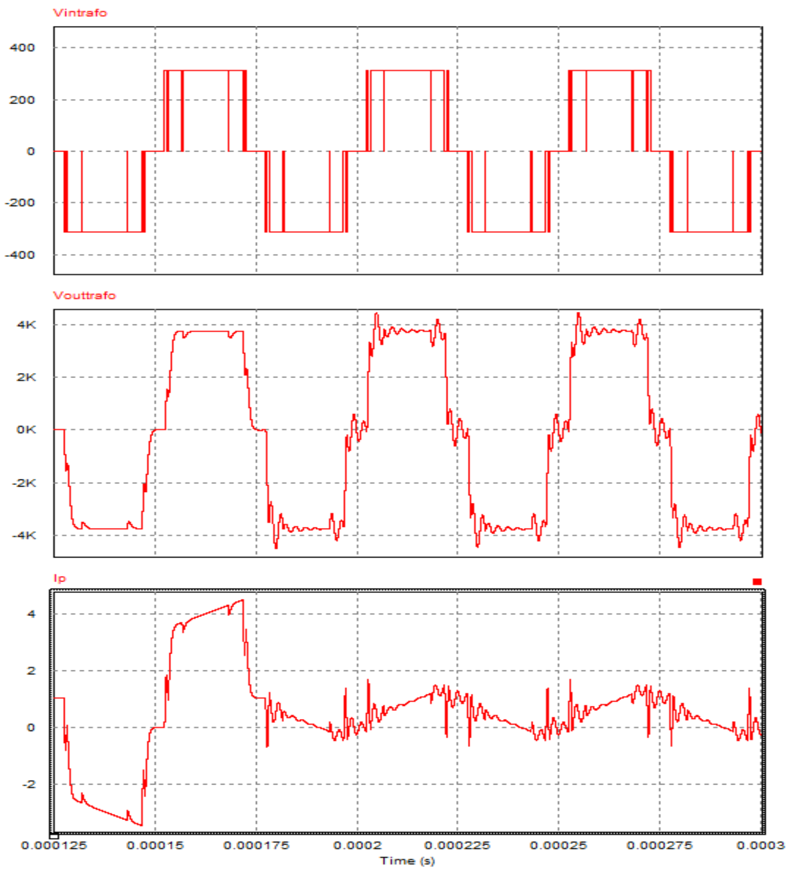

Figure 3.41 - Waveforms for the 1 kVA transformer with the 17th, 19th, 21st and 23rd harmonics elimination. From top to bottom: Primary voltage, secondary voltage and primary current.

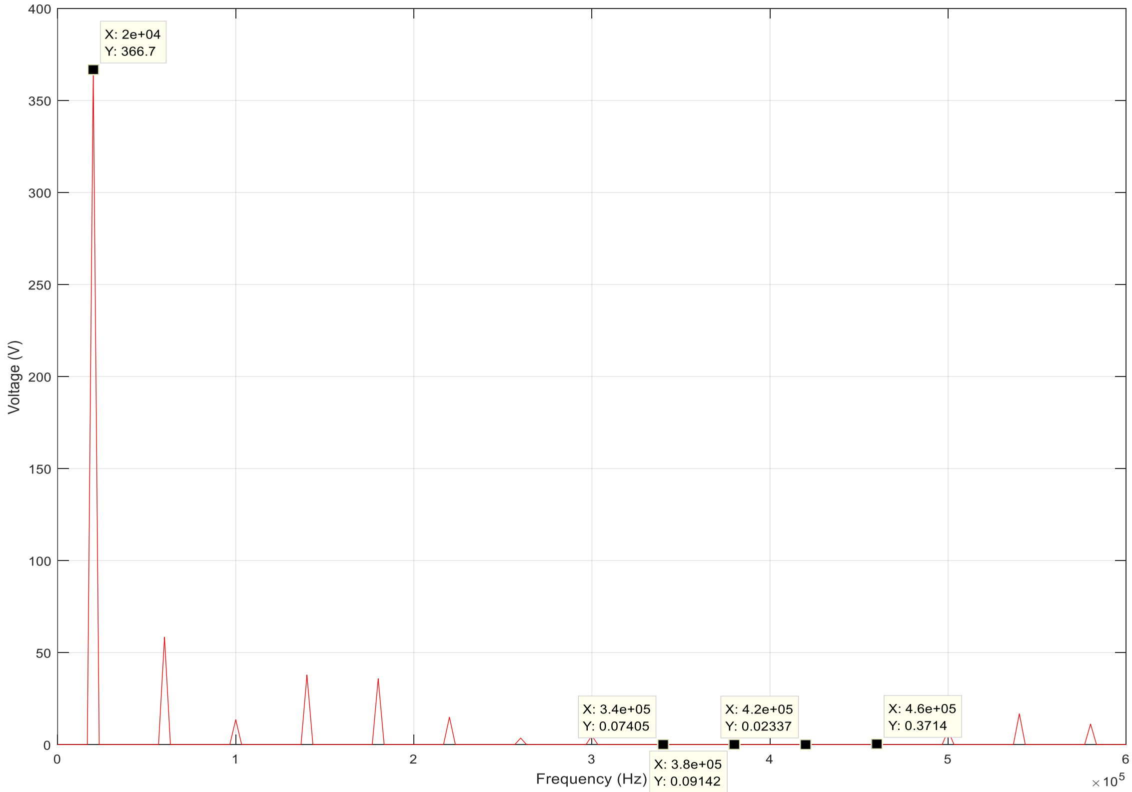

Figure 3.42 - Fourier analysis of the primary voltage of Figure 3.41.

Table 5- Comparison among the harmonic elimination technique for different number of eliminated harmonics.

Chopping angles	**Harmonics eliminated**	**Fundamental Component Amplitude (V)**	**Output RMS Voltage (kV)**	**Output power at nominal conditions (W)**	**Secondary open load voltage peak (kV)**
a1=8.57º	21st	394.9	3.6	899	4.5
a1=5.9º; a2= 10.9º; a3=12.6º	19th, 21st	391.2	3.5	854	3.94
a1=4.1º; a2= 43.1º; a3=44.4º; a4=89.4º	17th, 19th, 21st	384.4	3.5	865	4.77
a1=17.2º; a2= 20.4º; a3=23.8º; a4=48.8º; a5=49.2º	17th, 19th, 21st, 23rd	366.7	3.18	703	4.45

As a general approach, if the primary voltage waveform doesn't contain high frequency components, the resonance, perhaps will not be excited. One way to reduce the harmonic content is to produce a trapezoidal waveform or, at the limit, a sinusoidal waveform, instead of a rectangular or square wave. As the operation in the transistor active region is forbidden due to the losses, similar waveform only can be produced including an inductor or more complex circuitry in series with the primary, as a low-pass filter. However, the simplest alternative is the use of a single inductor. A combination of different strategies can also be applied, for example, eliminating a harmonic and using a voltage clamper, with reduced losses.

3.3.2 Overcurrent Protection Strategy

The primary overcurrent manifestation (besides the overcurrent presented in the magnetizing current due to the resonance excitation) happens when the load connected at the secondary side has a low resistance. The primary current must be monitored, so the converter is not damaged. Figure 3.43 shows the block diagram of the general overcurrent protection idea for the developing converter.

Figure 3.43-Overcurrent protection strategy general idea.

The primary current is measured, then a supervisory system verifies if the value is bellow a protective limit, and the converter operates normally. If an overcurrent is detected, the system is turned off immediately, turning off all the transistors. The current will flow through the diodes, until drops to zero.

As the load is variable, the overcurrent condition can be transient. So, after a while, the protection system verifies if the overcurrent event persists. If it seems to be permanent after some continuous verification (three, for example), the converter is permanently turned-off, and an alert signal is sent.

The primary current can be interrupted by different approaches, like turning off the inverter or disconnecting it from the transformer. The first can be made by interrupting the inverter switches' driving signals, and the second by putting a switch between the inverter and the transformer.

To implement the first approach a shunt resistor can be used to measure the inverter and so the primary current. The measured current is compared to a pre-determined limit. If so, the gate drive signals will be interrupted, turning off the inverter. This protection system is quite simple, and will be implemented in the 1 kVA converter, where the primary current is not so high, and the shunt resistor and circuitry necessary will not significantly change the general system dynamics. For the 3 and 10 kVA converter's version, a different protection system was developed, as shown in Figure 3.44. This protection system can also be applied in the development of a more powerful converter, with several transformers connected in parallel, fed by a single inverter [13] [47].

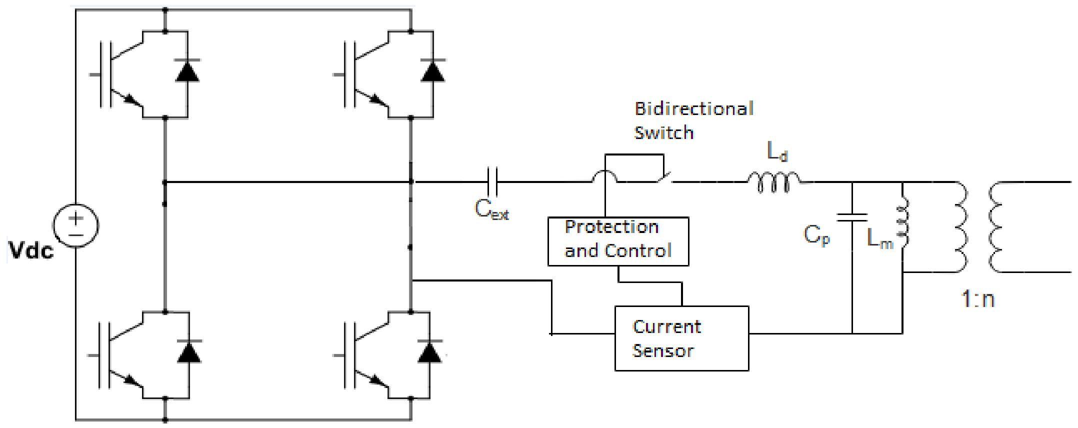

Figure 3.44-Overcurrent protection strategy based on an isolated current sensor and a bidirectional switch.

The primary current is measured by an isolated current sensor (as a Hall effect sensor), rectified and its value compared to a limit. If the current is above this limit, the protection and control system open the bidirectional switch. As the converter load is variable, maybe the overcurrent is temporary. A timer and a counter are activated. If the counter is not overflowed and the overcurrent situation disappears, the converter returns to its normal operation, if the counter is overflowed, what suggest that the short-circuit is permanent or will stay for a long time, the bidirectional switch opens permanently, sending an alert signal. The fluxogram for this overcurrent protection strategy is showed in Figure 3.45.

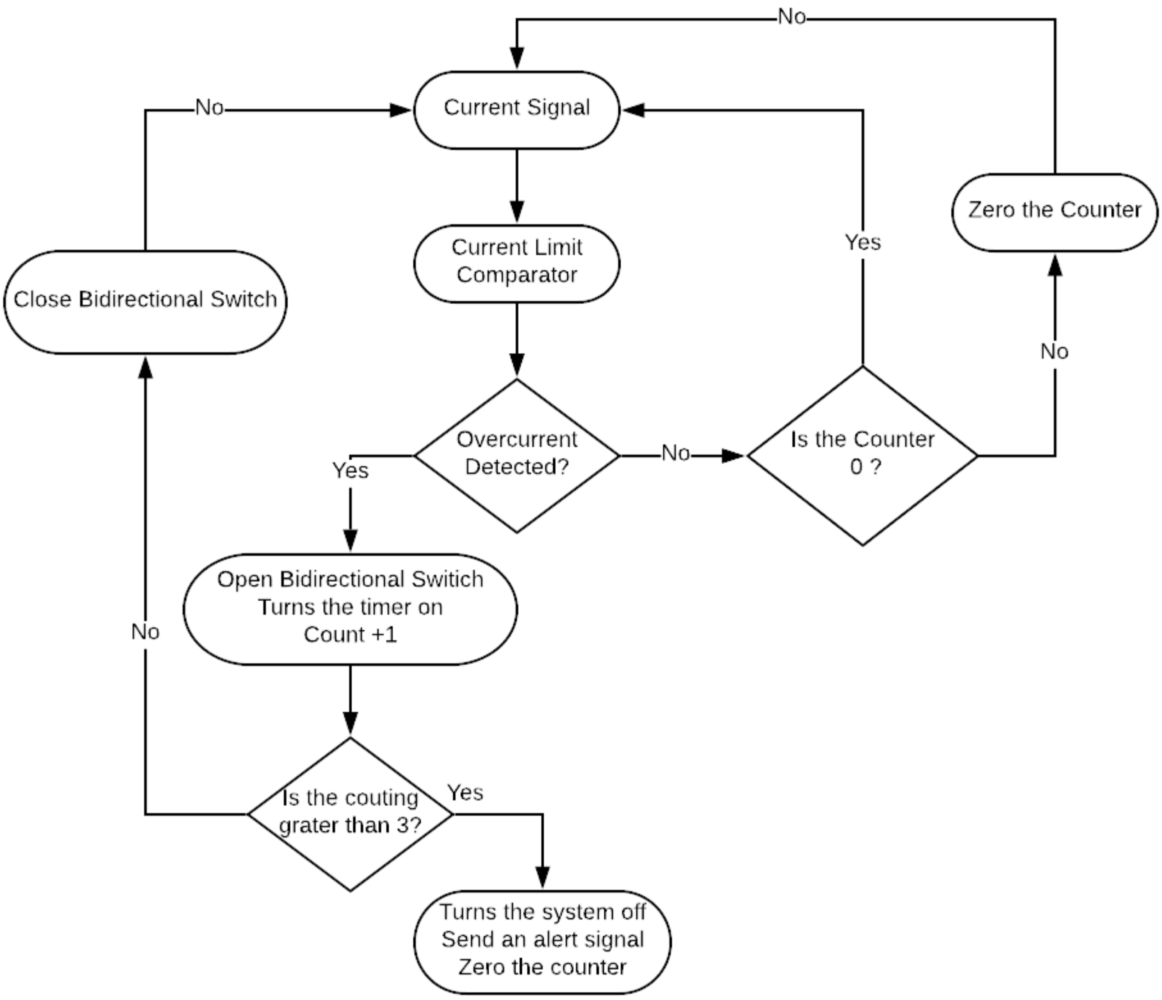

Figure 3.45 - Fluxogram for the overcurrent protection idea.

The current signal is converted to voltage and sent to a precision rectifier, as showed in Figure 3.46. The rectifier output is the input signal for a hysteresis comparator with a limit value determined by its reference value.

In the overcurrent occurrence, the comparator output changes its logical state, turning the timer on and opening the bidirectional switch. As the scale factor of the isolated sensor is high (like 1000:1 for example), the signal sent to the resistor is very small, that’s the reason why a conventional rectifier topology could not be used in this case, once the voltage drop on the diodes could compromise the correct protection system working.

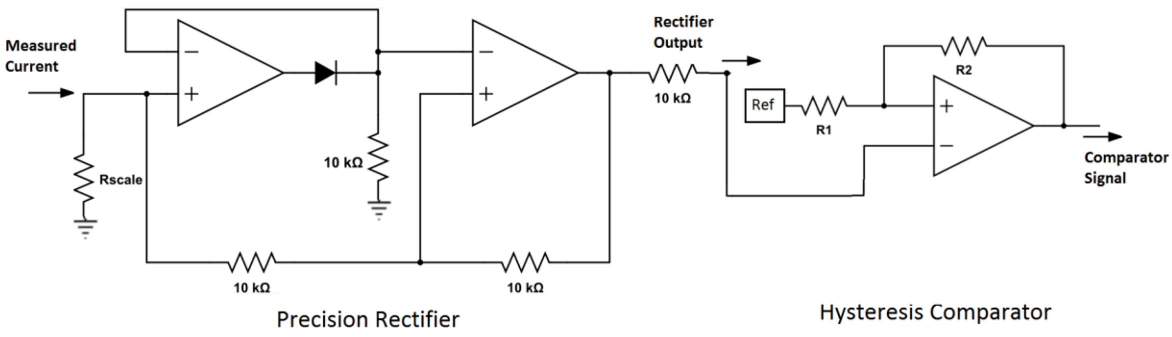

Figure 3.46-Measurement and monitoring circuits for the system represented by the fluxogram of Figure 3.44.

To implement the bidirectional switch [59] [60], two IGBTs are connected as in Figure 3.47. When the timer, that's going to be the enable signal, changes its logical state, the IGBTs gate signal is interrupted, taking them to the open circuit situation. The transistors association behaves as a controlled bidirectional switch. The RC snubber is used to absorb the energy delivered when the "inductive current" is interrupted, otherwise sparks could arise and damage the system.

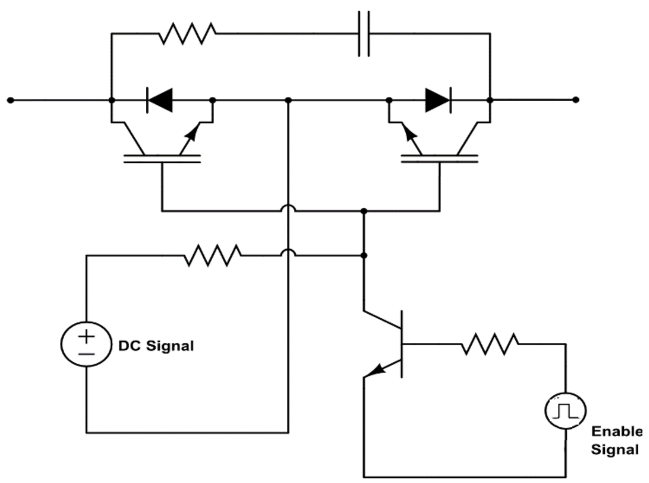

Figure 3.47-Bidirectional switch topology.

4 EXPERIMENTAL RESULTS AND ANALYSIS

To validate the theoretical calculations and the simulation analysis, experimental setups were built. Figure 4.1shows a block diagram of the system's main parts, Figure 4.2 shows the prototype for the 1 kVA converter feeding the resistive load, with its constituent parts identified according to Figure 3.8. Figure 4.3 shows the same converter, but with a more powerful inverter, and the external inductor and bidirectional switch already connected at the transformer primary.

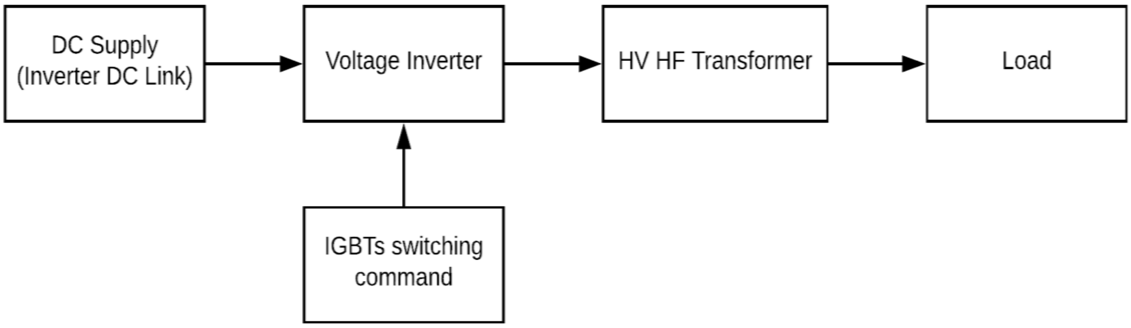

Figure 4.1 – System's general block diagram, identifying its main constituents.

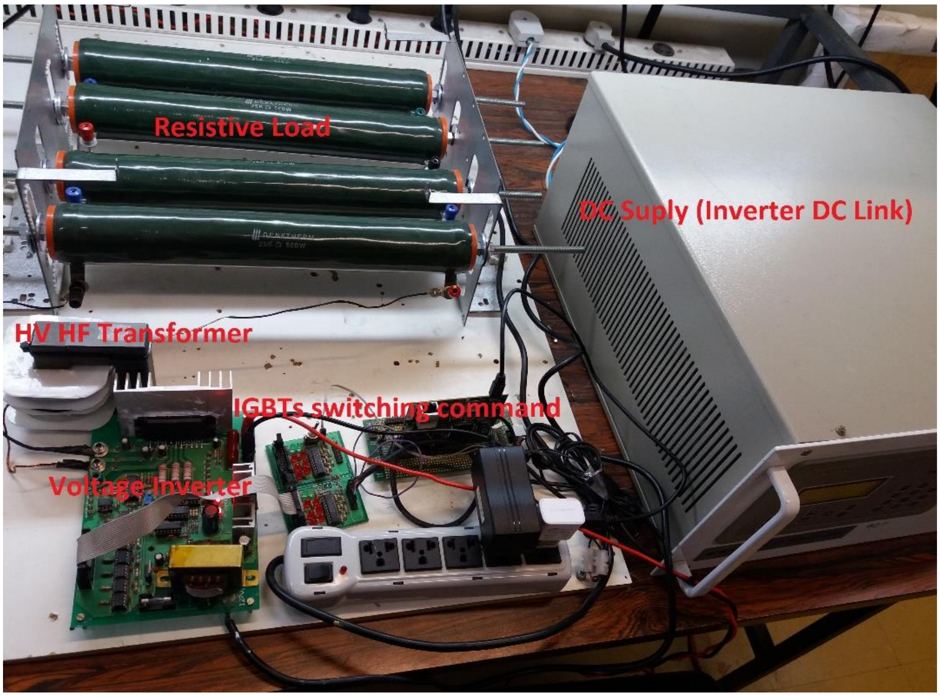

Figure 4.2 - Experimental setup for the 1 kVA version of the HV HF proposed converter.

Figure 4.3 - Experimental setup for the 3 kVA version of the HV HF proposed converter.

To measure the secondary voltage when the rated primary voltage is supplied, a High Voltage Probe Tektronix P 6015A was used [61]. This voltage probe has a relatively high capacitance (3 pF), that changes the resonance frequency to nearly 380 kHz for the 1 kVA transformer, and reduces the tank circuit impedance, increasing the current. Besides, there is a note in the probe instruction manual saying that for high frequency signal (as fast transients) ringing may occurs due to resonance between the probe's capacitance and the ground lead inductance, distorting the actual waveform [61]. Consequently, there will be some mismatches between simulation and experimental results. The voltage probes influence on the resonant behavior was already discussed in Figures 2.20 and 2.21.

4.1 1 KVA CONVERTER

Figure 4.4 shows the primary waveforms for the 1 kVA converter feeding a resistive load of 12.5 kΩ, for the same conditions of Figure 3.11, i.e., an inverter DC link of 311 V. The corresponding secondary voltage is shown in Figure 4.5. The waveforms have a well-defined square wave aspect, and the input power was almost 1.1 kW. The primary and secondary rms values were close to the expected, according to the transformer's specifications.

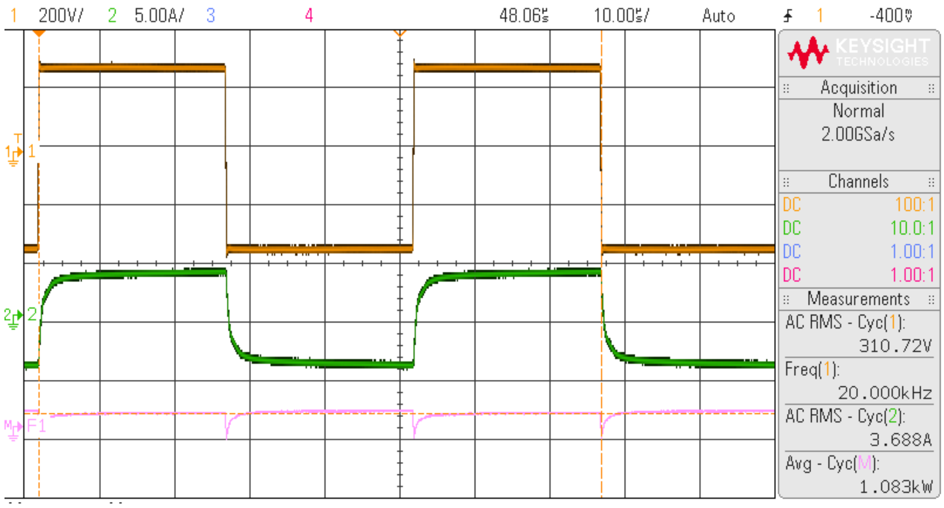

Figure 4.4 - Primary voltage (yellow), primary current (green) and input power (pink) for the 1 kVA converter feeding a secondary resistive load of 12.5 kΩ.

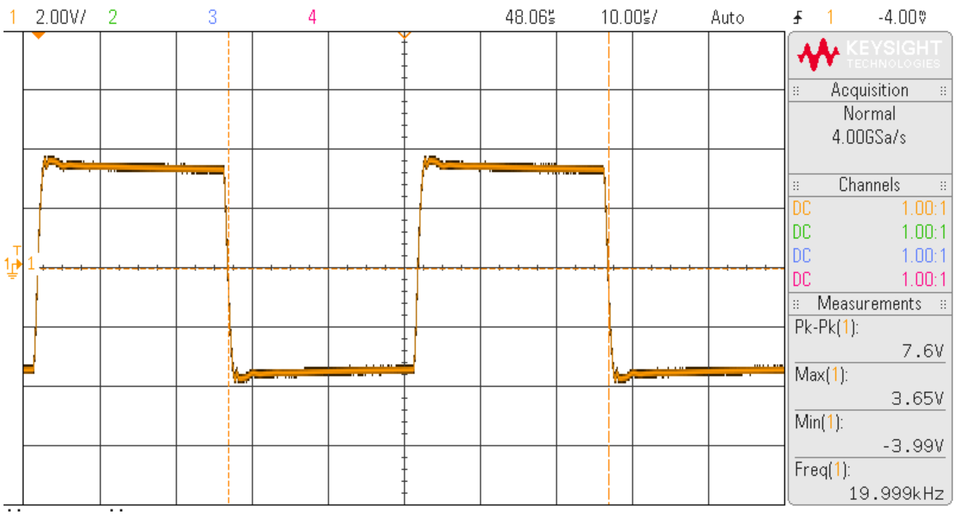

Figure 4.5 - Secondary voltage for the primary waveforms of Figure 4.4.

Figure 4.6 shows the primary waveforms for resistive loads of 25 kΩ and 50 kΩ, and Figure 4.8 the corresponding secondary voltages. Figure 4.7 shows the same waveforms for 75 kΩ and 100 kΩ, and Figure 4.9 the secondary voltage. As the resistive load value increases, the transformer secondary approximates to the open load condition, reducing the resonance damping and increasing the primary current and secondary voltage peaks. For a resistive load of 75 kΩ, the voltage peak is already two times the peak obtained in Figure 4.5.

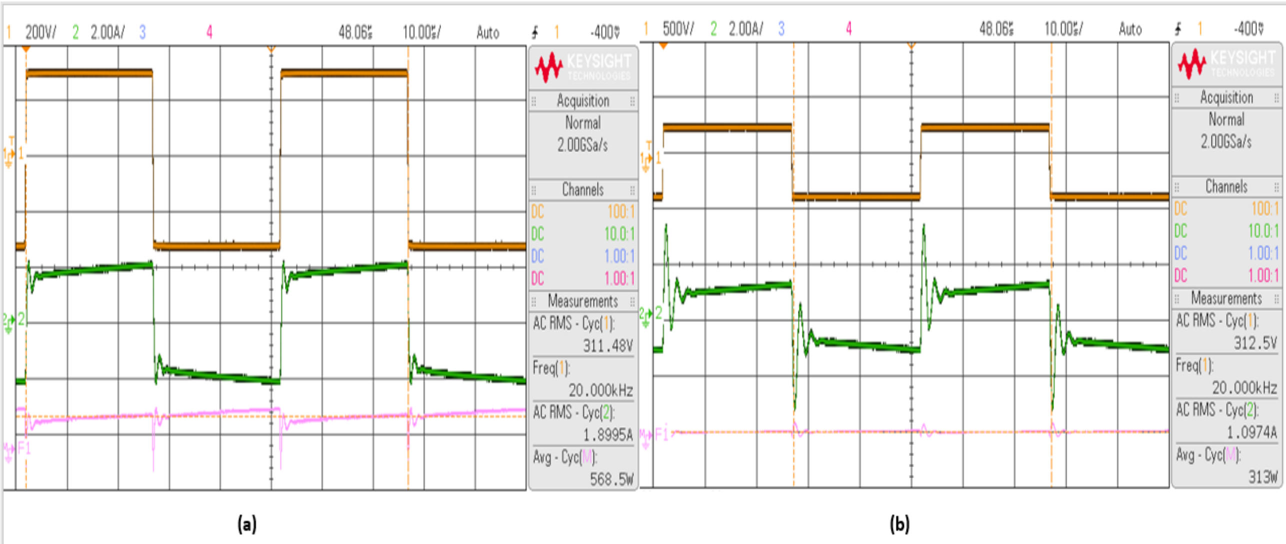

Figure 4.6- Primary voltage (yellow), Primary current (green) and input power (pink) for resistive loads of 25 kΩ (a) and 50 kΩ (b).

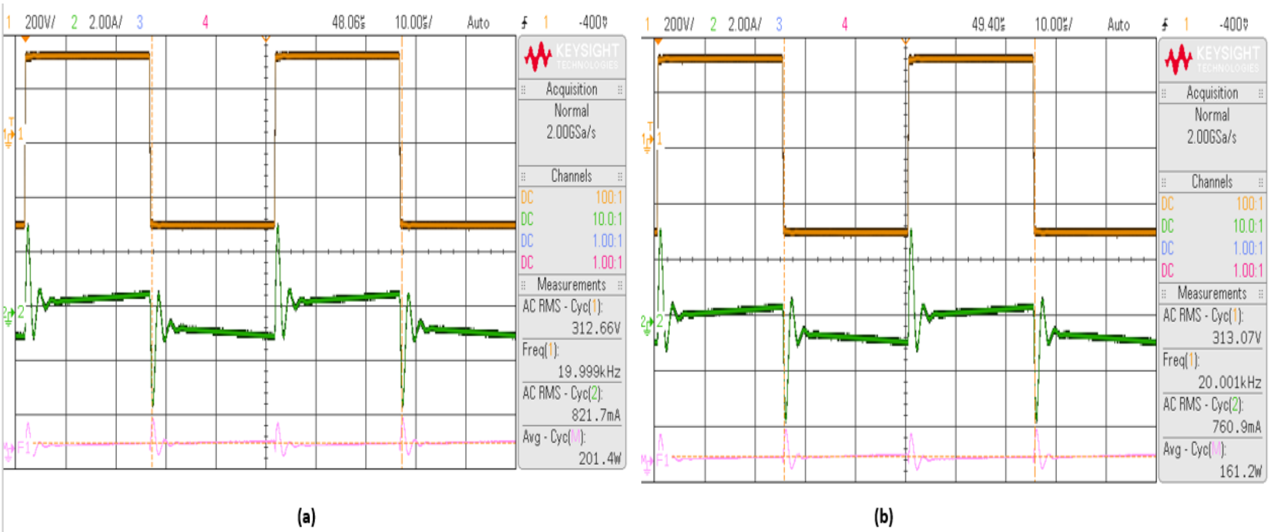

Figure 4.7 - Primary voltage (yellow), Primary current (green) and input power (pink) for resistive loads of 75 kΩ (a) and 100 kΩ (b).

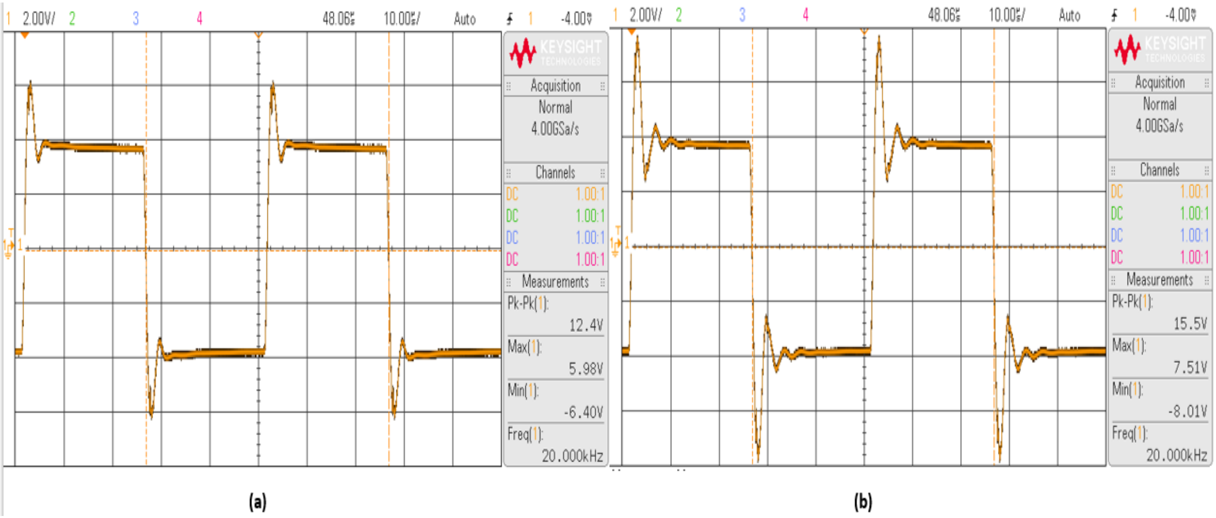

Figure 4.8 - Secondary voltages for the primary waveforms of Figure 4.5: Secondary loads of 25 kΩ (a) and 50 kΩ (b). Vertical scale 1:1000.

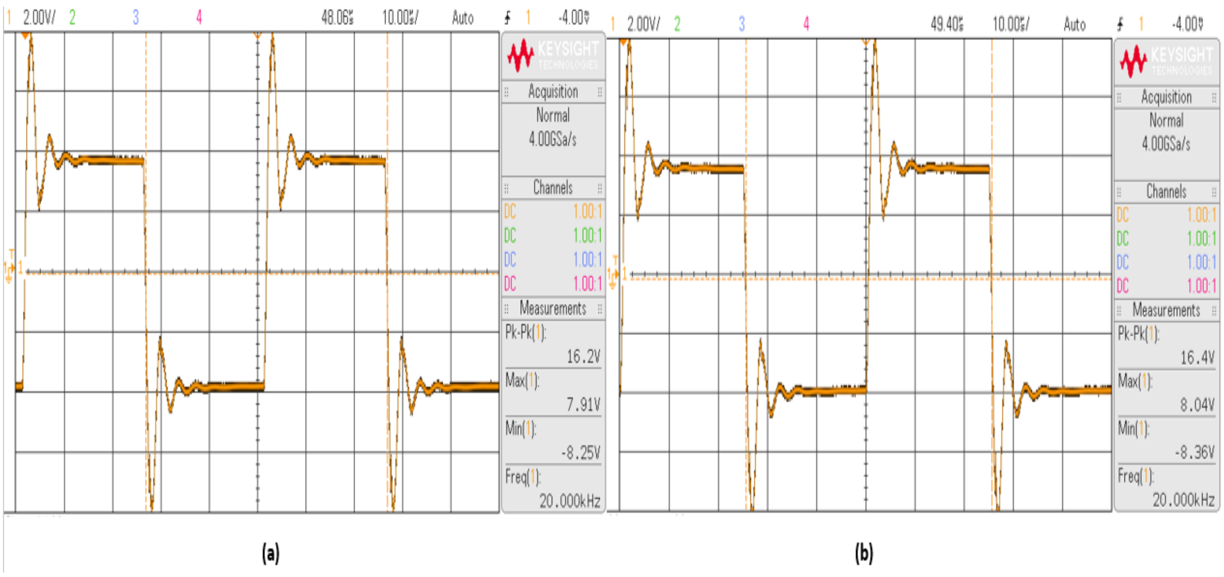

Figure 4.9 - Secondary voltages for the primary waveforms of Figure 4.6: Secondary loads of 75 kΩ (a) and 100 kΩ (b). Vertical scale 1:1000.

Table 6 shows a comparison between the simulated and measured input power. The error increases as the load approximates to the open load condition, but the difference between the measured and simulated values is almost constant and is probably due to transformer losses that were not accurately represented in the lumped model and are more evident for high resistive values. This loss is maybe associated to the thermal behavior, that was not considered in the modeling. As a matter of fact, the lumped model is only an approximation of the real phenomena, which is an “infinite” distribution of RLC branches.

Table 6 - Comparison between the simulated and measured input power.

Resistive Load (kΩ)	Simulated Power (W)	Measured Power (W)	Power Variation (W)	Error (%)
12.5	1169	1083	86	7.3
25	663	568.5	94.5	14.2
50	398	313	87	21.3
75	307	201	106	34.5
100	264	161.2	102.8	38.9

4.1.1 HV Clamper

The experimental setup with the high voltage clamper connected at the 1 kVA transformer secondary side is shown in Figure 4.10. To build the clamper’s capacitor, 5 high voltage capacitors of 4.7 nF available at the lab were connected in parallel and 30 kV diodes were used for the diode bridge. For the clamper’s resistance 6 resistors of 22 kΩ and 7 resistors of 100 kΩ were connected in series. The primary waveforms for the open load condition with the HV rectifier are shown in Figure 4.11 and the corresponding secondary voltage in Figure 4.12.

The secondary voltage peak was nearly 4.5 kV, 19 % more than the nominal peak and 12.5 % higher than the expected from the analytical calculations. The measured waveforms show the effectiveness of this strategy and validate the simulation results obtained in Figure 3.19. The total power dissipated in the primary windings for this strategy was 56.2 W, 5.62% of the transformer’s nominal power and are the losses added by the clamper’s resistor.

Figure 4.10 - Experimental setup for the HV Clamper strategy.

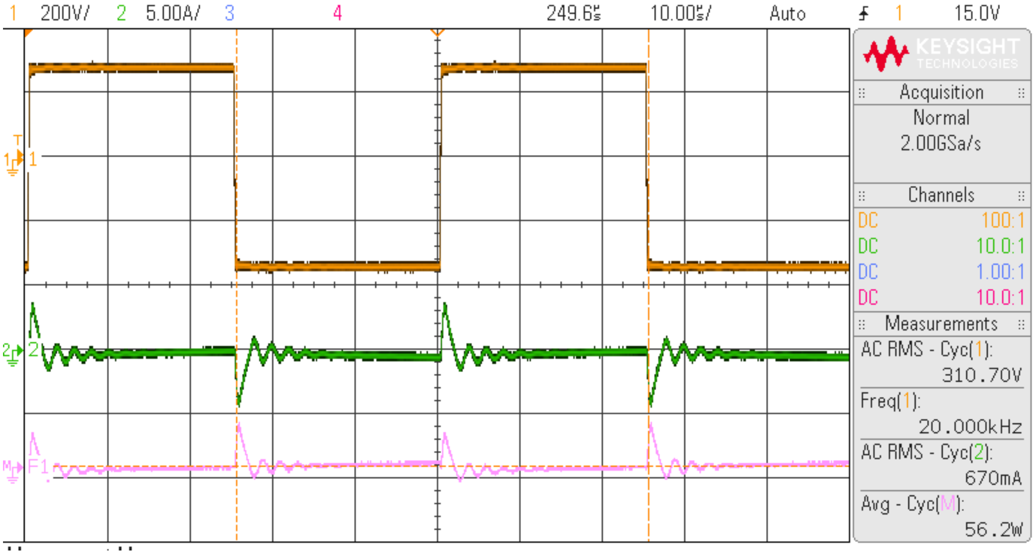

Figure 4.11- Primary waveforms for the setup of Figure 4.10. From top to bottom: Primary voltage (yellow), primary current (green) and input power (pink).

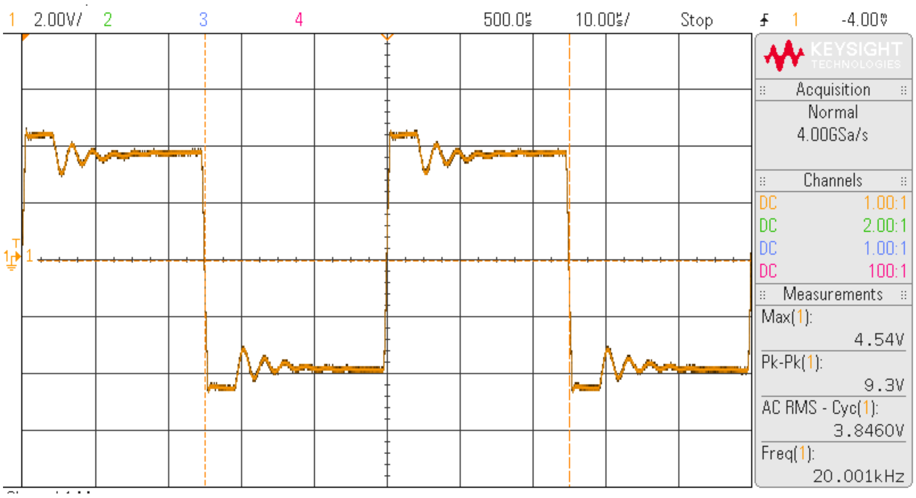

Figure 4.12 - Secondary voltage for the situation of Figure 4.11. Vertical scale 1:1000.

The primary waveforms for the feeding of resistive loads of 12.5 kΩ and 25 kΩ with the clamper are shown in Figure 4.13 and the corresponding secondary voltage in Figure 4.14. The primary current and secondary voltage had their aspect a little changed, because of the dynamics added by the clamper. The input power is higher compared to Figures 4.3 and 4.5, because of the power loss in the clamper.

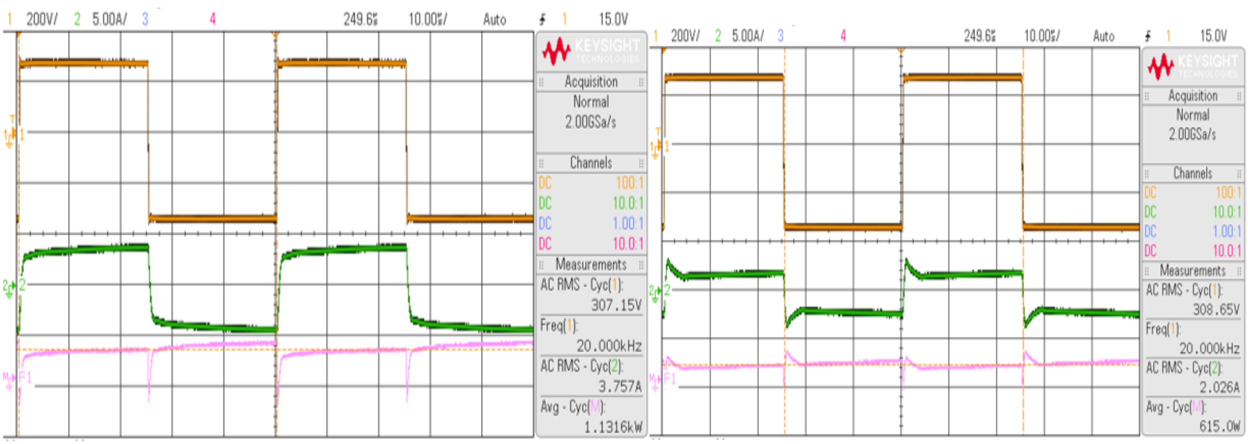

(a) (b)

Figure 4.13 - Primary waveforms for the 1 kVA converter feeding resistive loads with the clamper connected: Secondary loads of 12.5 kΩ (a) and 25 kΩ (b).

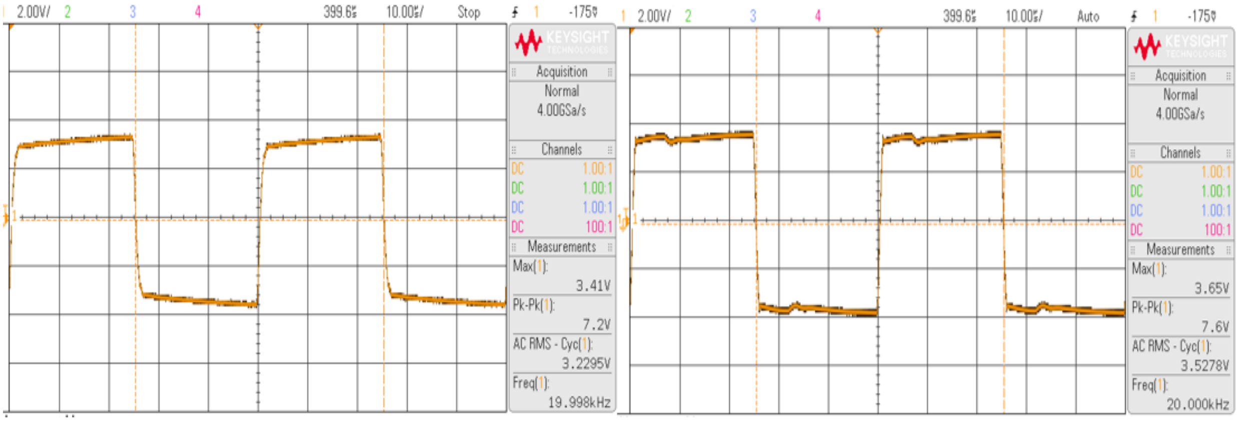

(a) (b)

Figure 4.14 - Secondary voltage corresponding to the waveforms of Figure 4.13: Secondary loads of 12.5 kΩ (a) and 25 kΩ (b).

4.1.2 External Inductor

A prototype for the external inductor strategy is shown in Figure 4.15 and the primary waveforms and the corresponding secondary voltage are shown in Figures 4.16 and 4.17, respectively. The experimental waveforms validate the external inductor simulation results, presented in Figure 3.23 and Table 2. The secondary voltage peak was 4.5 kV, 19% more than the nominal value. The primary input power loss in this case was only 10.2 W.

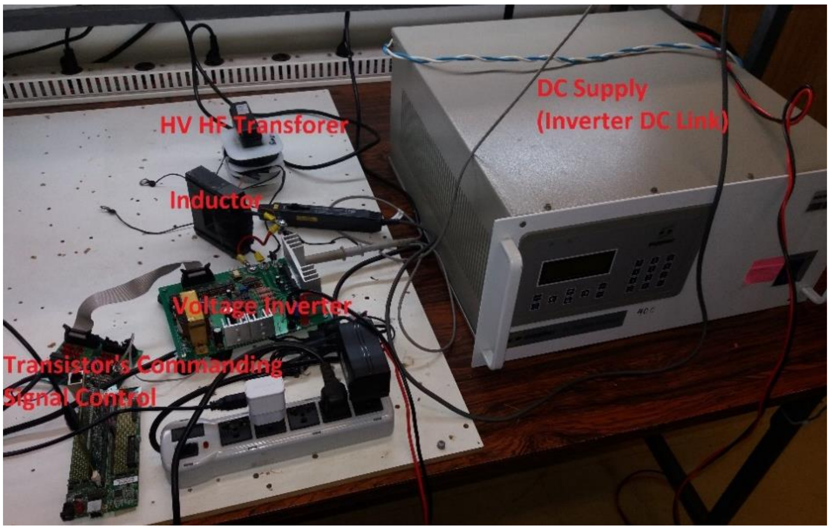

Figure 4.15- Experimental implementation of the external inductor strategy.

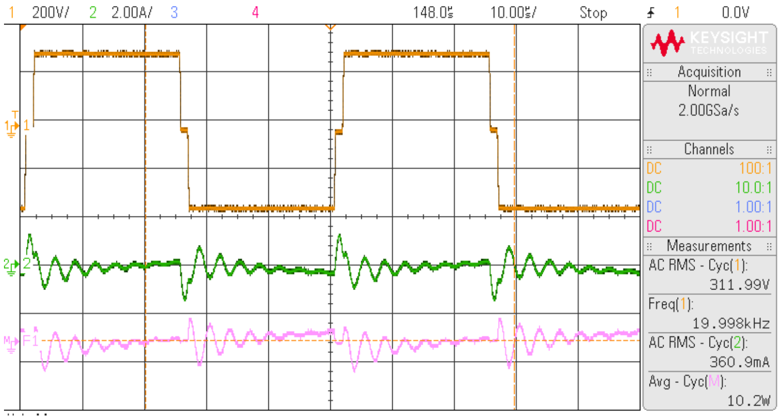

Figure 4.16 - Primary waveforms for the external inductor strategy.

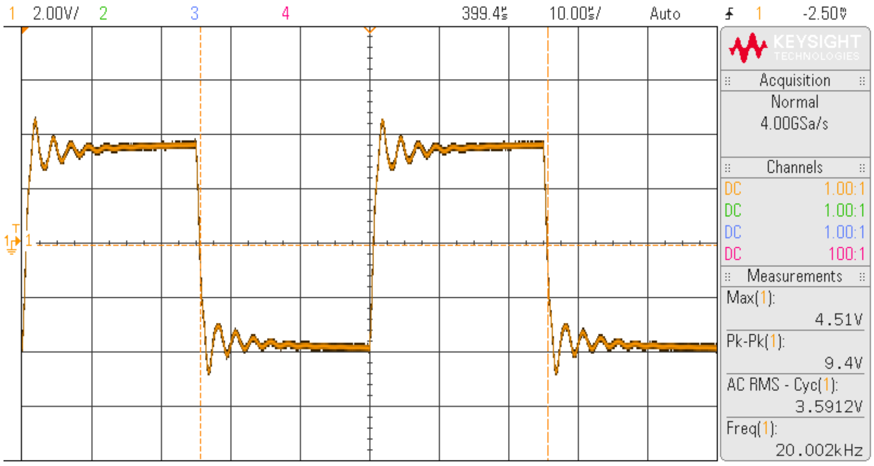

Figure 4.17 - Secondary voltage for the external inductor strategy.

The primary waveforms for the resistive loads feeding are shown in Figure 4.18, with the corresponding secondary voltages at Figure 4.19. The primary waveforms have the “dead-time” introduced by the inductor charging, as expected by the simulation results of Figure 3.24. The primary RMS voltage and current are reduced, reducing the transferred power, being the reduction higher for low resistive loads values, once the system presents an inductive behavior more evident in these cases. The power transferred to 12.5 kΩ and 25 kΩ were 879.5 W and 529.8W respectively, 18.8% and 7% less than the same situation without the external inductor.

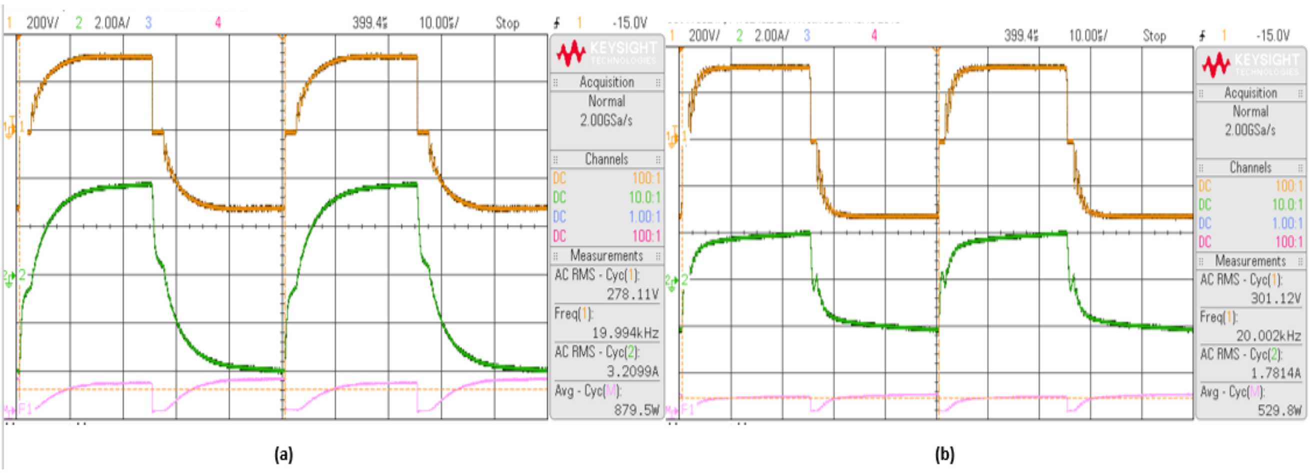

Figure 4.18 - Primary waveforms for the 1 kVA converter feeding resistive loads with the external inductor connected: Secondary loads of 12.5 kΩ (a) and 25 kΩ (b).

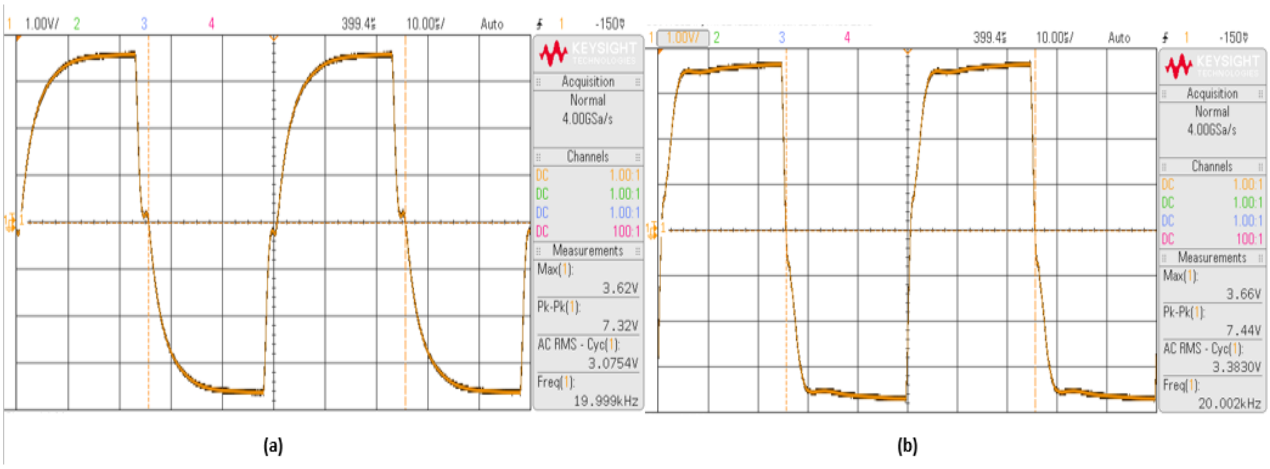

Figure 4.19 - Secondary voltage corresponding to the waveforms of Figure 4.18: Secondary loads of 12.5 kΩ (a) and 25 kΩ (b).

4.1.3 Harmonic Elimination

Figure 4.20 shows the primary waveforms for the selective harmonic elimination and Figure 4.21 the corresponding secondary voltage. The output wave form oscillation was reduced, due to the less harmonic content at the primary voltage, and the secondary open load voltage peak was 4.3 kV, 13% more than the output nominal value, showing the effectiveness of this strategy to protect the system against the overvoltage peaks and validating the simulation results of Figure 3.32. The primary input power loss was 17.6 W for this strategy.

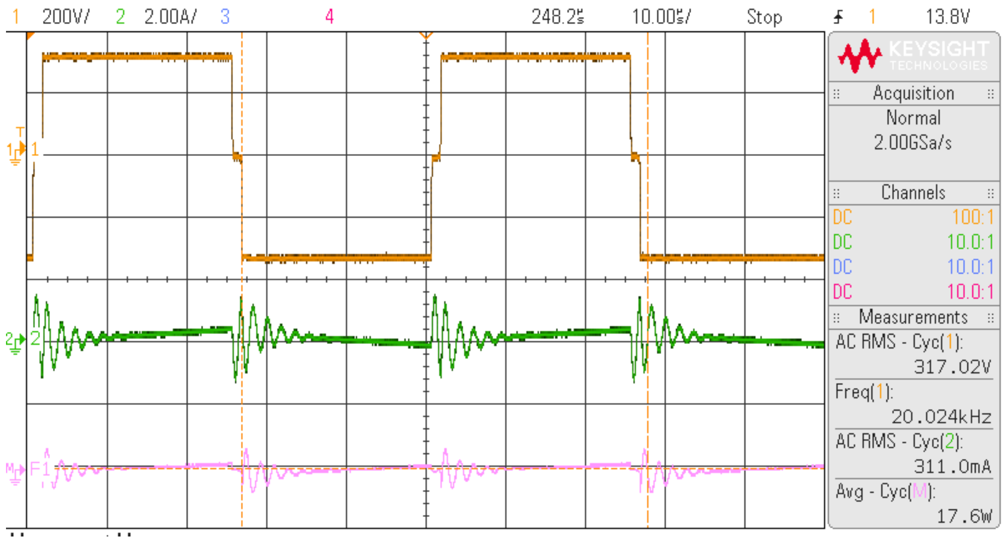

Figure 4.20 - Primary waveforms for the selective harmonic elimination.

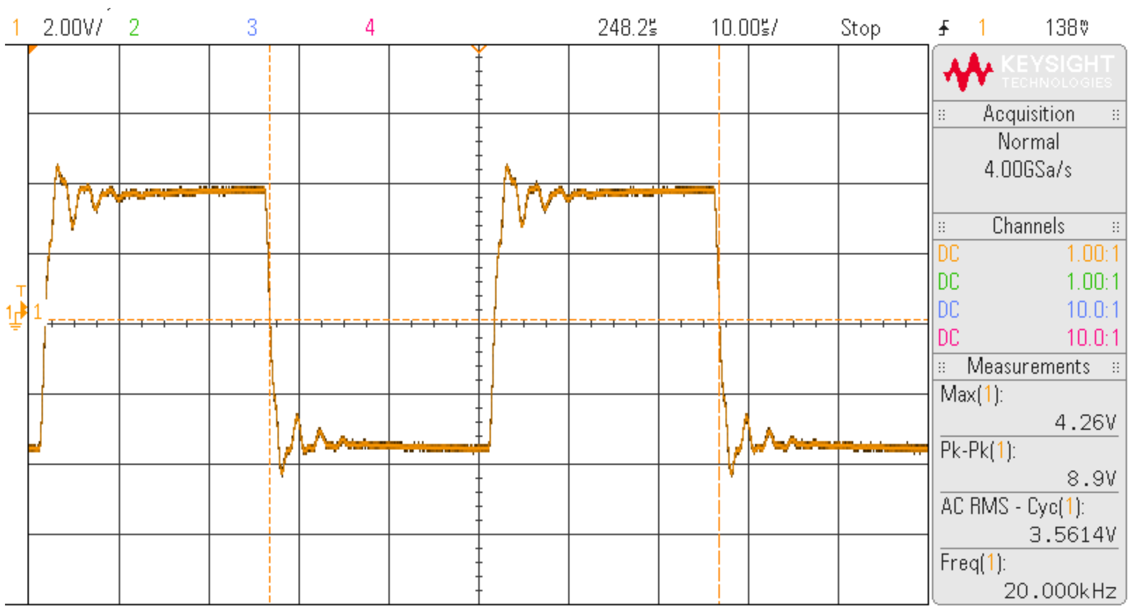

Figure 4.21- Secondary voltage for the situation of Figure 4.20.

Figure 4.22 shows the primary waveforms with the selective harmonic elimination feeding resistive loads, and Figure 4.23 the corresponding secondary voltage. The transferred power for 12.5 kΩ were 955 W, 11.8% less than the case with a full square-wave. The power reduction for 25 kΩ was not so expressive.

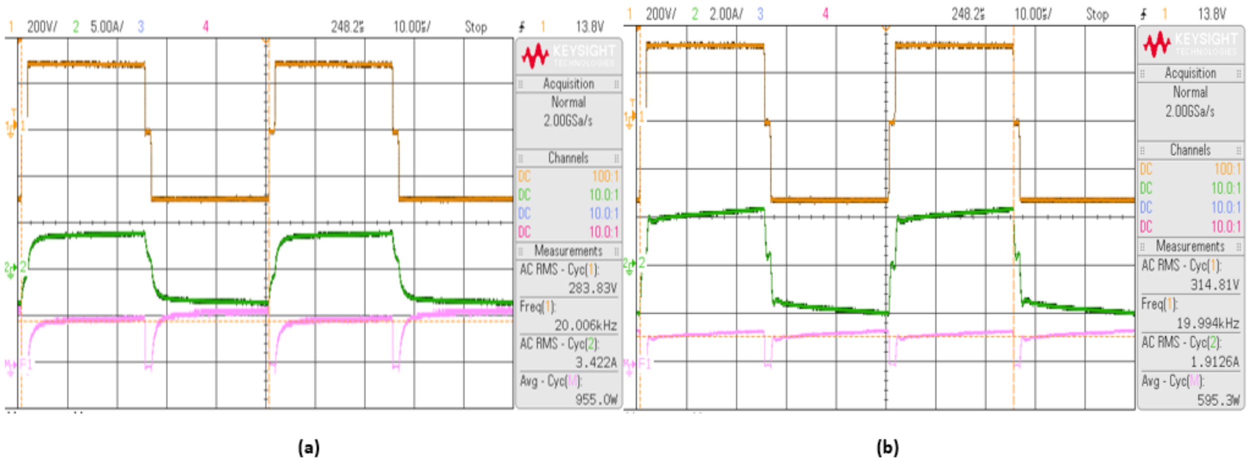

Figure 4.22- Primary waveforms for the 1 kVA converter feeding resistive loads with the SHE implementation: Secondary loads of 12.5 kΩ (a) and 25 kΩ (b).

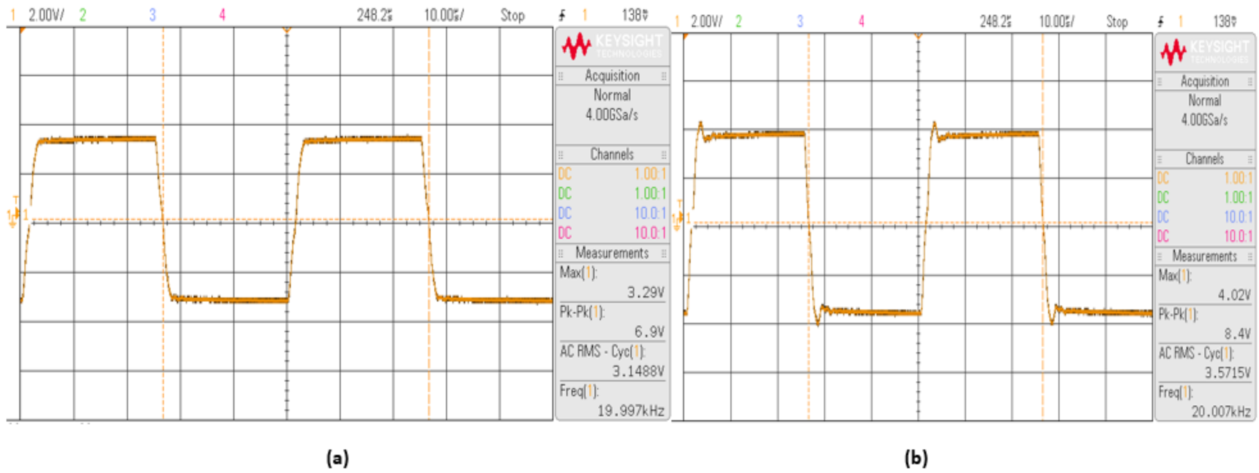

Figure 4.23- Corresponding secondary voltages for the primary waveforms of Figure 4.22: Secondary loads of 12.5 kΩ (a) and 25 kΩ (b).

4.2 3 KVA CONVERTER

The parameters values for the 3 kVA transformer are shown in Table 7, they were estimated using the same procedure described in section 2.2 and exemplified in section 2.4 for the 1 kVA transformer.

Table 7 – Estimated parameters values for the 3 kVA transformer.

Parameter	**Value**
n	20.14
Rd	0.126 Ω
Ld	5.99 µH
Lm	2.52 mH
Rp	880 Ω
fp	47 kHz
fs	822 kHz

The primary waveforms for the 3 kVA converter considering resistive loads of 13 kΩ and 25 kΩ connected at the transformer's secondary are shown in Figure 4.24 and the corresponding secondary voltage in Figure 4.25. The inverter's DC link is 311 V and the waveforms RMS values are next to the expected by the transformer's specifications. The power delivered to the first and second loads were about 2.7 kW and 1.5 kW, respectively, practically the same obtained by simulation results.

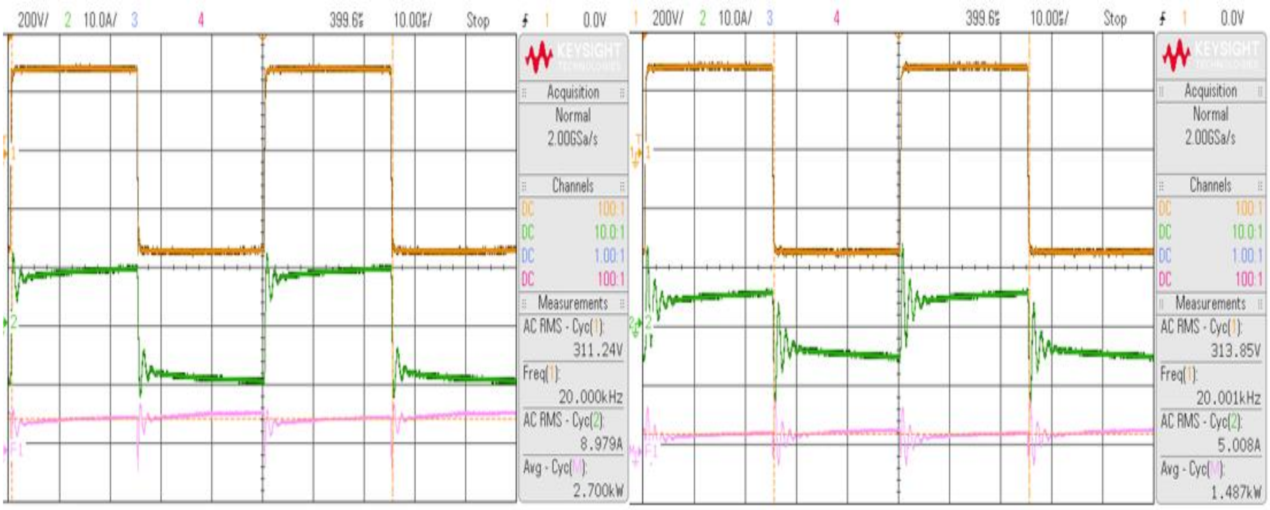

(a) (b)

Figure 4.24 - Primary waveforms for the 3 kVA converter feeding different secondary resistive loads: 13 kΩ (a) and 25 kΩ (b).

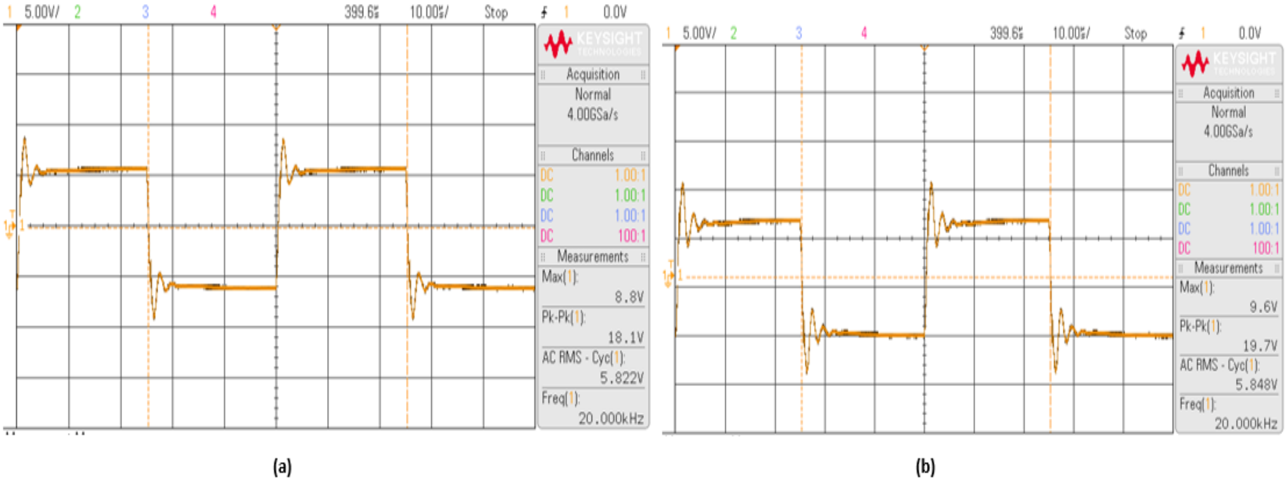

Figure 4.25 - Secondary voltage corresponding to the waveforms of Figure 4.24: Secondary loads of 13 kΩ (a) and 25 kΩ (b).

Figure 4.26 shows the voltage waveforms at open load condition for the 3 kVA system, with a reduced primary voltage, for an inverter's DC link of 30 V. The expected peak-peak voltage at normal operation for the conditions of Figure 4.26 is 1.3 kV and it was 2.13 kV due to the resonance. Operating like that the "effective voltage ratio" is practically 33.3 at such frequency, so for the nominal primary voltage, the secondary voltage peak is nearly 10.4 kV, 65% more than the expected at normal operation.

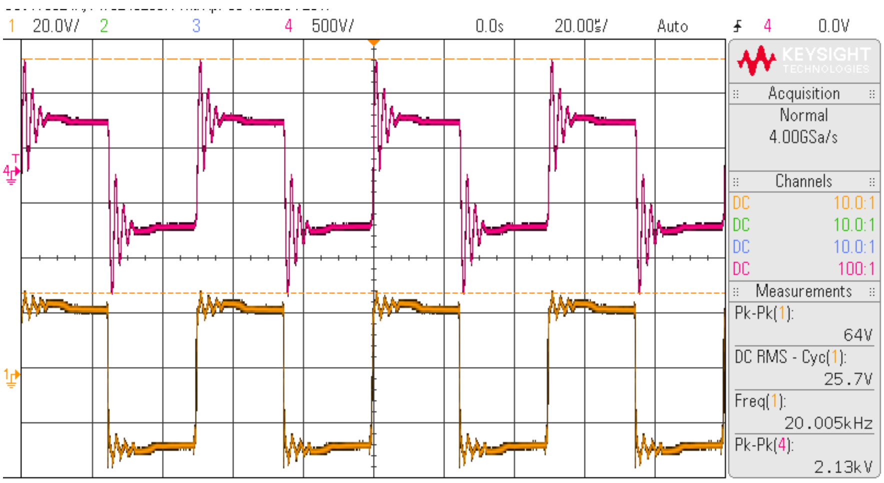

Figure 4.26 - Voltage waveforms for the 3kVA transformer open load condition, with a reduced primary voltage. From top to bottom: Secondary voltage (purple) and primary voltage (yellow)

4.2.1 External Inductor

Figure 4.27 shows the primary waveforms for the open load condition, and the corresponding secondary voltage is shown in Figure 4.28. The secondary voltage peak was almost the same as expected at normal conditions. The power dissipated at the primary side was 44 W, 1.5% the transformer's nominal power. The external inductor performance was better for the 3 kVA transformer in terms of the overvoltage reduction, once this transformer has lower leakage inductance than the 1 kVA.

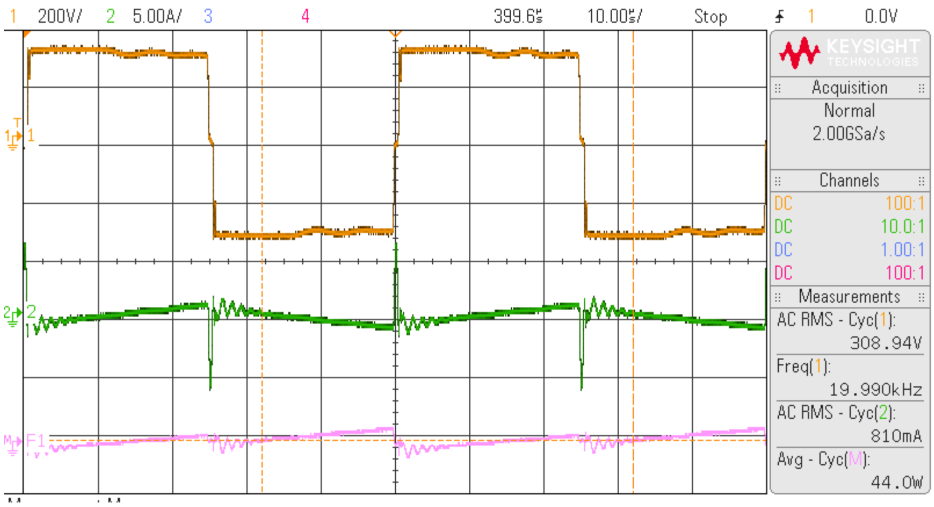

Figure 4.27- Primary waveforms for the 3 kVA converter at open load condition with the external inductor.

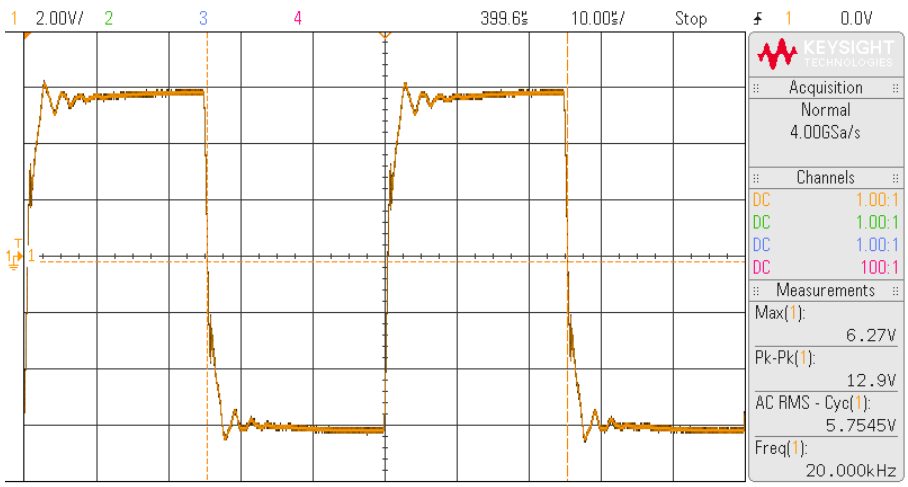

Figure 4.28- Secondary voltage for the 3 kVA transformer at open load condition with the external inductor.

Figure 4.29 shows the primary waveforms for the same situation of Figure 4.24 with the external inductor connected, and Figure 4.30 the corresponding secondary voltage. The waveforms square-wave aspect is affected, due to the high value of the series external inductance (almost 23 times the transformer's leakage inductance).

The power delivered for 13 kΩ and 25 kΩ were 1.27 kW and 1 kW, respectively, only 47% and 62.7% than the same conditions without the external inductor. The less power transferring is due to the voltage and current rms values reduction, caused by the external inductor strategy dynamics.

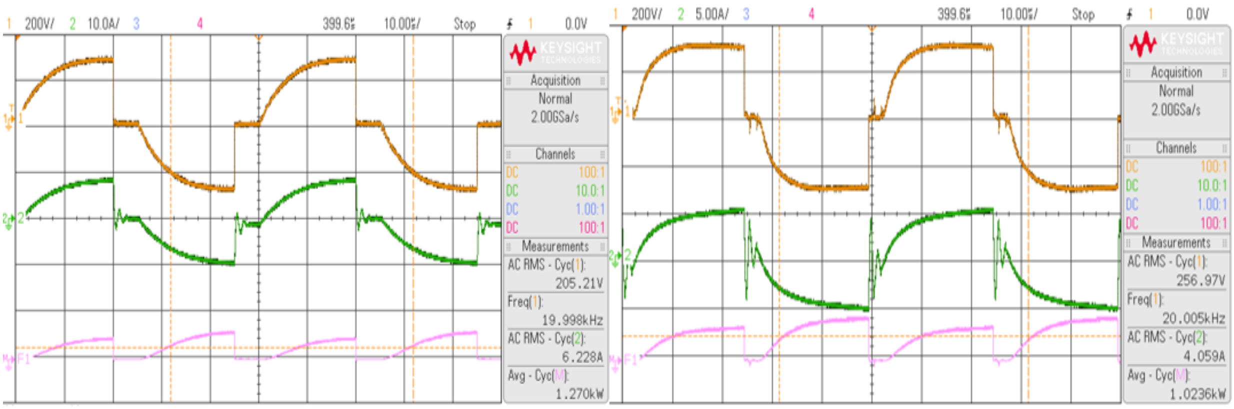

(a) (b)

Figure 4.29 - Primary waveforms for the 3 kVA converter with the external inductor feeding different secondary resistive loads: 13 kΩ (a) and 25 kΩ (b).

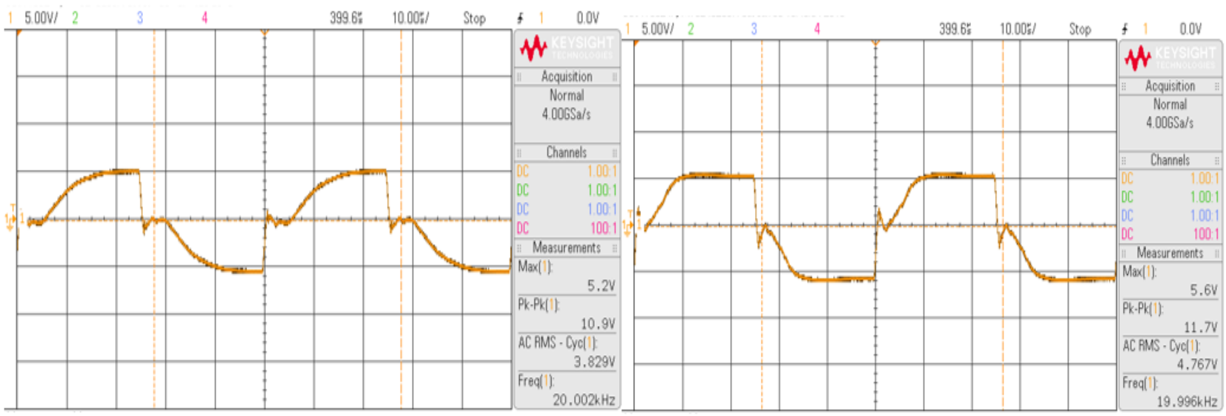

(a) (b)

Figure 4.30 - Secondary voltage corresponding to the primary waveforms of Figure 4.29: Secondary loads of 13 kΩ (a) and 25 kΩ (b).

4.2.2 HV Clamper and Harmonic Elimination

Table 8 shows the clamper components for the 3 kVA transformer, according to the overvoltage admissible. The capacitances are too high, expensive and difficult to obtain for the frequency and voltage level necessaries. Besides, the diodes must be fast enough to respond at the resonant period and support the voltage levels, which are higher than for the 1 kVA transformer.

Table 8-Parameters of the HV Clamper according to the overvoltage admissible

Overvoltage (kV)	Clamper Capacitor	Clamper Resistor
0.2	1.72 uF	1.2 MΩ
0.5	688 nF	480 kΩ
1	344 nF	240 kΩ
2	172 nF	120 kΩ

The series resonance happens near 820 kHz for the 3 kVA transformer, so the harmonic to be eliminated is the 41st. As this harmonic happens in an elevated order, it won’t significantly damp the overvoltage. Figure 4.31 shows the simulated secondary voltage with the 41st harmonic eliminated. The voltage peak is still almost 10 kV. The elimination of additional harmonics won’t help in the overvoltage reduction, as already showed for the 1 kVA transformer and because of the high frequency location of the resonance.

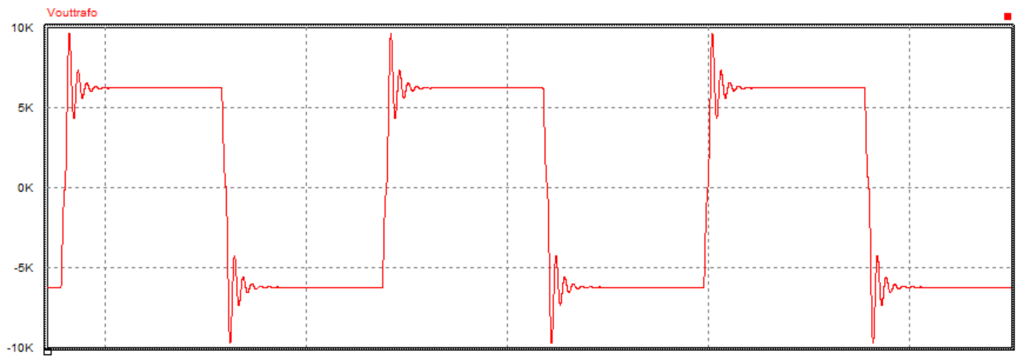

Figure 4.31- Secondary voltage for the elimination of the 41st harmonic from the input voltage of the 3 kVA transformer.

4.2.3 Overcurrent Protection System

The overcurrent protection system as described in Figure 3.45 was implemented in the form of two electronic boards. The first implementation had the bidirectional switch according to the configuration shown in Figure 3.47, as well as the DC source, a Hall effect current sensor and the decoupling capacitor C_{ext}. The schematic for this board is shown in Figure 4.32 and the corresponding PCB in Figure 4.33.

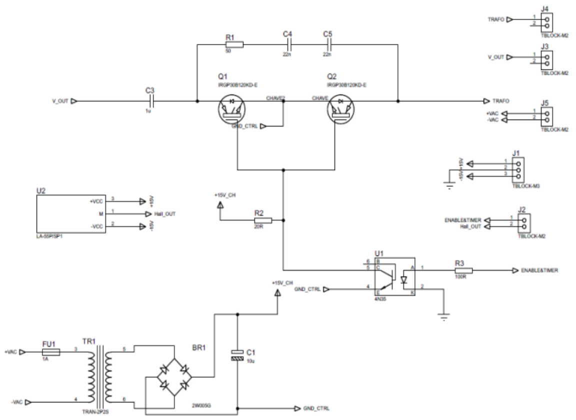

Figure 4.32- Schematic for the switches electronic circuit board.

Figure 4.33- PCB for the schematic of Figure 4.27.

The second board has the protection circuit described in Figure 3.46 and the timer that is the enable signal for the switches. Figure 4.34 shows the schematic for the protection system, and Figure 4.35 the corresponding PCB.

The protection board receives the measured current signal from the switches board and monitors if the current peak overcomes a specified limit. The limit established for testing the circuit with the 3 kVA converter is 20 A.

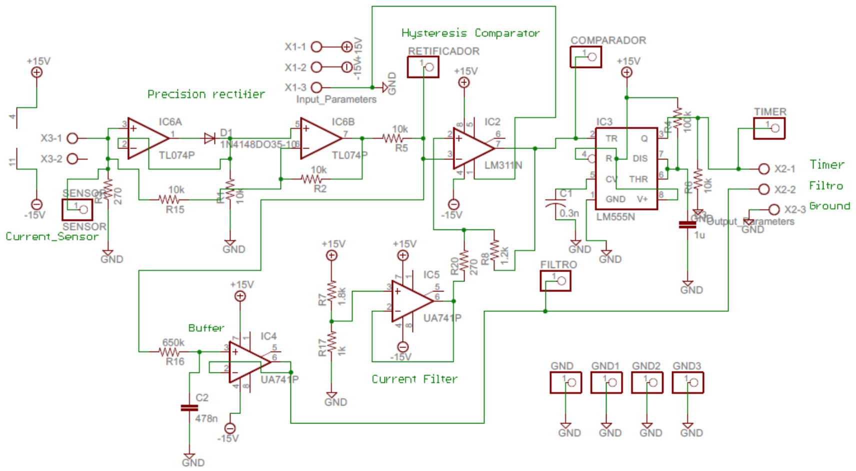

Figure 4.34 - Schematic for the protection system electronic circuit board.

Figure 4.35 - PCB for the schematic of Figure 4.29.

Figure 4.36 shows the primary voltage and current when the protection system activates. Although the showed value is 10 A, the value measured by the Hall sensor is 20 A, once the primary conductor passes two times through the sensor, what was made to prove the system’s working and good calibration in a more safety way.

The current was interrupt as expected, showing the effectiveness of this protection system for overcurrent protection. As the current is oscillatory, the system tries to turn on again every half-cycle, when the peak is again achieved, and the protection activates again, as showed by the little pulses presented in Figure 4.36.

This protection system has the advantages of easy implementation and calibration, and the isolated measurement of the current sensor. Nevertheless, the system may be sensitive to electromagnetic interference. The implementation of the parallel version of this converter will enable this analysis.

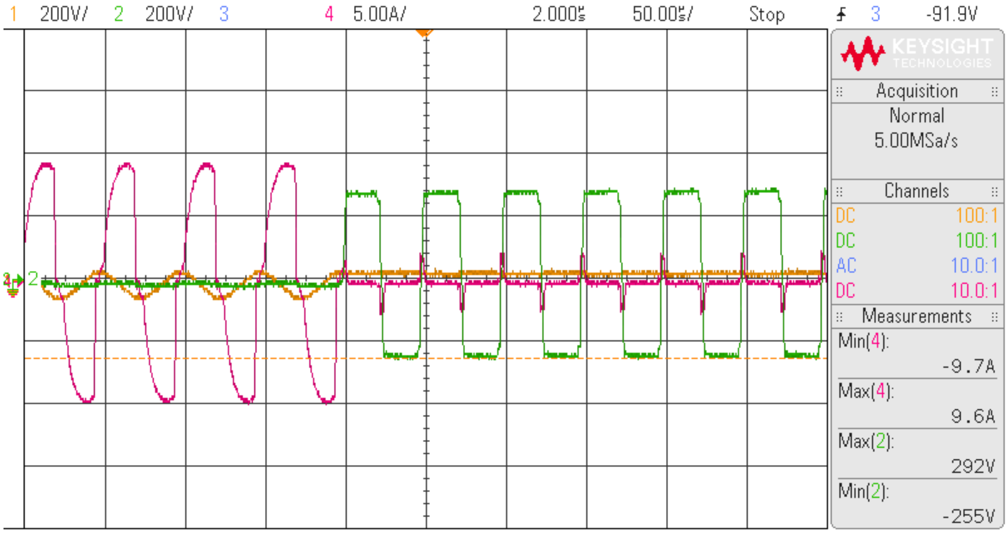

Figure 4.36 - Waveforms showing the actuation of the overcurrent protection system.

5 CONCLUSIONS AND FUTURE PERSPECTIVE

A high voltage high frequency converter for resistive load, with unpredictable variation, was detailed investigated, taking in account the high voltage high frequency converter particular behavior. Design and criteria for the converter's safety operation were defined. Simulation results and analytical calculations were performed and validated by experimental results.

The simplified approach to determine the converter's maximum power proved to be a good tool to give a general first view of the system's power transferring dynamics.

The series resonance happens inside the transformer and is caused by the leakage inductance and winding capacitance, whose are strongly dependent on the transformer building procedures. This resonance can cause high overvoltage peaks at the transformer's secondary and can only be mitigated by external procedures and, as the load dynamics is too fast for this converter, control strategies are not effective.

The HV clamper has a good result, but may be too expensive for high power applications, because of the high voltage high frequency components necessity and must be verified if the clamper's components determined by the design equations are reasonable with the commercially available. The external inductor is easy to implement and have a good effect in the overvoltage damping, but can only be applied when the leakage inductance has a low value.

The selective harmonic elimination is easy to implement, but has only a good result if the resonance happens in a low frequency range, where the harmonic amplitudes are higher, and must be carefully implement, taking in account the dynamics that the parasitic capacitances add to the open load behavior, once the ${dV}/{dt}$ associated to them can delay the primary voltage turning off, making the zero time interval lower than necessary, and not effectively eliminating the desired harmonic . The elimination of several harmonics doesn't have significant impact in the overvoltage damping when compared to one or two harmonics elimination, and increases the switching stress on the inverter's transistors.

The accurate measurement of the secondary voltage with the resonance manifestation is a challenge, once the voltage probe capacitance cannot be neglected when the series resonance happens in a high frequency range.

The electronic protection system based on the transistors' bidirectional switch and precision rectifier has a good result for the overcurrent protection.

In the continuity of this work, a more powerful converter can be built, with a more powerful inverter feeding several transformers, each one with an individual overvoltage protection and bidirectional switch, or even several individual converters, working in parallel, fed by the same energy source to deliver high power levels. This configuration would be interesting specially from the application point of view, once the several branches could work independently, and if a branch fails, the other continue to deliver power. Electromagnetic noise may be generated by this converter's configuration, and the effects of these noises in each "converter's module" must be analyzed.

In terms of the transformer, new studies can be made to minimize the effects of the series resonance excitation. This work showed the effectiveness, limitations and drawbacks of three different strategies. Continuing from that point, the combination of strategies can be explored, like the elimination of harmonics and the use of a clamper with reduced losses and simpler components, or the use of an external inductor and a clamper or a SHE, as the inductor changes the resonance frequency, the use of low pass filters etc. All the alternatives must be analyzed in terms of facility and cost of implementation, effectiveness and drawbacks.

REFERENCES

1. OLIVEIRA, L. A. F. D. **Study of High Frequency Transformers Models (in Portuguese)**. Belo Horizonte: UFMG, 2011. Master Dissertation.

2. MCLYMAN, C. W. T. **Transformer and Inductor Design Handbook**. 3. ed. New York: Marcel Dekker Inc, 2004.

3. PETROV, R. Optimum Design of High-Power, High-Frequency Transformer. **IEEE Transactions on Power Electronics**, v. 11, n. 1, p. 33-42, January 1996.

4. RAZAK, A. R. A.; TAJB, S. **Design considerations of a high frequency power transformer**. National Power Engineering Conference (PECon). Bangi: [s.n.]. 2003.

5. POMILIO, J. A.; BET, O.; VIEIRA, M. P. High-Voltage Resonant Converter with Extreme Load Variation: Design, Criteria and Applications. **International Journal of Electrical, Computer, Electronics and Communication Engineering**, v. 8, n. 12, p. 1764-1769, 2014.

6. LU, H. Y. et al. Measurement and Modeling of Stray Capacitances in High Frequency Transformers. **Power Electronics Specialists Conference**, 1 July 1999. 763-768.

7. LU, H. Y.; ZHU, J. G.; HUI, S. Y. R. Experimental Determination of Stray Capacitances in High Frequency Transformers. **IEEE Transactions on Power Electronics**, v. 18, n. 5, p. 1105-1112, September 2003.

8. BIELA, J.; KOLAR, J. W. Using transformer parasitics for resonant converters-a review of the calculation of the stray capacitance of transformers. **IEEE 40th Industry Applications Society Conference (ISA)**, v. 3, p. 1868-1875, 2005.

9. COGITORE, B.; KERADEC, J. P.; BARBAROUX, J. The two-winding transformer: experimental method to obtain a wide frequency range equivalent circuit. **IEEE Transactions on Instrumentation and Measurement**, v. 43, n. 2, p. 364-371, 1994.

10. LEON, F. D.; SEMLYEN, A. Efficient calculation of elementary parameters of transformers. **IEEE Transactions on Power Delivery**, v. 7, n. 1, p. 376-383, 1992.

11. KANE, M. M.; KULKARNI, S. V. MTL-Based Analysis to Distinguish High-Frequency Behavior of Interleaved Windings in Power Transformers. **IEEE Transactions on Power Delivery**, v. 28, n. 4, p. 2291-2299, 2013.

12. SPERANDIO, G. S.; POMILIO, J. A. **High-efficiency, high-frequency inverter for silent discharge load**. Brazilian Power Electronics Conference. Blumenau: [s.n.]. 2007.

13. TARDIVO, D. T.; POMILIO, J. A. **Resonant High-voltage supply for multiple paralleled loads with parameters equalization**. Brazilian Power Electronics

Conference. Natal: [s.n.]. 2011.

14. SHEN, W. **Design of High-Density Transformers for High-Frequency High-Power Converters**. Blacksburg: Virginia Polytechnic Institute State University, 2006. Doctorate Thesis.

15. MUHAMMED, A. H. **High Frequency Transformer, Design and Modeling Using Finite Element Technique**. Newcastle Upon Tyne: University of Newcastle Upon Tyne, 2000. Doctorate Thesis.

16. BAHMANI, M. **Design and Optimization of HF Transformers for High Power DC-DC Applications**. Göteborg: Chalmers University of Technology, 2014. Thesis for Degree of Licentiate.

17. KAZIMIERCZUK, M. K.; CZARKOWSKI, D. **Resonant Power Converters**. [S.l.]: John Wiley & Sons, 2001.

18. PEREZ, M. A. et al. A New Topology for High Voltage High Frequency Transformers. **IEEE Applied Power Electronics Conference and Exposition**, v. 2, p. 554-559, 1995.

19. BIBEROGLU, M.; GÜCIN, N. T.; FINCAN, B. Analyzing the influences of high frequency transformers utilized in parallel resonant converters. **IEEE International Conference on Renewable Energy Research and Applications**, p. 983-988, 2016.

20. ATALLA, A. et al. Advancements in high power high frequency transformer design for resonant converter circuits. **IEEE Energy Conversion Congress and Exposition**, p. 1-8, 2016.

21. PATTERSON, O.; DIVAN, D. **Pseudo-Resonant Converter Technologies**. IEEE 18th Power Electronics Specialists Conference (PESC). Blacksburg: [s.n.]. 1988.

22. LIU, J. et al. Design of High Voltage, High Power and High Frequency Transformer in LCC Resonant Converter. **Applied Power Electronics Conference and Exposition**, 15-19 February 2009. 1034-1038.

23. SULLIVAN, C. R.; ZHANG, R. Y. Simplified Method for Litz Wire. **IEEE Applied Power Electronics Conference and Exposition**, p. 2667-2674, 2014.

24. PAGAN, C. J.; POMILIO, J. A. Resonant High-Voltage Source Working at Resonance for Pulsed Laser. **Proc. of IEEE Power Electronics Specialists Conference**, Baveno, Italy, 24-27 June 1996.

25. ALONSO, J. et al. Analysis, desing and experimentation of a high-voltage power supply for ozone generation bsed on current-fed parallel-resonant push-pull inverter. **IEEE Transactions on Industry Applications**, v. 41, n. 5, p. 1364-1372, September-October 2005.

26. BONALDO, J. P.; POMILIO, J. A. Control Strategies for High Frequency Voltage Source Converter for Ozone Generation. **IEEE International Symposium on Industrial Electronics (ISIE)**, Bari, Italy, 4-7 July 2010. 754-760.

27. LU, S. et al. Modeling of Neon Tube Powered by High Frequency Converters. **IEEE IECON**, 2002. 288-293.

28. RIBAS, J. et al. High Frequency Electronic Ballast for Metal Halide Lamps Based on a PLL Controlled Class E Resonant Inverter. **IEEE PESC**, 2005. 1118-1123.

29. GONZÁLES, S. A.; VALLA, M.I.; MURAVCHIK, C.H. Analysis and Design of Clamped-Mode Resonant Converters with Variable Load. **IEEE Transaction on Industrial Electronics**, v. 48, n. 4, p. 812-819, August 2001.

30. BAIZAN, J. et al. Converter with four quadrant switches for EDM Applications. **IEEE Industry Applications Society Annual Meeting**, 2013.

31. CASANUEVA, R. et al. Resonant converters: properties and applications for variable loads. **31 st Annual Conference of IEEE Industrial Electronics Society**, 2005.

32. MIZUNO, A. et al. A Portable Weed Control Device using High Frequency AC Voltage. **IEEE Industry Application Soc. Annual Meeting**, 1993. 2000-2003.

33. ZASSO Brazil. Available at: <www.zasso.com.br>. Accessed in: August 2018.

34. BRIGHENTI, A. M.; BRIGHENTI, D. M. Weed Control in organic soybean using electrical discharge. **Ciência Rural**, Santa Maria, v. 39, n. 8, p. 2315-2319, November 2009.

35. SHAFIEI, N. et al. Analysis of a Fifth-Order Resonant Converter for High-Voltage DC Power Supplies. **IEEE Transactions on Power Electronics**, v. 28, n. 1, p. 85-100, January 2013.

36. SEN, P. C. **Principes of Electric Machines and Power Electronics**. New York: John Wiley & Sons, 1997.

37. CHAN, Y. P.; PONG, M. H. Leakage inductance calculation of complex transformer constructions based on a simple two-coil inductor model. **37th IEEE Power Electronics Specialists Conference (PESC)**, 2006. 1-4.

38. KAYMAK, M.; SHEN, Z.; DONCKER, R. W. D. Comparison of analytical methods for calculating the AC resistance and leakage inductance of medium-frequency transformers. **IEEE 17th Workshop on Control and Modeling for Power Electronics (COMPEL)**, 2016. 1-8.

39. BAKAR, M. A.; BERTILSSON, K. An improved modelling and construction of power transformer for controlled leakage inductance. **IEEE 16th International Conference on Environment and Electrical Engineering (EEEIC)**, 2016. 1-5.

40. ROSSMANITH, H.; STENGLEIN, E. **Prediction of the leakage inductance in high frequency transformers**. IEEE 18th European Conference on Power Electronics and Applications. [S.l.]: [s.n.]. 2016.

41. HARADA, K.; NINOMIYA, T.; KAKIHARA, H. **Effects of stray capacitances between transformer windings on the noise characteristics in switching power converters**. IEEE Power Electronics Specialists Conference. Boulder: [s.n.]. 1981.

42. MAYER, P.; GERMANO, P.; PERRIARD, Y. FEM modeling of skin and proximity effects for coreless transformers. **IEEE 15th International Conference on Electrical Machines and Systems (ICEMS)**, p. 1-6, 2012.

43. ROßKOPF, A.; BÄR, E.; JOFFE, C. Influence of Inner Skin and proximity Effects on Conduction Litz Wires. **IEEE Transactions on Power Electronics**, v. 29, n. 10, p. 5454-5461, 2014.

44. SADIKU, M. N. O. **Elements of Electromagnetics**. 3rd. ed. New York: Oxford University Press, 2000.

45. MORAG, Y.; TAL, N.; LEVRON, Y. **The effects of radiation resistance on the signal to noise limits of magnetic sensors and communication systems**. IEEE International Conference on Microwaves, Communications, Antennas and Electronic Systems (COMCAS). Tel Aviv: IEEE. 2015.

46. CONTRERAS, S. A. D. **Study of the Application of Intercellular Transformers in Voltage Inverters (in Portuguese)**. Belo Horizonte: UFMG, 2014. Doctorate Thesis.

47. RODRIGUES, D. T. **Balance power of high voltage resonant loads fed in parallel, through electronic compensation of the parameters (in Portuguese)**. Campinas: Unicamp, 2012. Master Dissertation.

48. SPERANDIO, G. S. **High-voltage AC resonant source for ozonizers (in Portuguese)**. Campinas: Unicamp, 2007. Master Dissertation.

49. BONALDO, J. P. **Power converter feeding ozone generation cells (in Portuguese)**. Campinas: Unicamp, 2010. Master Dissertation.

50. ROCABERT, J. et al. A regenerative active clamp circuit for DC/AC converters with high-frequency isolation in photovoltaic systems. **IEEE 35th Annual Power Electronics Specialists Conference**, v. 3, p. 2082-2088, 2004.

51. TSAI, F.; LEE, F. C. **A complete dc characterization of a constant-frequency, clamped-mode, series-resonant converter**. IEEE 19th Power Electronics Specialists Conference (PESC). Kyoto: [s.n.]. 1988.

52. ALEXANDER, C. K.; SADIKU, M. N. O. **Fundamentals of Electric Circuits**. 5th. ed. New York: McGraw-Hill, 2013.

53. STEIN, E. M.; SHAKARCHI, R. **Princeton Lectures in Analysis I Fourier Analysis An introduction**. New Jersey: Princeton University Press, 2002.

54. BHADRA, S.; GROGORY, D.; PITANGIA, H. **An analytical solution of switching angles for Selective Harmonic Elimination (SHE) in a cascades seven level inverter**. IEEE 2nd Southern Power Electronics Conference. Auckland: [s.n.]. 2016.

55. DAHIDAH, M. S. A.; KONSTANTINOU, G.; AGELIDIS, V. G. A Review of Multilevel Selective Harmonic Elimination PWM: Formulations, Solving Algorithms, Implementation and Applications. **IEEE Transactions on Power Electronics**, v. 30, n. 8, p. 4091-4106, 2015.

56. KUMAR, N. V. et al. **Selective harmonic elimination:** An comparative analysis for seven level inverter. IEEE Students' Technology Symposium (TechSym). Kharagpur: [s.n.]. 2016.

57. SAHALI, Y.; FELLAH, M. K. **Selective harmonic eliminated pulse-width modulation technique (SHE PWM) applied to three-level inverter/converter**. IEEE International Symposium on Industrial Electronics (ISIE). Rio de Janeiro: [s.n.]. 2003.

58. SIRISUKPRASERT, S. **Optimized Harmonic Stepped-Waveform for Multilevel Inverter**. Blacksburg: Virginia Polytechnic Institute State University, 1999.

59. SOKOLOVS, A.; GALKIN, I. **Cost and space effective IGBT gate drive circuit for bi-directional switch of matrix converter**. 11th International Biennial Baltic Electronics Conference. Tallinn: [s.n.]. 2008. p. 293 - 296.

60. ITOH, J.-I.; NAGAYOSHI, K.-I. **A New AC Bidirectional Switch with Regenerative Snubber to Realize a Simple Series Connection for High Power AC/AC Direct Converters**. IEEE 38th Power Electronics Specialists Conference (PESC). Orlando: [s.n.]. 2007. p. 3009-3014.

61. TEKTRONIX. **Instruction Manual P6015A 1000X High Voltage Probe 070-8223-05**. [S.l.].